ABSTRACT

RESOANCES OF PERIODIC METAL-DIELETRIC MESHES IN THE INFRARED WAVELENGTH REGION

by

Oren Sternberg

Metal meshes have been used as reflectors in radar receivers for wavelength much longer than the periodic constant of the conducting wires and as optical reflectors in a Fabry-Perot in the far infrared. Cross shaped metal meshes can be used as band pass filters but the design theory and near field properties have not been known.

Transmittance of thin, single-layer and multiplayer metal meshes has been investigated using Micro-Strips, yielding numerical solutions of Maxwell's equations. The near field effect was studied for two alignment configurations of cross shaped metal meshes, both free standing and with dielectrics, and transmission line theory was applied for the interpretation as an oscillator mode model. The model for the interpretation of the mode of a single mesh uses a pair of coupled surface wave (that is one standing wave on each side). The transmittance of multi-layer metal meshes are interpreted as modes composed of resonance modes of the single mesh, the Fabry-Perot modes depending on the separation of the meshes, and their interaction.

Experimental data for thick inductive cross shaped metal meshes agree very well with Micro-Stripes calculations in the long wavelength region and with Fourier Modal method calculations in the short wavelength. The transmittances of all these meshes show

similar resonance peaks and the same dependence on thickness of the short wavelength peaks, suggesting that the interpretation using the oscillator mode model is valid in the short and long wavelength region.

Stacks of thin metal meshes have been studied with Micro-Strips and transmission line theory. Narrow transmission regions for inductive meshes and narrow bandgap regions for capacitive meshes may be obtained from layered structures for the aligned configuration and spacing of 1/4 resonance wavelength of a single layer.

RESONANCES OF PERIODIC METAL-DIELECTRIC STRUCTURES AT THE INFRARED WAVELENGTH REGION

by
Oren Sternberg

A Dissertation
Submitted to the Faculty of the New Jersey Institute of Technology and
Rutgers, the State University of New Jersey - Newark
In Partial Fulfillment of the Requirements for the Degree of
Doctor of Philosophy in Applied Physics

Federated Physics Department

August 2002

APPROVAL PAGE

RESONANCES OF PERIODIC METAL-DIELECTRIC STRUCTURES

AT THE INFRARED WAVELENGTH REGION

Oren Sternberg

Dr. Karl D. Möller, Dissertation Advisor — Date
Research Professor, Department of Physics, NJIT

Dr. Haim Grebel, Dissertation Co-Advisor — Date
Professor, Department of Electrical and Computer Engineering, NJIT

Dr. Daniel E. Murnick, Committee Member — Date
Professor, Department of Physics, Rutgers University

Dr. John F. Federici, Committee Member — Date
Professor, Department of Physics, NJIT

Dr. Zafar Iqbal, Committee Member — Date
Professor, Department of Chemistry, NJIT

Dr. Kenneth P. Stewart, Committee Member — Date
Department of the NAVY, Naval Research Laboratories

BIOGRAPHICAL SKETCH

Author: Oren Sternberg

Degree: Doctor of Philosophy

Date: August 2002

Undergraduate and Graduate Education:

- Doctor of Philosophy in Applied Physics
  New Jersey Institute of Technology, 2002

- Bachelor of Science in Applied Physics
  New Jersey Institute of Technology, 1998

Major: Applied Physics

Publications:

O. Sternberg, K.D. Möller, H. Grebel K.P Stewart, and R. M. Henry. (2002). Accepted Infrared Physics.

Karl D. Möller, Oren Sternberg, Haim Grebel, and Kenneth P. Stewart. (2002). Inductive cross-shaped metal meshes and dielectrics. Applied Optics, 41, 3919-3926.

K.D. Möller, Oren Sternberg, H. Grebel , Philippe Lalanne. (2002). Thick inductive cross shaped metal meshes. Applied Physics, 91, 9461-9465.

Karl D. Möller, Oren Sternberg, Haim Grebel, and Kenneth P. Stewart. (2002). Near-field effects in multilyer inductive metal meshes. Applied Optics, 41, 1942-1948.

K.D. Möller, K.R. Farmer, D.V.P. Ivanov, O. Sternberg, K.P. Stewart, and P. Lalanne. (1999). Thin and thick cross shaped metal grids. Infrared Physics, 40, 475-485.

K.D. Möller, K.R. Farmer, D.V.P. Ivanov, O. Sternberg, K.P. Stewart, P. Lalanne. (1998) Band Pass Filters for the Mid-Infrared", 23rd International Infrared and Millimeter Wave Conference, Colchester, U.K, 191-192.

To my grandfathers, Chaim Sternberg, and Mendel Gercht, for
their honor, loyalty, and fighting spirits

ACKNOWLEDGMENT

I would like to recognize and thank Professor Karl Dieter Moeller for his direction, advice and patience, and Professor Haim Grebel for his advice, and participation in many useful suggestions.

I would like to thank Professor Daniel Murnick, Professor Zafar Iqbal and Professor John F. Federici for their interest in my work and the service on the committee. I thank Dr. Kenneth P. Stewart of the Naval Research Laboratories for his support, advice and service on the committee, and Dr. D. V. P. Ivanov for advice and help in the NJIT-cleanroom, as well as Dr. K. R. Farmer.

My efforts would not be possible without the machine time and funding of the Electronic Imaging Center (NJIT), a grant of the National Science Foundation and the Naval Research Laboratory, and the support of the Goddard Space Flight Center for far infrared spectroscopy.

TABLE OF CONTENTS

TABLE OF CONTENTS
(Continued)

TABLE OF CONTENTS
(Continued)

Chapter **Page**

TABLE OF CONTENTS
(Continued)

Chapter **Page**

TABLE OF CONTENTS
(Continued)

Chapter **Page**

LIST OF TABLES

LIST OF FIGURES

LIST OF FIGURES
(Continued)

LIST OF FIGURES
(Continued)

Figure **Page**

LIST OF FIGURES
(Continued)

LIST OF FIGURES
(Continued)

Figure **Page**

LIST OF FIGURES
(Continued)

Figure **Page**

LIST OF FIGURES
(Continued)

Figure **Page**

LIST OF FIGURES
(Continued)

LIST OF FIGURES
(Continued)

Figure **Page**

LIST OF FIGURES
(Continued)

Figure **Page**

LIST OF FIGURES
(Continued)

Figure **Page**

CHAPTER 1

INTRODUCTION

1.1 Metal Meshes and Applications in the Infrared and mm-Region

Metal meshes have been used as reflectors for many years. In the 1940's and 1950's radar receivers were constructed with metal grids as reflectors for wavelength much longer than the periodic constant of the conducting wires. In the 1960's Ulrich *et al.*[1] constructed a far infrared Fabry-Perot device with electroformed metal meshes as reflectors and operated a Fabry-Perot spectrometer in the 100μm to 600μm region. These meshes showed in transmission a strong maximum at a wavelength larger than the periodicity constant and high reflectivity for long wavelength. The inverse structure of a metal grid, that is a periodic array of metal squares, has first been published by Ressler and Möller[2] and showed a strong minimum in reflection at the same wavelength as for the metal grid.

Ulrich[3] used transmission line theory to develop a model for the meshes, and described the metal meshes as electromagnetic oscillators similar to a two dimensional array of dipoles. He used electromagnetic circuit elements for the description of the resonance wavelength and studied arrays of metal meshes as multiple mesh filters[1]. The theory was semi-empirical and needed input data from experiments. Ulrich[1,3] named the metal grids inductive meshes and the inverse structure capacitive meshes and used a combination of inductive and capacitive meshes to manufacture meshes with cross shaped pattern, see Figure 1.1. The transmittances of cross shaped inductive meshes were studied by Chase and Joseph[4] and the dependence on the geometrical parameters studied.

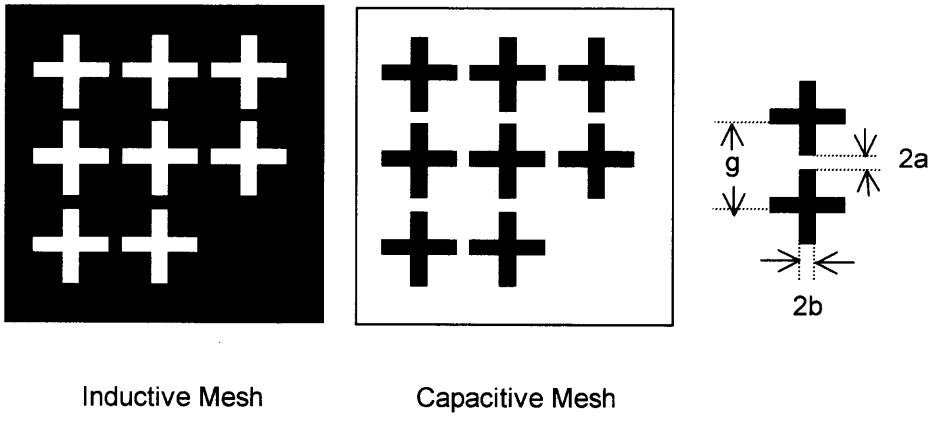

Figure 1.1 Geometrical overview of crosses. Geometrical constant g, separation of cross 2a, width of cross arms 2b, and metal thickness t. (a) Inductive mesh (b) Capacitive mesh.

Theoretical calculations on thin metal meshes have been done by Golden[5], Compton[6] and Porterfield[7] using various computational methods for solving the electromagnetic boundary value problem. These calculations were applied in the long wavelength region to lithographically produced metal meshes, where the metal thickness is small compared to the wavelength and periodicity constant. In the short wavelength region, free standing metal meshes, on account of their mechanical stability, have a thickness not small compared to the periodicity constant resonance wavelength and are called thick metal meshes. Lalanne[8] has used the Fourier modal method in the 1μm region for calculations of the transmittance of thick metal meshes with cross shaped openings. In this dissertation the Micro-Stripes program is employed to calculate the transmittance of thin and thick metal meshes. Solutions of Maxwell's equations with appropriate boundary conditions are used for a wide range of geometrical parameters and several values of refractive indices.

The use of metal meshes in Fabry-Perot spectrometers led to the design and construction of Fabry-Perot etalons as filters for specific wavelength in the long wavelength region. The COBE (Cosmic Backbround Explorer) satellite used such cross shaped metal mesh etalons as filters, designed by Möller *et al.*[9].

The Micro-Stripes[10] program allows the investigation of aspects of photonic crystals constructed of stacks of thin and thick inductive and capacitive metal meshes, see References [9] and [10]

1.2 The Micro-Stripes Simulation Program

The Micro-Stripes simulation program was used for the calculation of the transmittance of metal meshes, free standing or in contact with dielectrics. The program solves Maxwell's equations for 3D periodic structures and needs as input data the geometrical parameters, boundary conditions, the surface impedance of the metal and the dielectric constants of the dielectrics. A description is presented in Appendix A.

The transmittances of accurately manufactured thick metal meshes were used to determine the surface impedance of the metal mesh by matching the simulated intensity to the observed transmittance. These transmittance calculations of inductive metal meshes of various thicknesses were used as justification of the Micro-Stripes calculations, see Figure 1.2. The experimental results of eight transmittance peaks were reproduced with an average accuracy of 1% of the measured values[11]. Therefore, using the adjusted surface impedance, we consider the Micro-Stripes simulations "as good as experiments".

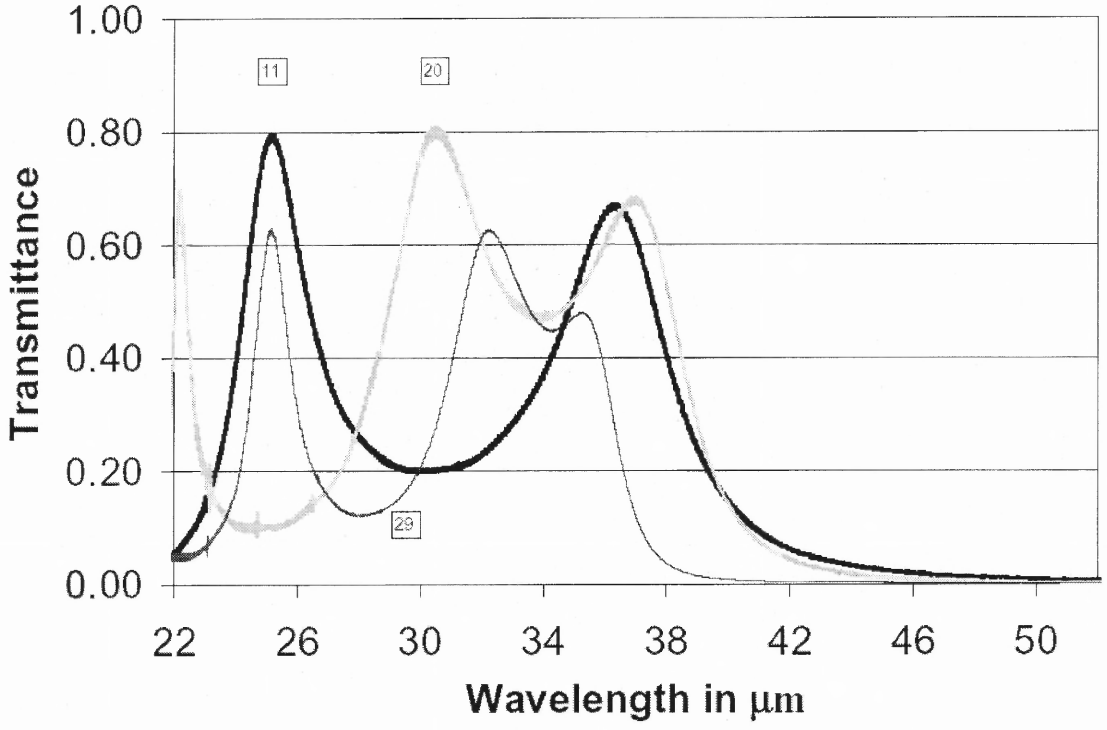

Figure 1.2 Micro-Stripes calculated transmittance of free standing metal meshes of thicknesses 11, 20 and 29μm. The parameters of the cross are g = 20, 2a = 1.5 and 2b = 3μm.

1.3 Interpretation of the Results of Simulations

Simulations are applied to specific sets of parameters and are similar to the numerical results of an equivalent specific experiment. Variation of the parameters supplies clues for the description using the laws of physics. For the interpretation, a number of models are discussed, each describing a certain point of view of the physics involved.

1.3.1 Metal Meshes as Long Wavelength Reflectors

The reflectivity of metal meshes depends on the ratio of the wavelength to the periodicity constant of the mesh, and for large ratios one may get 95% reflection or even higher.

Square shaped metal meshes are commercially available as electroformed meshes with periodicity constants from 25μm to the millimeter region and a thickness of a few microns. In the far infrared, at around 100μm, metal meshes have been used as Fabry-Perot reflectors. Metal meshes were used in this spectral region because they show considerably less absorption than semi-transmissive thin metal films, as used in the short wavelength region for the same purpose.

1.3.2 Inductive and Capacitive Meshes

Metal meshes made of wires in a two dimensional periodic arrangement are called inductive meshes, and the inverse structure a capacitive mesh, both shown for cross shaped pattern in Figure 1.1. The capacitive meshes need a substrate for their realization. Ulrich[3] has studied inductive and capacitive metal meshes with transmission line theory and represented the meshes by electrical circuit elements. Since the incident light induces currents along the wires of a wire grid, he called them inductive mesh, while in the inverse structure positive and negative charges are produced on metals separated by a dielectric gap, he called them capacitive mesh.

1.3.3 Diffraction, Resonance Peaks and Babinet's Principle

Electromagnetic radiation is considered incident in normal direction on inductive and capacitive meshes with the same size of the crosses and periodicity constant. Both meshes will show the same diffraction pattern for wavelength smaller than the periodicity constant, similar to what one would have for a two dimensional grating, according to

Babinet's principle in *scalar wave formulation*[12,13,14]. The transmittance of radiation with wavelength longer than the periodicity constant is shown in Figure 1.3.

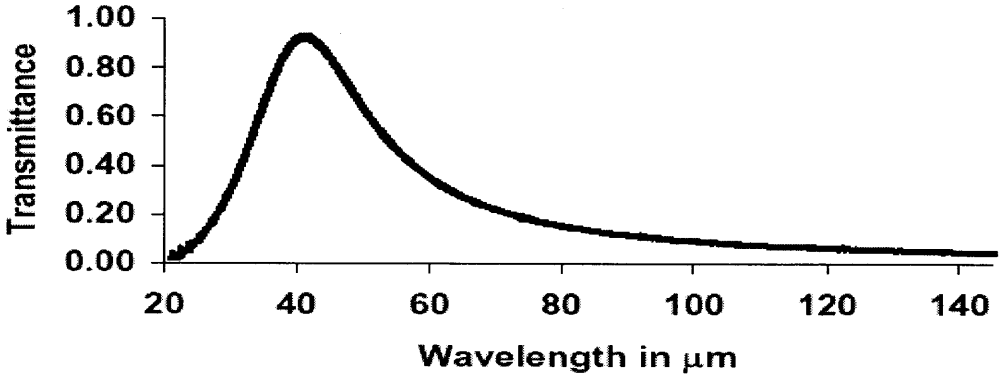

(a) Transmittance of Inductive Mesh

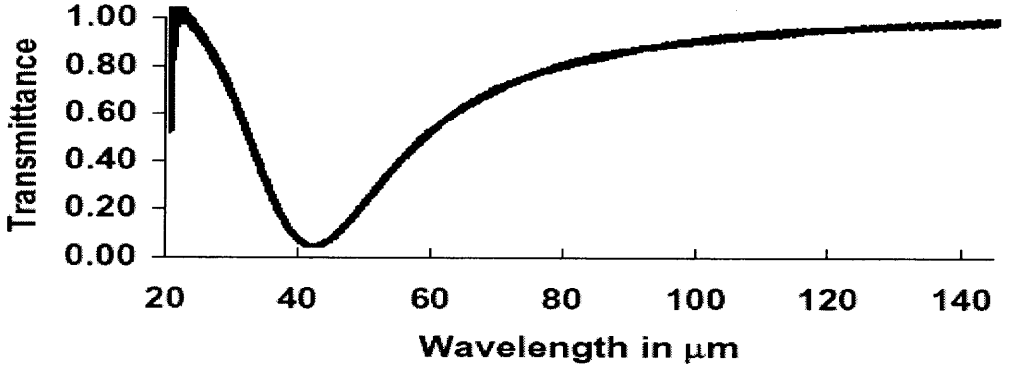

(b) Transmittance of Capacitive Mesh

Figure 1.3 Demonstration of Babinet's Principle(a) Inductive Mesh (b) Capacitive Mesh.

The inductive mesh has a resonance maximum at around 40μm while the capacitive mesh shows a resonance minimum at the same wavelength, see Figure 1.3. According to Babinet's principle in *electromagnetic formulation*[12,13,14] complementary screens will show complementary transmittance pattern. The maximum of an inductive mesh has the

same wavelength as the minimum of the capacitive mesh provided that the geometrical parameters are the same.

1.3.4 Resonance Mode and Intensity

The relation of the resonance wavelength of a mesh to the periodicity constant may be seen considering a one dimensional capacitive grid that is chain of metal pieces separated by dielectric gaps. The incident light induces changes in the distribution of the charges in the metal and the vibrating positive and negative charges form a chain of vibrating electrical dipoles. There is similarity to a vibrating chain of NaCl molecules. In the fundamental mode all Na atoms move in phase against all Cl atoms and the resonance wavelength of this fundamental mode is the vibrational wavelength of one NaCl molecule vibrating with respect to its center of gravity. Similarly, the resonance wavelength of the chain of vibrating dipoles has the resonance wavelength $2L$ for a dipole of length L. When using the periodicity constant g for the representation of the resonance wavelength one has for the resonance wavelength $2g$ minus two times the width of the gap between the metal pieces. With respect to Babinet's principle, one can make an argument of "dipoles of the openings"; that is the incident light excites the vibration of all dipoles in the fundamental mode and all dipoles reflect in phase the incident light at the resonance wavelength of a dipole. The incident light is strongly reflected at this wavelength, producing a minimum in transmission, similar to constructive interference at a periodic array of source points. In contrast, a random array of source points will show a much less pronounced minimum at the resonance wavelength of the dipole.

1.3.5 Surface Waves and Modes

The incident light induces a pair of surface waves on both sides of the mesh, and these surface waves transfer the incident light into the reflected and transmitted light. The induced longitudinal electromagnetic surface waves are standing waves with resulting wave vector equal to zero and resonance wavelength depending on the periodicity of the mesh. The two pairs of surface waves on the front and back side of a metal mesh oscillate with the same resonance wavelength and form the resonance mode.

When a metal mesh is placed on a dielectric substrate, the resonance wavelength shifts to longer wavelength by a factor smaller than the refractive index n of the substrate. When the mesh is embedded in a dielectric, the resonance wavelength changes by the refractive index *n*. The shifting of the resonance wavelength may be seen considering a chain of metal rectangles of a two dimensional capacitive mesh. At the gap between the rectangles one side has positive charges, on the other side has negative charges and in the gap, a dielectric of refractive index *n*. For refractive indices *n* larger than 1, the corresponding capacitance is increased. Since, in transmission line theory the resonance wavelength is proportional to the square root of the inductance times the capacitance, there is an increase of the capacitance resulting in a shift to longer wavelengths of the resonance wavelength.

1.3.6 Thick Metal Meshes and the Waveguide Modes

Thick metal meshes show a similar transmission spectrum to for thin metal meshes when the metal thickness is 1/100 of the periodicity constant. With increasing thickness, at a metal thickness of about 1/10 of the periodicity constant, a new peak appears. The peak

corresponds to a wave guide mode of the openings of the inductive mesh and transfers energy from the surface waves on the front to the back side. The wavelength of the thickness peak is obtained from the vector addition of wavevector k of the surface waves and the wave guide modes.

CHAPTER 2

FREE STANDING CROSS SHAPED MESHES

2.1 Single Mesh

2.1.1 Geometrical Parameters

Electroformed metal meshes have been used in the far-infrared spectral region as well as in the mm region as reflectors because of their high reflectivity and small losses. These meshes with square shaped openings were called by Ulrich[1,3], Inductive meshes. They show a resonance transmittance at a wavelength close to the periodicity constant and high reflectivity in the long wavelength region. The high and lossless reflectivity of the meshes in the long wavelength region was used in Fabry-Perot spectrometers[1,15] and Fabry-Perot etalons and the resonance transmittance for the construction of multi-layer band pass filters. The width of the transmittance band may be made narrower if the square shaped openings are changed to cross shaped openings. Inductive, metal meshes with cross-shaped pattern, see Figure 2.1, are metal foils with cross-shaped openings in a periodic array.

In the astrophysical community, there is a great need of narrow bandpass filters in the mid and far infrared spectral region. Cross shaped meshes have one geometrical parameter more than square shaped meshes. The resonance wavelength of cross shaped meshes may be designed at a position not as close to the limiting periodicity region that one would have with square shaped meshes, thus allowing greater flexibility. A cross will have narrower bandpass characteristics than that of a square shaped mesh. In addition, crosses have the advantage that there is no preference with respect to polarization of the

incident light. The resonance wavelength as well as the bandwidth of crosses depend on the choice of the parameters *a* and *b* with respect to the periodicity constant *g*. The shape of the crosses for certain ratios of *a/g* and *b/g* are shown in Figure. 2.2

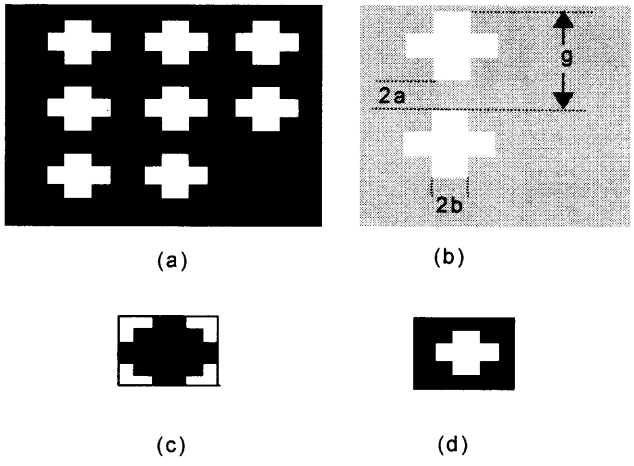

Figure 2.1 (a) Pattern of inductive meshes; openings are white, and metal film is black. (b) Geometrical parameters g, a, and b of a cross. (c) Cross in shifted position. (d) Cross in the lined-up position.

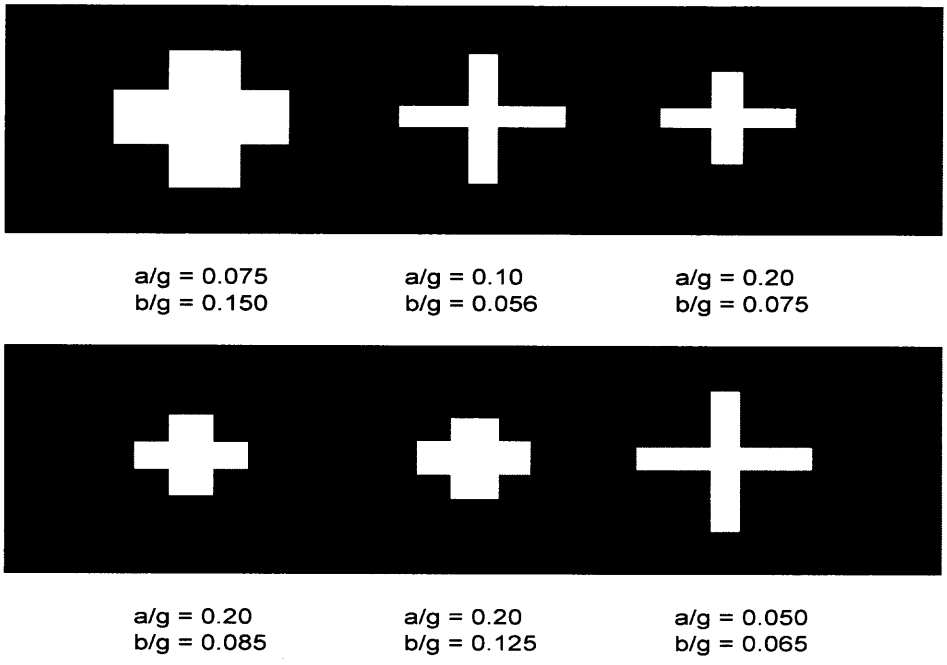

Figure 2.2 Inductive Cross meshes, a/g and b/g values corresponding to certain cross shapes, (Chase and Joseph see Reference [4]).

2.1.2 Modes of Metal Meshes

An inductive cross shaped metal mesh diffracts all light of wavelength shorter than the periodicity constant and reflects most of the light of wavelength larger than the periodicity constant. However, around a wavelength twice as large as the periodicity constant, all incident light is transmitted. The interaction of the light with the mesh may therefore be considered as an excitement of an oscillator by the incident light, and transfer of energy of the incident light into the reflected and transmitted light. An analysis of free standing inductive metal meshes has been presented by Ulrich[16].

To describe the interaction process, one assumes a plane wave propagating in z direction, perpendicular to the surface of the mesh in the x-y plane. The plane wave, incident in normal direction, induces currents in the metal. As a result, longitudinal surface waves are induced on the front and back side of the mesh. The surface waves appear as pairs of traveling waves in opposite direction with wave vectors parallel to the x-y direction. Since the incident light has a wave vector perpendicular to the x-y plane, the surface waves are standing waves with resulting wave vector equal to zero. The pairs of standing waves on the front and back side of the mesh form an oscillator mode of the mesh.. The induced mode transfers the incident light into the reflected and transmitted light. For thin meshes, the surface waves are tightly coupled through the openings. Figure 2.3, shows a schematic of the interaction of the light with the mesh.

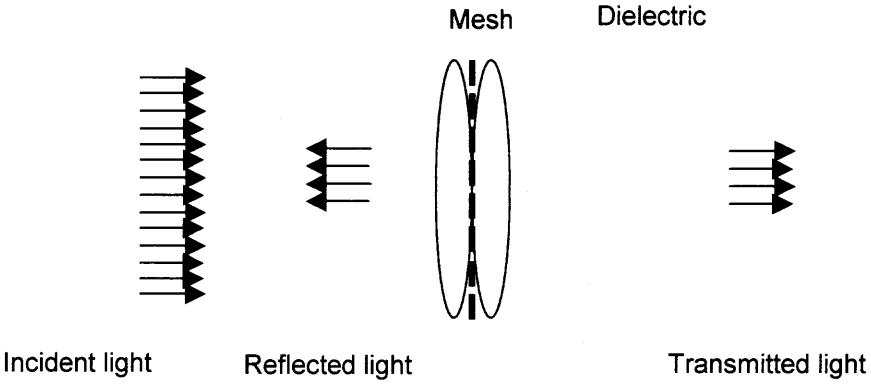

Figure 2.3 The incident light induces a mode of the mesh, consisting of two pairs of standing surface waves on each side of the mesh. For a thin mesh, the two pairs are coupled tightly through the openings. The excited mode transfers the incident light into the transmitted and reflected light.

The charge fluctuations may be looked at as a periodic array of oscillating dipoles as positive and negative charges oscillate in the well known linear chain of solid state physics. The fundamental mode of such a chain has the wavelength of 2 times the length of one dipole. In the case of cross shaped meshes, the resonance wavelength turns out to be close to two times the periodicity constant, but depends on the shape of the crosses.

2.2 Resonance Wavelength

2.2.1 Empirical Formula

Ulrich used a combination of capacitive and inductive meshes for the manufacturing of cross shape meshes and Chase and Joseph[4] investigated the transmittance of six types of cross shaped meshes with shape parameters of a/g between 0.05 and 0.2 and b/g between 0.56 and 0.15. They presented an empirical formula for the resonance wavelength, see Equation (2.1a). a least squares fit calculation using six observed values of resonance

wavelengths to determine the coefficients of g, a and b. An empirical formula on the basis of dipole interaction was derived by Möller et al[8,9], shown in Equation (2.1b).

The Golden program[5,8] was used for the calculation of the transmittance of thin metal meshes. The input data are the geometrical parameters of the crosses. The Golden program assumes for the calculations, infinite conductivity. A least squares fit for the formula is displayed in Equation (2.1c).

A computation of the transmission of six different types of cross shaped grids[4] using the Fourier Modal Method[8] in the near infrared was done as well. This rigorous method relies on a Fourier decomposition of electromagnetic fields on the surface of the periodic structure of the mesh. Symmetry consideration were exploited to reduce the number of Fourier orders, and the results of computed data had an absolute error smaller than 0.01. The calculations were performed on a nickel film surrounded by air with a periodicity contact of g = 2.14 μm and the real and imaginary part of the refractive index of nickel were interpolated from tabulated data[8]. The resulting formula is shown in Equation (2.1d).

$$\lambda_R = 2.1g - 4.2a + 2.1b \quad (2.1a)$$

$$\lambda_R = 2g - 4a - 2b \quad (2.1b)$$

$$\lambda_R = 2g - 3.6a - 2.7b \quad (2.1c)$$

$$\lambda_R = 2.6g - 4.3a - 3.9b \quad (2.1d)$$

The resonance wavelengths given in the four formulas are in general consistent with experimental results. All formulas have a first term of about $2g$ and are modified by

the parameters *a* and *b* of the shape of the crosses. The main difference with these linear relations is the sign + or – for the *2b* factor. For thin free standing meshes, the formulation of Equation (2.1b) deems to be more appropriate, while the formula with *+2b* is better for thin meshes on a thin substrate.

2.2.2 Micro-Stripes Results

The Micro-Stripes program[10] provides 3D electromagnetic analysis of arbitrary geometries, yielding results in time/frequency domain and uses the Transmission Line Matrix(TLM). This method is based on establishing a network of transmission lines that represents the physics of the problem, and finding equivalence between the electrical solutions of that network and the physical parameters of the problem.

The Micro-Stripes program was used to calculate the resonance wavelength λ_R and width of resonance RW for twenty-five sets of *g, a*, and *b*(free standing). In Figure 2.4 the resonance is plotted for a wavelength λ_R, calculated for $g = 20\mu m$, $2a = 3, 4, 6, 8, 9\mu m$ and $2b = 2, 4, 5, 6, 7\mu m$. The resonance wavelength λ_R is plotted depending on *a* and *b*. The Micro-Stripes data have been presented by a non-linear formula (Equations (2.2a). The coefficient were calculated by a best-fit.[17]. Assuming that realistic input data would have only two significant decimal places, Equations (2.2b)) appears without second order *b* term.

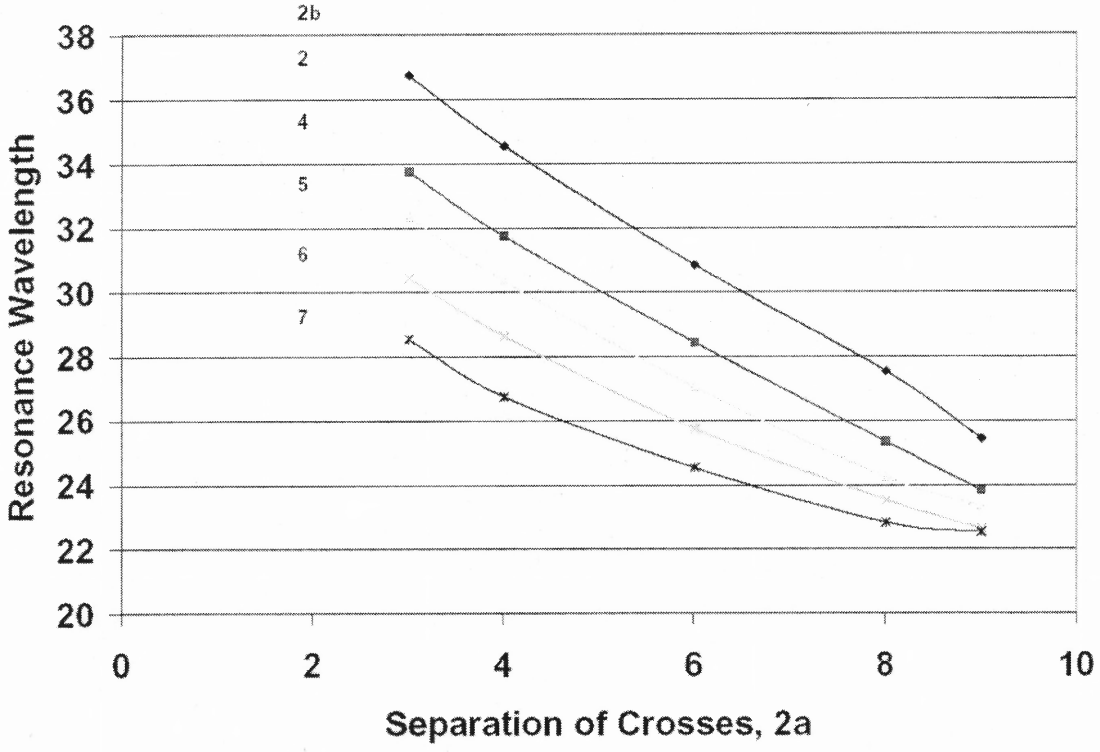

Figure 2.4 Resonance wavelength verses cross separation. Geometrical parameters: g=20μm, 2a = 3, 4, 6, 8, 9μm and 2b = 2, 4, 5, 6, 7μm.

$$\lambda_R = 2.4539\ g - 6.2444\ a - 4.3527\ b + (0.2933\ a^2 - 0.0032\ b^2) + 0.657\ (a\ b) \qquad (2.2a)$$

$$\lambda_R = 2.45\ g - 6.24\ a - 4.35\ b + 0.29\ a^2 + 0.67\ (a\ b) \qquad (2.2b)$$

A linear chain of dipoles of length g would have for the fundamental mode a wavelength of *2g*. The terms depending on *a* and *b* modify the resonance wavelength by changing the shape of the crosses. The non-linear relation was based upon 25 data sets of different cross shape parameters, and the formula is accurate within a standard deviation of 0.2μm.

2.3 Width of Resonance

An empirical formula for the bandwidth was given by Chase and Joseph[4]. The width of the band over the center wavelength was presented by a constant of 0.15 and an additional term ¼ (a/b).

The Micro-Stripes program was used to calculate the width of the resonance (WR) defined as width at half height ($\Delta\lambda/\lambda$). In Figure 2.5 one shows WR for g = 20 depending on a/g and b/g. The values chosen were b/g = 0.05, 0.1, 0.125, 0.15, 0.175 and calculated the resonance wavelength depending on a/g = .075, 0.1, 0.15, 0.2, 0.225 for each of these values.

The results of the Micro-Stripes program have been presented with a non-linear formula and the coefficient calculated by a best fit[17], see Equation 2.3a. Assuming that realistic input data would have only two significant decimal places, one can use Equation (2.3b).

$$\Delta\lambda/\lambda = -2.441(a/g)^2 - 2.7827(b/g)^2 - 21.7103(a/g)(b/g) + 0.9677(a/g)+0.58824(b/g) \quad (2.3a)$$

$$\Delta\lambda/\lambda = -2.44(a/g)^2 - 2.78(b/g)^2 - 21.71(a/g)(b/g) + 0.96(a/g)+0.59(b/g) \quad (2.3b)$$

and the standard deviation was obtained as 0.023. The change of width of resonance depending on changes of cross parameters a and b for fixed periodicity g may be seen from Figure.2.5. The smallest width is obtained for large a/g and large b/g, and the largest width for small a/g and b/g values

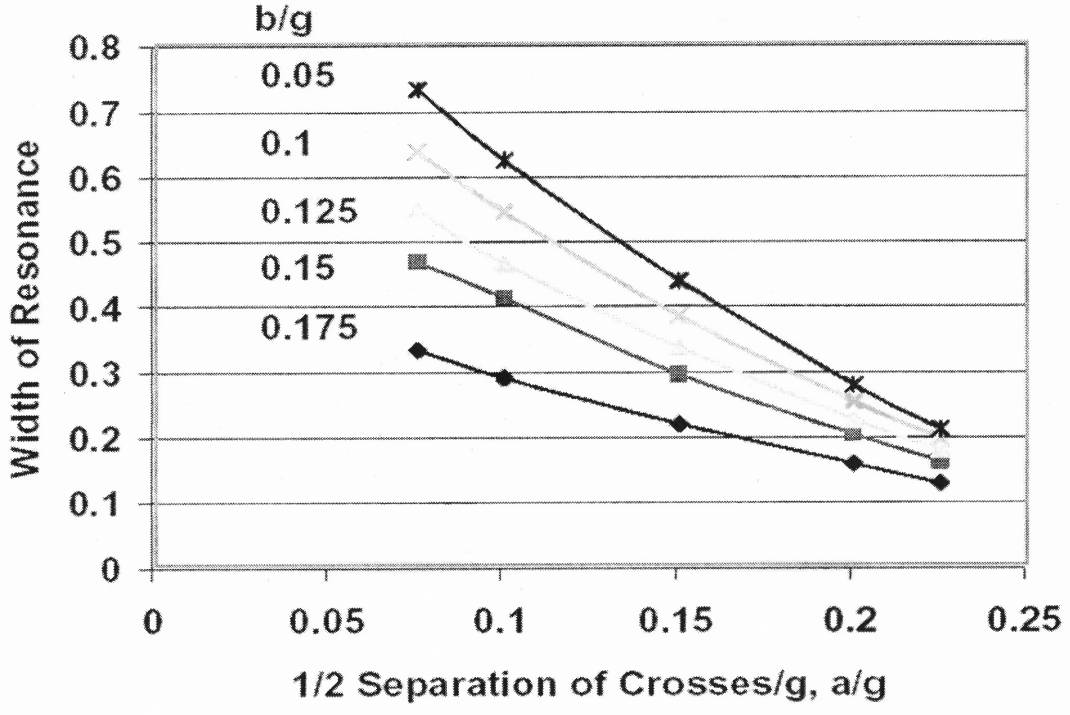

Figure 2.5 Width of Resonance Vs Cross separation relation (a/g). g = 20μm and sets of a/g = .075, 0.1, 0.15, 0.2, 0.225 and b/g = 0.05, 0.1, 0.125, 0.15, 0.175.

2.4 Width of Resonance and Intensity

Both the peak intensity resonances and the width to resonances depend on the shape of the cross. This is shown for a few cross parameters a and b and fixed g = 24 μm, see Figure.2.6. The parameters are for (1) a = 5.6 μm and b = 0.2 μm, (2) a = 5.2 μm and b = 1.0 μm, (3) a = 4.8 μm and b = 1.2 μm, (4) a = 4.4 μm and b = 0.26 μm, and (5) a = 3.2 μm and b = 5 μm.

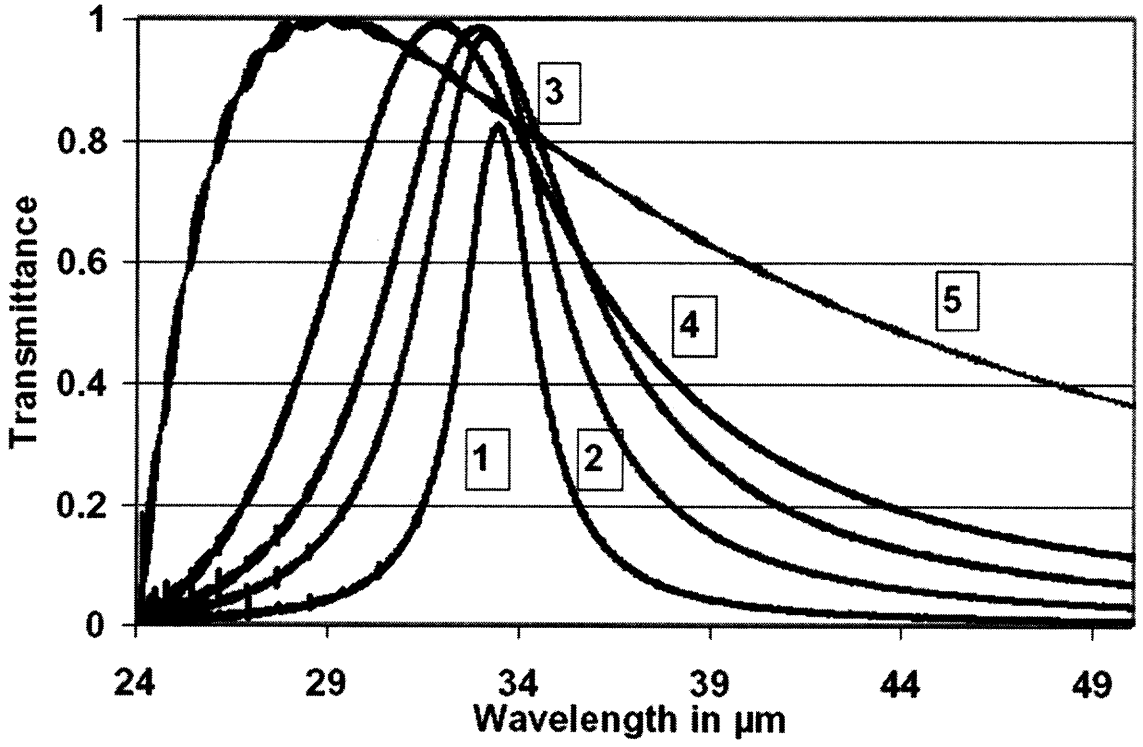

Figure 2.6 Cross shaped meshes, g=24μm. The parameters are for (1) a = 5.6 μm and b = 0.2 μm, (2) a = 5.2 μm and b = 1.0 μm, (3) a = 4.8 μm and b = 1.2 μm, (4) a = 4.4 μm and b = 0.26 μm, and (5) a = 3.2 μm and b = 5 μm.

The change of the intensity depends on changes of WR, while WR depends on the shape parameters a and b, as shown in Figure 2.5. The Micro-stripes program was used to study the dependence of the intensity on WR and in turn on the dependence on cross shape parameters. In Figure 2.7 the intensity is plotted depending on WR for g = 20 and sets of a/g = .075, 0.1, 0.15, 0.2, 0.225 and b/g = 0.05, 0.1, 0.125, 0.15, 0.175.

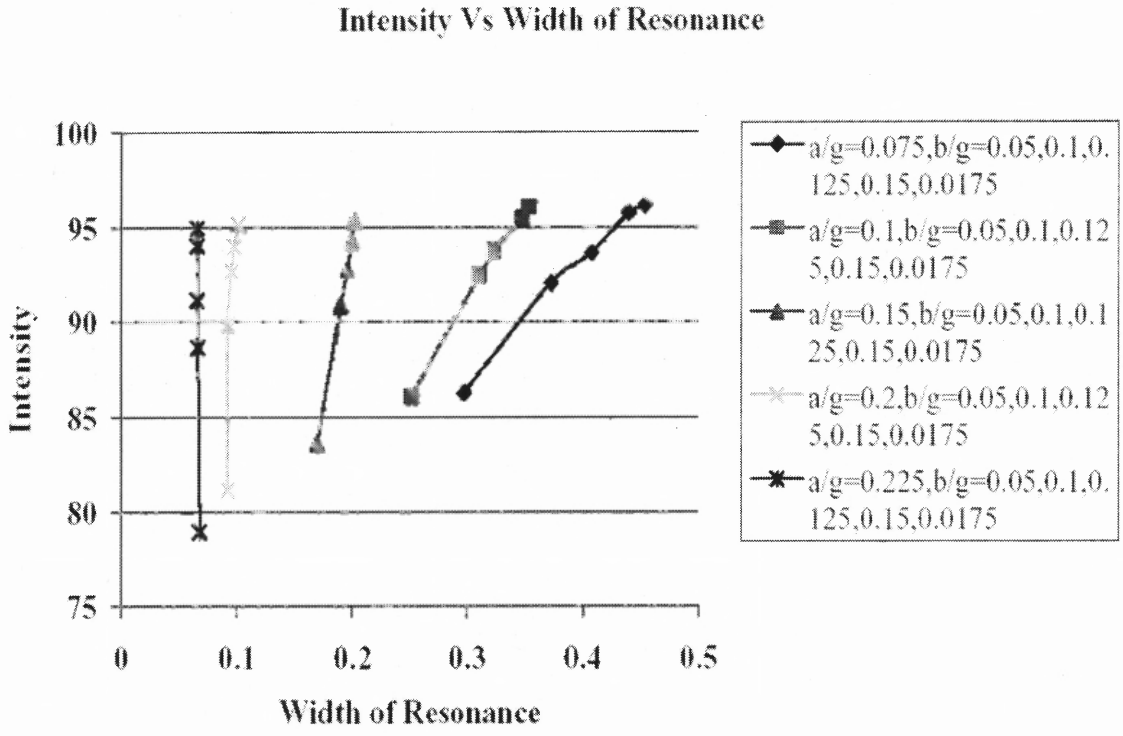

Figure 2.7 Intensity Verses Width of Resonance. Cross Shapes for g = 20 and sets of a/g = .075, 0.1, 0.15, 0.2, 0.225 and b/g = 0.05, 0.1, 0.125, 0.15, 0.175.

The transmittance was calculated for each of these sets of parameters and the intensity obtained. For all calculations of Figure 2.6 and Figure 2.7 the metal thickness was 0.2μm and surface impedance 1.635Ω.

One finds that broader WR corresponds to higher intensity, and vice versa. The optimum intensity will correspond to small separation of the crosses and large cross areas. It has been observed when the opening size are increased so does the intensity. One can believe the reason for such a behavior is corresponding stronger coupling between the surface waves through the cross openings.

2.5 Micro-Stripes & Transmission Line Theory

2.5.1 Micro-Stripes Results as Input Parameters of TLT

In the past all calculations with transmission line theory needed input data obtained from experiments. The Micro-Stripes program, after adjustment to the empirical parameters of experiments, yields results corresponding to a relevant class of related experiments. Since the study of dependence on a wide range of parameters can be done much faster with transmission line theory than with the Micro-Stripes program, parameters and results of the Micro-Stripes program are used as input data for transmission line theory.

There are three important parameters used in transmission line theory of metal meshes. The parameters are the resonance wavelength, width of band and the loss parameter. The transmittance of a mesh with resonance wavelength λ_R of a single mesh, corresponding to the normalized frequency $\omega_0=g/\lambda_R$, is obtained from Micro-Stripes calculations and used as parameter in transmission line theory, see Figure.2.8. The width of resonance band parameter A1 is obtained by adjusting the transmission line transmittance curve to the Micro-Stripes transmittance curve. The loss parameter a1 is taken as 0.001 from Reference [18] and [19]

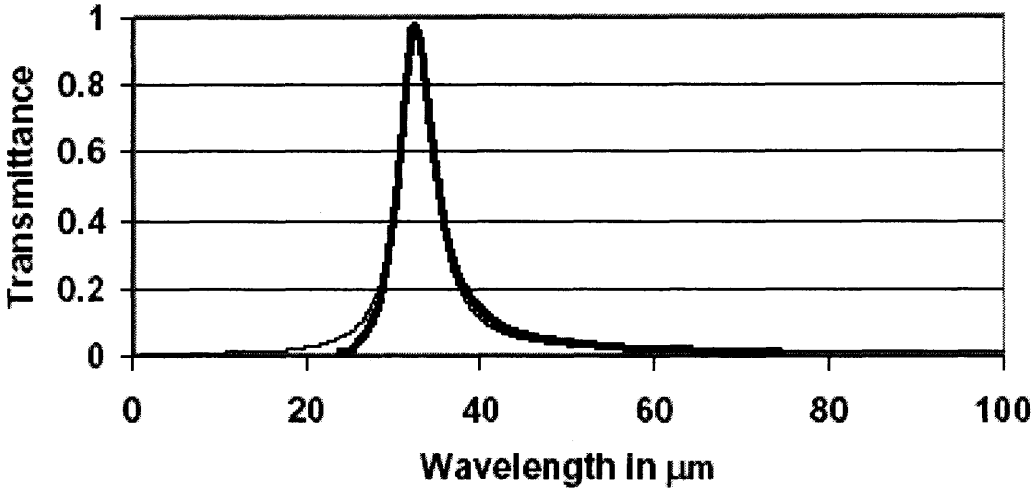

Figure 2.8 Two free standing meshes with parameters g = 24μm, 2a = 9.6μm, 2b =3.6μm and t = 0.2μm. Bold Line: Micro-Stripes program calculation Thin line: Transmission line theory using parameters λ_0 = 32.4μm, A1 = 0.1, a1 = 0.001.

2.5.2 Transmission Line Theory

Transmission line theory uses complex quantities and electrical parameters for the description of the mesh. Ulrich developed transmission line theory for calculation of reflection and transmission of thin metal meshes[1]. A short description is given in Reference [15]. Ulrich's formulation has been corrected by Whitbourn and Compton[19] and is used here. In order for the analysis to be valid, the most important assumption is that the wavelength must be greater than the periodicity constant *g*, to avoid diffraction.

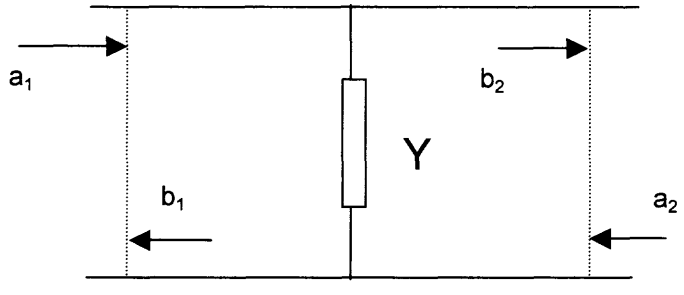

Figure 2.9 Shunt impedance with incident and reflected waves on both sides.

2.5.2.1 Parameters of a Single Mesh. A single mesh is characterized by three parameters, the resonance frequency ω_0, the bandwidth parameter A1, and the metal loss parameter a1. An inductive thin metal mesh is described by a resonance oscillator and a shunt impedance is used, see Figure 2.9.

The shunt impedance for the case of a freestanding thin inductive mesh is taken as

$$Y(\lambda) = 1/[a1 - i(\omega_o A1)/\Omega(\lambda)] \tag{2.4}$$

where $\omega_o = g/\lambda_R$ is the normalized frequency, g is the periodicity constant, λ_R the resonance wavelength of one mesh, A1 the bandwidth parameter and a1 the loss parameter of the metal mesh. The "generalized wavelength" is defined as

$$\Omega(\lambda) = g/\lambda\omega_o - \lambda\omega_o/g. \tag{2.5}$$

2.5.2.2 Cascading Matrices. To calculate the transmittance of the mesh, one can consider the shunt impedance in Figure 2.9, and assume incident and reflected waves $a_1$and b_1, transmitted wave b_2 and backward traveling wave a_2. The waves are related by the matrix M as[20]

$$b_1 = m_{11}\, a_2 + m_{12}\, b_2 \tag{2.6}$$

$$a_1 = m_{21}\, a_2 + m_{22}\, b_2 \tag{2.7}$$

Assuming no backward traveling waves, that is $a_2 = 0$, one has for the ratio of reflected wave b_1 to the incident wave a_1

$$b_1/a_1 = m_{12}/m_{22} \tag{2.8}$$

and for the ratio of transmitted wave b_1 to the incident wave a_1

$$b_2/a_1 = 1/m_{22} \tag{2.9}$$

The matrix M1 describes the impedance at the interface of a plane with refractive index $n_1 = 1$ on both sides

$$m1_{11} = (-Y/2 + 1) \qquad m1_{12} = -Y/2$$

$$m1_{21} = Y/2 \qquad m1_{22} = (Y/2 + 1), \tag{2.10}$$

The matrix M2 describes a transmission line of length d without losses in the medium with refractive index 1

$$m2_{11} = \exp(-i2\pi d)/\lambda \qquad m2_{12} = 0$$

$$m2_{21} = 0 \qquad m2_{22} = \exp(i2\pi d)/\lambda \tag{2.11}$$

2.6 Two meshes, Four meshes

2.6.1 Micro-stripes Calculations and Alignments, Two-Four Meshes, Cross Shaped

The Micro-Stripes program uses a unit cell for the calculation of the transmittance of a periodic array. One may think of a waveguide with square-shaped cross and reflecting walls. There are two different placements of the cross which preserve the symmetry of

the mesh: one with ¼ cross at each corner see Figure 2.10(c) and one with the cross at the center, see Figure 2.10(d). Two meshes will have either the crosses lined up the in normal direction, called symmetric geometry, filter (A), or the crosses are not lined up, called asymmetric geometry, filter (B). In Figure 2.10, the alignments are shown schematically.

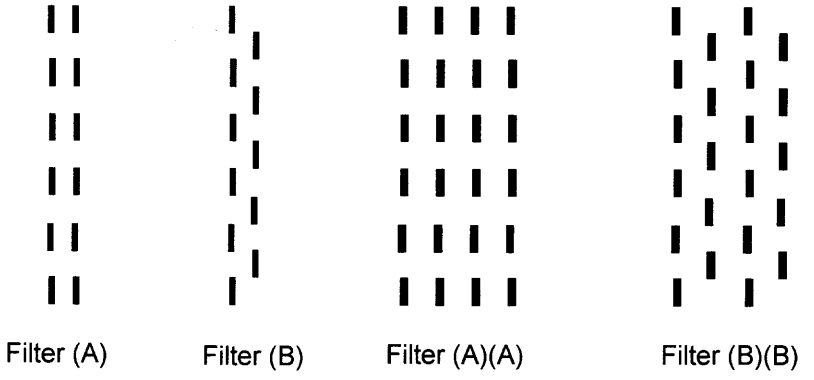

Figure 2.10 Positioning of crosses in two and four mesh filters. Filter (A): crosses of the two meshes are lined-up. Filter (B): crosses in second mesh are shifted with respect to first. Filter (A)(A): crosses of all meshes are lined-up. Filter (B)(B): the crosses of second and fourth mesh are shifted.

2.6.2 Two Meshes, Matrix Representation

Experimentally assembled two-mesh filters have usually no-aligned crosses. While Micro-Stripes calculations are used for the configurations of filter (A) and (B), transmission line theory calculates the transmittance corresponding to experimentally assembled two or four meshes, *ignoring any alignment of the crosses.*

A combination of several matrices of the type M1 and M2 will now be used for the calculation of the transmittance of multi-layer metal meshes at a given spacing. The matrix M1 describes the impedance at the interface of a plane with refractive index $n_1 = 1$ on both sides. And matrix M2 describes a transmission line of length d without losses in

the medium with refractive index n_1 = 1. The two metal meshes with a spacer of thickness d will be described by the matrix product Mf =M1M2M1 (See Appendix B)

2.6.3 Two Meshes at Separation of d = 4, 8, 12 and 16μm

In this section TLT will serve as a guide for the splitting of the resonance modes and the wavelength position of resonance and Fabry-Perot modes. The interpretation of the transmittance of two meshes at distance d is done using the mode model, see Figure 2.3. One considers only the fundamental mode composed of pairs of surface waves of resonance wavelength λ_R and tightly bound by the openings. It is advantageous to calculate with transmission line theory the wavelength peak of transmittance for all separations from d=0 to d=45μm, shown in Figure 2.11.

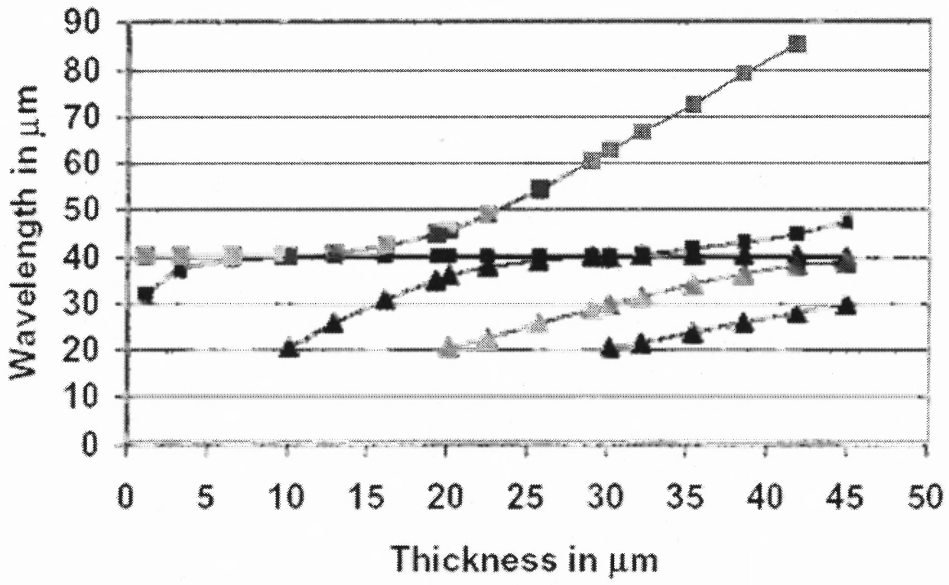

Figure 2.11 Transmission line calculations for two meshes at separation d and mesh parameters g = 24μm, 2a = 9.6μm, 2b =3.6μm and t = 0.2μm. Peak resonance wavelength (squares) and Fabry-Perot peaks (triangles).

There are two resonance peaks, appearing with different wavelength for small values of *d* and merge into one peak for separation at around 10μm. At that distance, the interaction has decreased, the two resonance wavelengths have the same value, and a series of new peaks appear. I shall define them as Fabry-Perot modes, generated between the two meshes and transferring energy through the mesh. These calculations serve as guide for the interpretation of the Micro-Stripes calculation of filter (A) and (B).

Micro-Stripes and Transmission line theory were applied to the calculation of the transmittance of two mesh filters for spacings of 4, 8, 12, and 16μm, shown in Figures. 2.12-2.15. The transmittances are shown for filter (A) and (B) and of the experimental type represented by transmission line theory (TLT).

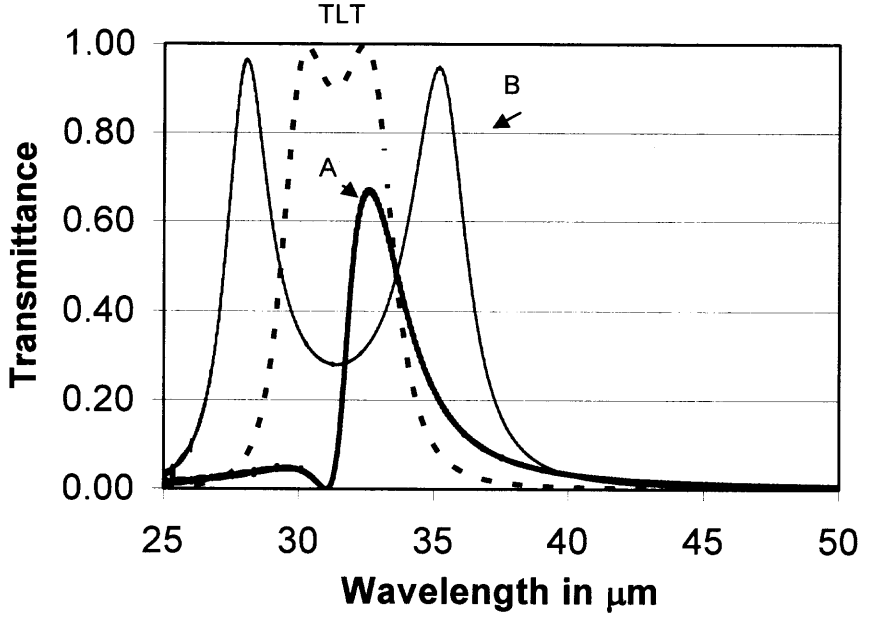

Figure 2.12 Calculated transmittance of two free standing meshes with parameters g = 24μm, 2a = 9.6μm, 2b =3.6μm and t = 0.2μm at distance of 4μm. Bold line: Micro-Stripes program calculation of filter (A). Solid line: Micro-Stripes program calculation of filter (B). Broken line: Transmission line theory using parameters λ_o = 32.4μm, A1 = 0.1, a1 = 0.001.

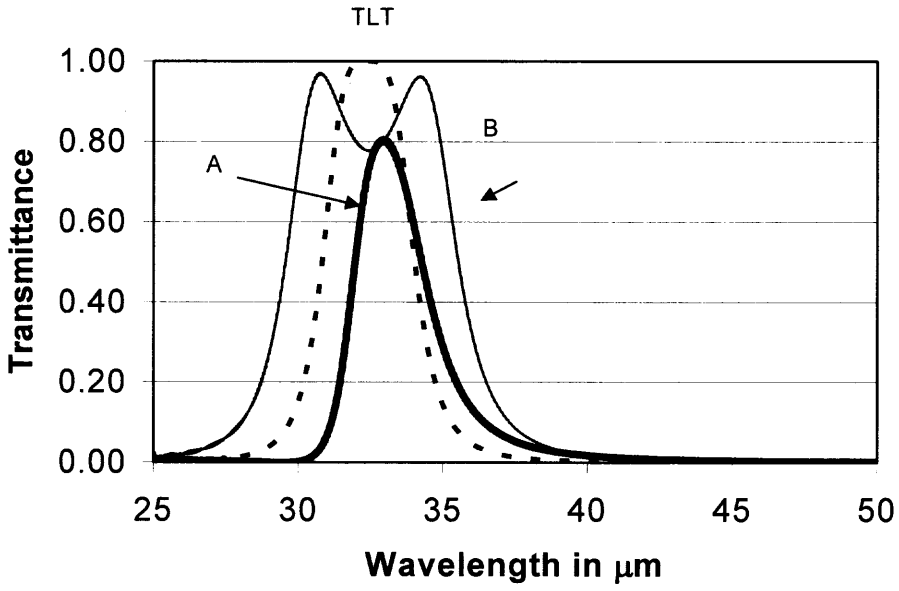

Figure 2.13 Calculated transmittance of two free standing meshes with parameters g = 24μm, 2a = 9.6μm, 2b =3.6μm and t = 0.2μm at distance of 8μm. Bold line: Micro-Stripes program calculation of filter (A). Solid line: Micro-Stripes program calculation of filter (B). Broken line: Transmission line theory using parameters λ_o = 32.4μm, A1 = 0.1, a1 = 0.001.

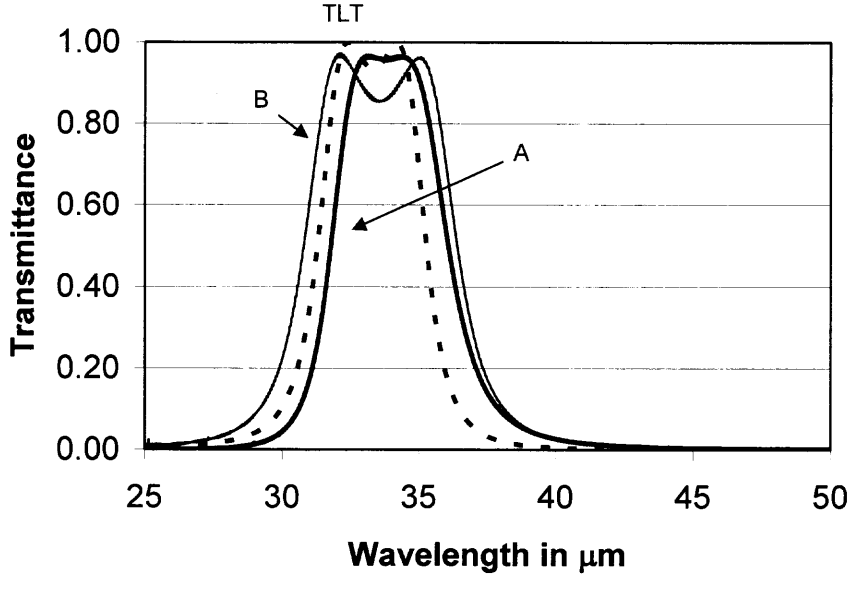

Figure 2.14 Calculated transmittance of two free standing meshes with parameters g = 24μm, 2a = 9.6μm, 2b =3.6μm and t = 0.2μm at distance of 12μm. Bold line: Micro-Stripes program calculation of filter (A). Solid line: Micro-Stripes program calculation of filter (B). Broken line: Transmission line theory using parameters λ_o = 32.4μm, A1 = 0.1, a1 = 0.001.

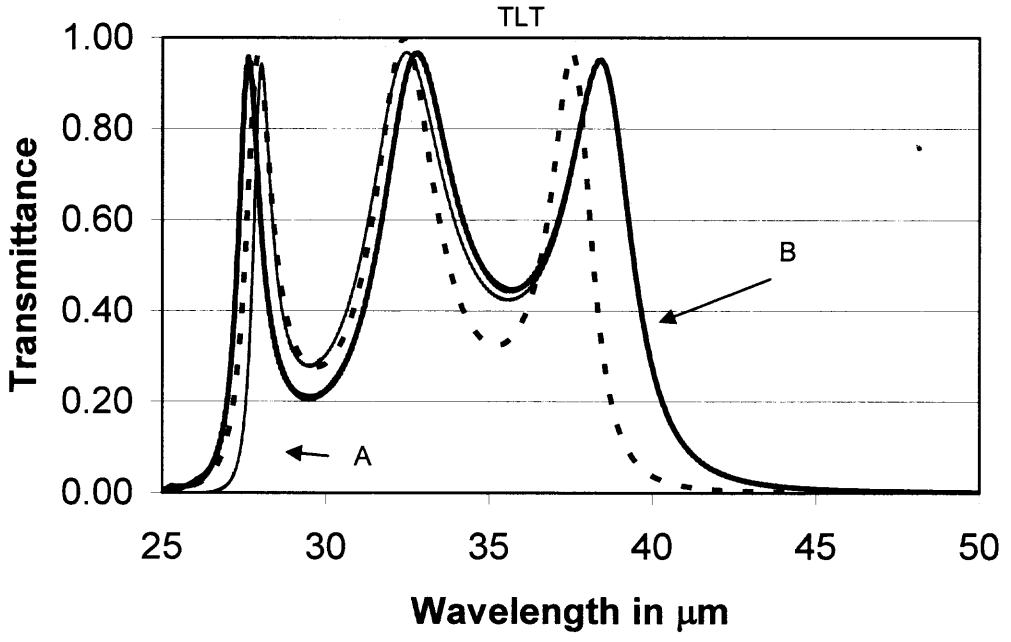

Figure 2.15 Calculated transmittance of two free standing meshes with parameters g = 24μm, 2a = 9.6μm, 2b =3.6μm and t = 0.2μm at distance of 16μm. Bold line: Micro-Stripes program calculation of filter (A). Solid line: Micro-Stripes program calculation of filter (B). Broken line: Transmission line theory using parameters λ_o = 32.4μm, A1 = 0.1, a1 = 0.001.

The Transmittances shown in Figures 2.12-2.15 are interpreted as follows:

(i) The modes of filter (TLT, broken line) that is for the case of non-aligned crosses, show interaction for all distances except for a distance of 8μm, that is, at $\lambda_R/4$ where oscillators have minimum interaction.

(ii) The modes of filter (A), that is, for symmetrically aligned crosses, show minimum interaction for small separation, because of symmetric geometry, and the interaction increases with increasing distance.

(iii) The modes of filter (B), that is for asymmetrically aligned crosses, show interaction for all distances, because of asymmetric geometry.

If one looks at two meshes, at the distance of 16μm, one can observe three peaks, two are from the resonance wavelength of the meshes and the short wavelength peak is of the Fabry-Perot mode, see Figure 2.11.

The near-field effect is seen when one compares the transmittance at spacing of 4 and 16μm, see Figures 2.12 and 2.15. At 4μm, filter (A) shows no interaction of the resonance wavelengths; filter (TLT), small interaction; and filter (B), large interaction. In comparison, at 16μm all three filters show the same degree of large interaction. For small spacing the geometry of the alignment of the crosses is attributed to the differences whereas for large spacing the effect of the alignment of the crosses disappears.

A filter should have one peak wavelength, as observed for filter(A) and (TLT) at spacer distance of $\lambda_R/4$ see Figure 2.13, where oscillators have minimum interaction. At that spacing, filter (TLT) shows a bandwidth of ~ 10% with 100% transmittance, whereas the bandwidth of filter (A) is 8% but with less than 100% transmittance. At a larger distance of 12μm one has only a small increase of interaction for both filters. If the filters with a dip are acceptable, one may select the desired filter bandwidth and shape for filters (TLT) and (A) by finding the corresponding spacing between at $\lambda_R/4$ and at $\lambda_R/2$, and one may consider filter (B), which shows two peaks for all distances and is in general less suitable as a filter.

2.7 Four Meshes

2.7.1 Transmission Line Matrix

Four metal meshes separated by three spacers with refractive index n = 1 are described by the matrix product Mff = M1M2M1M2M1M2M1, The matrix M1 describes the impedance at the interface of a plane with refractive index n_1 = 1 on both sides and matrix M2 describes a transmission line of length d without losses in the medium with refractive index 1, see also Appendix B.

2.7.2 Four Meshes at Separation of d = 4, 8, 12 and 16μm

Micro-Stripes and Transmission line theory were applied to the calculation of the transmittance of four mesh filters for spacings of 4, 8, 12, and 16μm, shown in Figures 2.16 to 2.19.

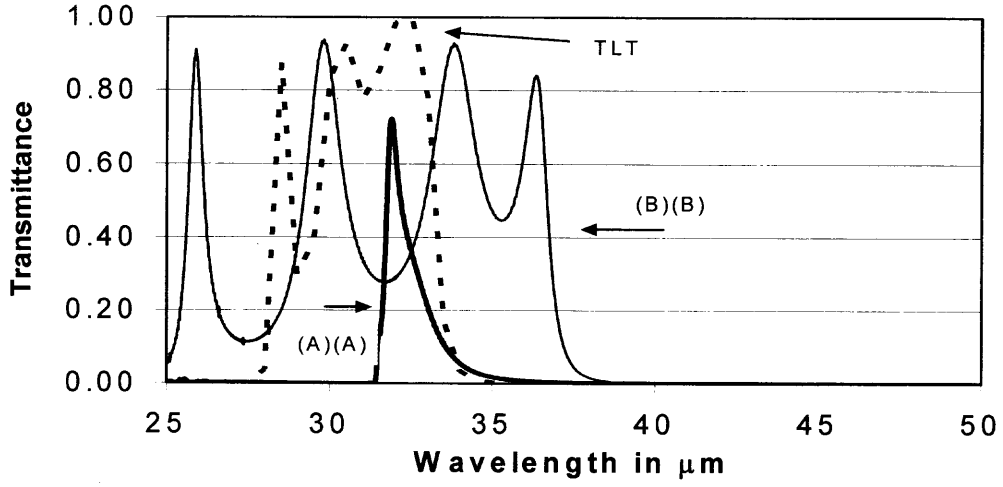

Figure 2.16 Calculated transmittance of four free standing meshes with parameters g = 24μm, 2a = 9.6μm, 2b =3.6μm and t = 0.2μm at distance of 4μm between each two. Bold line: Micro-Stripes program calculation of filter (A)(A). Solid line: Micro-Stripes program calculation of filter (B)(B). Broken line: Transmission line theory using parameters λ_o = 32.4μm, A1 = 0.1, a1 = 0.001.

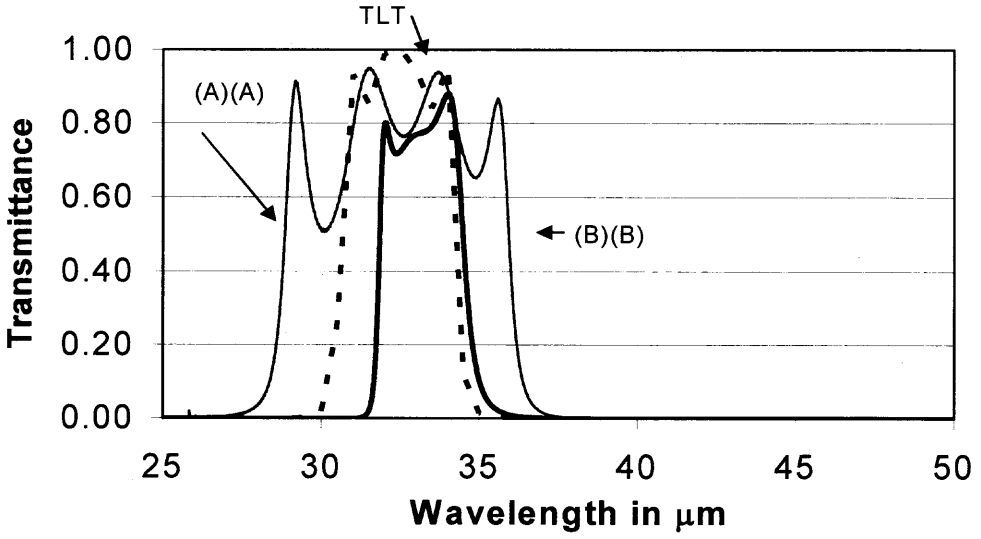

Figure 2.17 Calculated transmittance of four free standing meshes with parameters g = 24μm, 2a = 9.6μm, 2b =3.6μm and t = 0.2μm at distance of 8μm between each two. Bold line: Micro-Stripes program calculation of filter (A)(A). Solid line: Micro-Stripes program calculation of filter (B)(B). Broken line: Transmission line theory using parameters λ_o = 32.4μm, A1 = 0.1, a1 = 0.001.

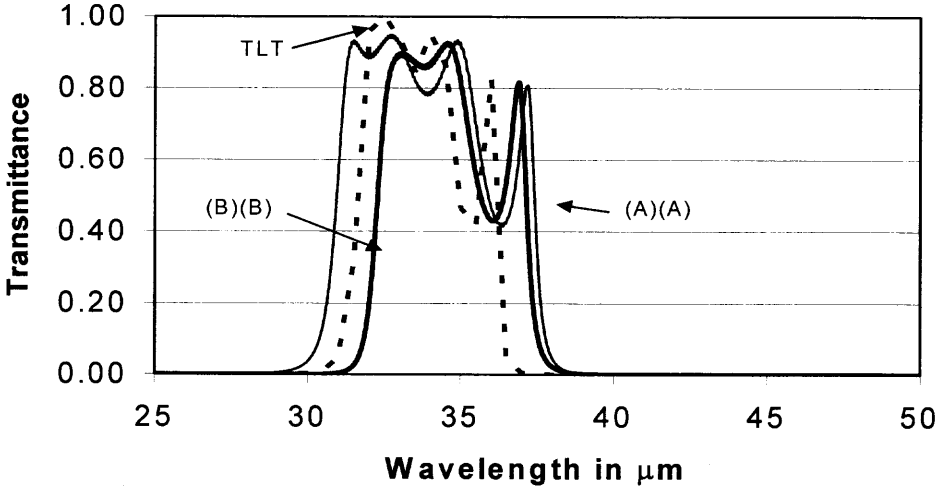

Figure 2.18 Calculated transmittance of four free standing meshes with parameters g = 24μm, 2a = 9.6μm, 2b =3.6μm and t = 0.2μm at distance of 12μm between each two. Bold line: Micro-Stripes program calculation of filter (A)(A). Solid line: Micro-Stripes program calculation of filter (B)(B). Broken line: Transmission line theory using parameters λ_o = 32.4μm, A1 = 0.1, a1 = 0.001.

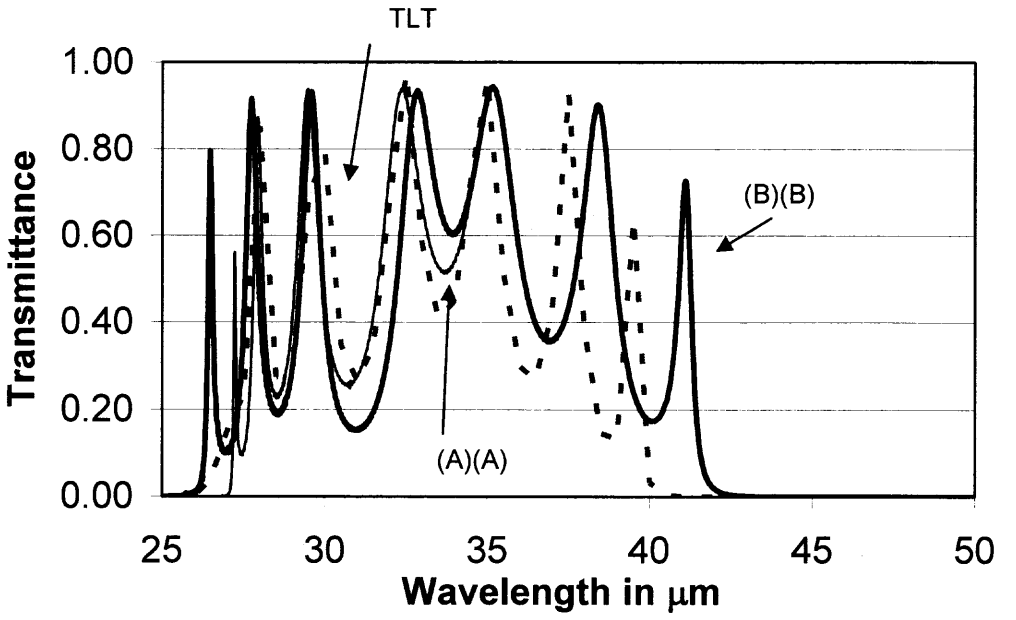

Figure 2.19 Calculated transmittance of four free standing meshes with parameters g = 24μm, 2a = 9.6μm, 2b =3.6μm and t = 0.2μm at distance of 16μm between each two. Bold line: Micro-Stripes program calculation of filter (A)(A). Solid line: Micro-Stripes program calculation of filter (B)(B). Broken line: Transmission line theory using parameters λ_o = 32.4μm, A1 = 0.1, a1 = 0.001.

The transmittances are shown for a symmetric filter (A)(A) and asymmetric filter (B)(B) and of the experimental type represented by transmission line theory (TLT).

The transmittances shown in Figures. 2.16-19 are interpreted as follows:

(i) The modes of filter (TLT) that is, for nonaligned crosses, show interaction for all distances except for a distance of 8μm, that is, at $\lambda_R/4$ where oscillators have minimum interaction.

(ii) The modes of filter (A)(A), that is, for symmetrically aligned crosses, show minimum interaction for a distance 4μm. The interaction increases for 8μm and shows a box-shaped contour. For larger distances the interaction increases.

(iii) The Modes of filter (B)(B), that is, for asymmetrically aligned crosses, show interaction for all distances, because of asymmetric geometry.

Four mesh filters have a maximum of four resonance peaks. For special purposes, one may consider filter (A)(A) at 4μm as a very narrow band pass filter and at 8μm as a band pass filter approaching a box shape contour, even if there are dips and less than 100% transmittance. Filter (B)(B) shows four peaks and filter (TLT) three peaks for distances of 4 μm to 12 μm and all resonance and Fabry-Perot peaks for 16 μm, making these four mesh filters less suitable as filters.

2.8 Summary, Free Standing Cross Shaped Meshes

The Micro-Stripes program has reproduced, with high accuracy, the experimental resonance wavelength of a single mesh using the geometry parameters of the shape of the opening and the periodicity constant. The material constant of the metal surface impedance was determined by adjustment of the reproduce intensities to the experimental one.

The resonance wavelength and WR were determined for a range of geometrical parameters and very well presented by analytical formulas. The model of a linear chain of vibrating dipoles serves well for the description of the resonance wavelength. The mode model is used for the interpretation of the calculations of Micro-Stripes program and transmission line theory on sequences of two and four meshes. The transmittance of two mesh filters may be describes by the interaction of two resonance modes and one Fabry-Perot mode, whereas for four meshes, by four resonance modes and three Fabry-Perot modes. The resonance modes of the three differently aligned meshes couple differently

for different separation of the meshes and show for large distance minimum coupling. For small distances, a near-field effect is apparent. At a spacing of $\lambda_R/4$, filters of (TLT) and (A) show for two meshes filters just one peak, indicating minimum interaction of the modes as expected from oscillator theory. For four layer meshes a more square like shape of the transmittance was obtained.

CHAPTER 3

METAL MESH ON DIELECTRIC SUBSTRATE/EMBEDDED

3.1 Metal Mesh on Thick Dielectric Substrate

3.1.1 Transmission Line Theory

Transmission line theory (TLT) has been used by Ulrich[1] to develop the oscillator model, to calculate the transmittance of metal meshes, and to model multiple mesh filters. Whitbourn and Compton[19] have corrected the theory and expanded the model to include metal meshes on dielectrics or embedded in it. A shift of the resonance wavelength factor $((n_1^2+ n_2^2)/2)^{1/2}$ was predicted for metal meshes on the interface of two infinitely long dielectrics of refractive index n_1 and n_2. For the case of a metal mesh on a thick Silicon substrate n = 3.4 the shift factor of the resonance wavelength was calculated to be 2.5. TLT does not include a dependence of the resonance wavelength of the mesh, on the thickness of a dielectric layer. TLT is limited to wavelengths larger than the periodicity constant.

3.1.1.1 Thin Metal Mesh on Dielectric. Only thin metal meshes are considered and the shunt impedance Y of a freestanding thin inductive mesh is taken as

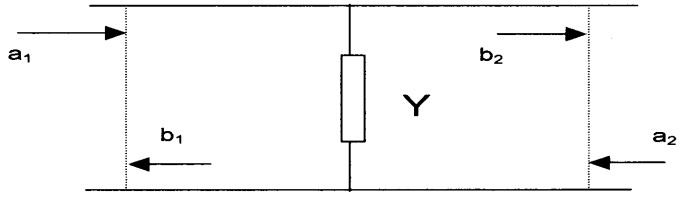

Figure 3.1 Shunt impedance with incident and reflected waves on both sides.

$$Y(\lambda) = 1/[a1 - i(\omega\ A1)/\Omega(\lambda) \quad (3.1)$$

where $$\omega = \omega_o[2/(n_1^2 + n_2^2)]^{1/2} \quad (3.2)$$

and normalized frequency $$\omega_o = g/\lambda_R \quad (3.3)$$

and $$\Omega(\lambda) = g/\lambda\omega - \lambda\omega/g \quad (3.4)$$

The refractive indices of the media on each side of the mesh are described by n_1 and n_2, g is the periodicity constant, ω_o is the resonance frequency of a single mesh, A1 is the bandwidth parameter and a1 is the loss parameter.

3.1.1.2 Cascading Matrices. A single mesh is described by the shut impedance Y. The waves on the left side of the impedance Y are related to the waves on the right side by a matrix M as

$$b_1 = m_{11}\ a_2 + m_{12}\ b_2$$
$$a_1 = m_{21}\ a_2 + m_{22}\ b_2 \quad (3.5)$$

For $a_2 = 0$ one has for the ratio of reflected wave b_1 to the incident wave a_1

$$b_1/a_1 = m_{12}/m_{22} \quad (3.6)$$

and for the transmitted wave

$$b_2/a_1 = 1/m_{22}. \quad (3.7)$$

The cascading matrix M1 describes the impedance at the interface of a metal mesh with dielectric of refractive index n_1 on the left and n_2 on the right and is given as

$$m1_{11} = (-Y + (n_1 + n_2))/2n_1 \qquad m1_{12} = (-Y + (n_1 - n_2))/2n_1$$

$$m1_{21} = (Y + (n_1 - n_2))/2n_1 \qquad m1_{22} = (Y + (n_1 + n_2))/2n_1, \tag{3.8}$$

The cascading matrix M2 describes the impedance at the interface of a dielectric with refractive index n_1 on the left and n_2 on the right and is given as

$$m2_{11} = (n_1 + n_2)/2n_1 \qquad m2_{12} = (n_1 - n_2)/2n_1$$

$$m2_{21} = (n_1 - n_2))/2n_1 \qquad m2_{22} = (n_1 + n_2)/2n_1 \tag{3.9}$$

The Matrix M3 describes a transmission line without losses of length d in the medium with refractive index n.

$$m3_{11} = \exp(-i2\pi dn)/\lambda \qquad m3_{12} = 0$$

$$m3_{21} = 0 \qquad m3_{22} = \exp(i2\pi dn)/\lambda \tag{3.10}$$

The combination of several matrices of type M1, M2 and M3 were used for the calculation of the transmittance of various combinations of metal meshes and dielectric layers. Two metal meshes with a dielectric spacer will be described by a matrix product Mb = M1M3M1', where M1 represents the metal mesh on the interface of the outside

medium with n_1 and the spacer with index n_2, M3 the spacer of thickness d and refractive index n_2, and M1' the mesh on the interface of the spacer and the outside medium.

3.2 Comparison with Experiments,

Micro-Stripes and Transmission Line Theory Calculations

3.2.1 Resonance Wavelength

Cross shaped metal meshes on Silicon substrate have been manufactured in the far-IR by Sternberg *et al.*[17], Möller *et al.*[8], and Hicks *et al*[21]. Metal meshes of aluminum with thickness t = 0.2μm, periodicity g = 20μm, separation $2a$ = 8μm, and arm width $2b$=6μm, have been produced and compared with the Micro-Stripes calculations[17]. The meshes were deposited on a silicon wafer with a thickness of 550μm, with resistivity of 15ohm-cm. The experimental transmittance showed a peak wavelength at 71.3μm compared to 70.2μm as result of the Micro-Stripes calculations, see Figure 3.2.

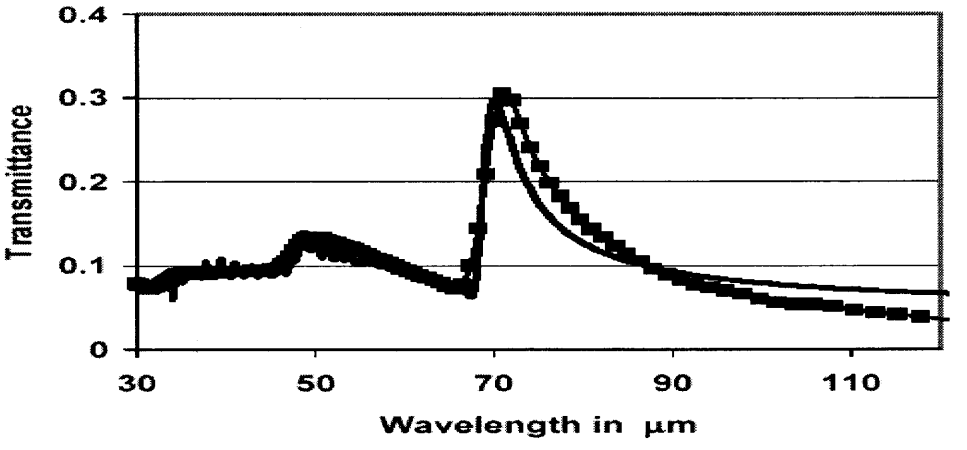

Figure 3.2 Inductive cross shaped metal mesh of thickness 0.2μm on a Silicon substrate of thickness of 550μm depending on the wavelength. The mesh has geometrical parameters g = 20, 2a = 8, 2b = 6μm. (a) Bold Line- Measured (Experimental) resonance wavelength at 71.3μm (b) Squares- Micro-Stripes Simulation wavelength at 70.2μm.

There is good agreement of the overall intensity, confirming the validity of the used surface impedance values for the metal and the conductivity value for the dielectric. A comparison was made between the experimental resonance wavelengths values, of Micro-Stripes and TLT, see Table 3.1.

Table 3.1 Values of Resonance Wavelengths, Thin Metal Thick Dielectric. (Thin Metal Meshes on Top of Silicon Substrate. First Column Displays the Cross Parameters, Second Column Displays Experimental Results, Third Column 3 Displays Micro-Stripes Results. Fourth Column Displays TLT*Whitbourn Factor. (The Free Standing Value Was Obtained Using Micro-Stripes).

	Experimental $\lambda_R(\mu m)$	Micro-Stripes $\lambda_R(\mu m)$	TLT*W Factor
Cross[8] g = 26.4 2a = 3.2 2b = 4.8 a/g = 0.06 b/g = 0.09	124.9	115.2	129.75
Cross[8] g = 16.4 2a = 2.5 2b = 4.8 a/g = 0.0762 b/g = 0.0146	61	67.2	58.75
Cross[8] g = 20 2a = 2.4 2b = 3.6 a/g = 0.06 b/g = 0.09	83.6	90.8	81.75
Cross[17] g = 20 2a = 8 2b = 6 a/g = 0.2 b/g = 0.15	71.3	70.2	58.87

3.3 Micro-Stripes Calculations of Dependence on Cross Parameters on Thick Silicon Substrate or Embedded in it

3.3.1 Resonance Formula

The resonance wavelength shifts to a longer wavelength when the mesh is deposited on a dielectric substrate or embedded in it. The shift of λ_R to a longer wavelength is smaller than the refractive index n when on a substrate and equal to the refractive index n when a metal mesh is embedded in a thick dielectric layer. The shift has been observed experimentally[8,17] by comparing the resonance wavelength of the mesh on a silicon substrate to a free standing mesh. The Micro-Stripes program was applied to the calculations of the resonance wavelength λ_R and width of resonance WR for meshes with g = 20μm and $2a$ = 3, 4, 6, 8, 9μm and $2b$ = 2, 4, 5, 6, 7μm on a silicon wafer of thickness of 550μm with resistivity of 15Ω. The Micro-Stripes data[17] of the resonance wavelength are presented by a nonlinear best-fit formula with a standard deviation of 0.323. Assuming that realistic input data would have only two significant decimal places, one has Equation (3.11b).

$$\lambda_R = 1.1475\, a^2 - 0.1146\, b^2 + 1.7115\, a\, b - 15.9656\, a - 8.3165\, b + 6.0544\, g \qquad (3.11a)$$

$$\lambda_R = 1.15\, a^2 - 0.11\, b^2 + 1.71\, a\, b - 15.966\, a - 8.32 b + 6.05\, g \qquad (3.11b)$$

In Figure 3.3, the resonance wavelength λ_R is plotted depending on *a/g* and taking *b/g* as parameter.

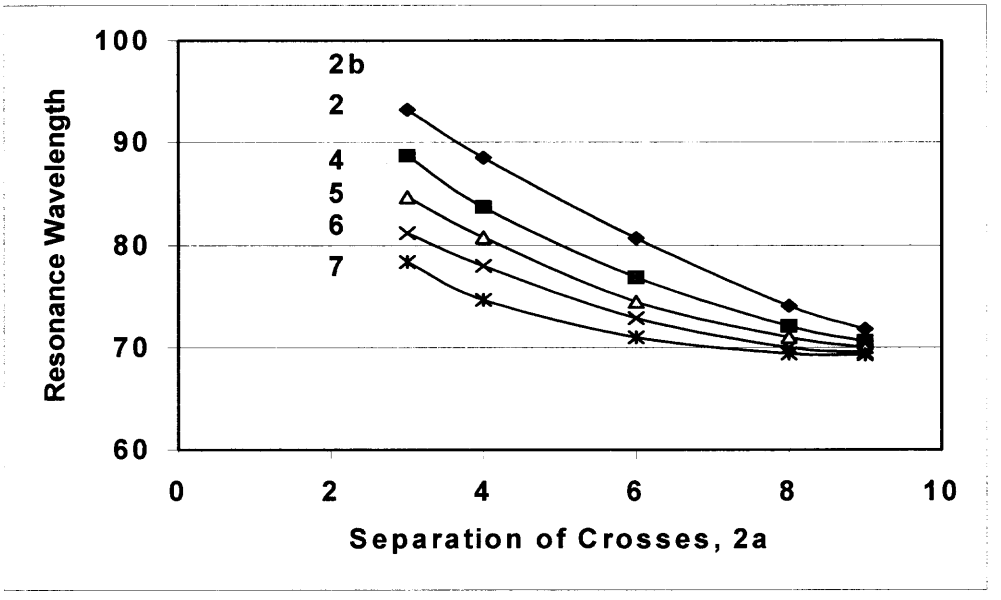

Figure 3.3 Micro-Stripes calculations of the resonance wavelength of an inductive cross shaped metal mesh of thickness 0.2μm and surface impedance of Z = 1.635Ω. The mesh was assumed to be on a silicon substrate of thickness of 550μm and surface resistance of 15 ohm-cm. The dependence on the separation of the crosses and the width of the cross arms is shown for the range of a/g = 0.075, 0.1, 0.15, 0.2, 0.225 and b/g = 0.05, 0.1, 0.125, 0.15 and 0.175.

3.3.2 Width of Resonance

The width of resonance (WR) for a thin cross shaped metal mesh on top of a thick silicon substrate was studied with the Micro-Stripes program. The WR was defined as width at half height ($\Delta\lambda/\lambda$) and in Figure 3.4, the dependence of WR on *a/g* and *b/g* is shown for *g* = 20μm. A calculation of a best-fit formula was performed giving standard deviation of 0.075.

$$\Delta\lambda/\lambda = -4.34(a/g)^2 - 10.21(b/g)^2 - 17.98\,(a/g)(b/g) + 1.09\,(a/g) + 5.31\,(b/g) \qquad (3.12)$$

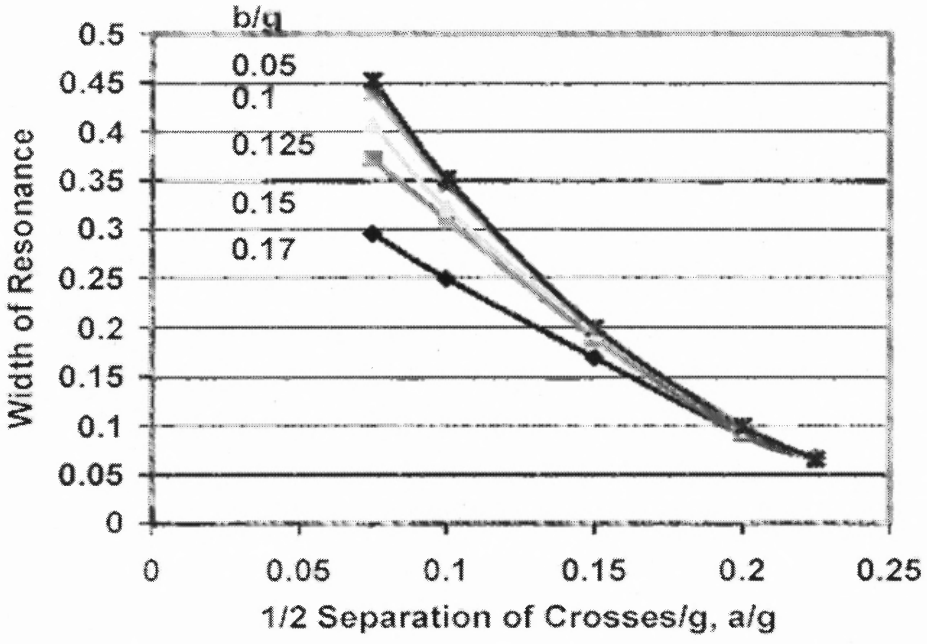

Figure 3.4 Micro-Stripes calculations of the width of resonance. Inductive cross shaped metal mesh of thickness 0.2μm and surface impedance of Z = 1.635ohm-cm. The mesh was assumed to be on a Silicon substrate of thickness of 550μm and surface resistance of 15 ohm-cm. The dependence on the separation of the crosses and the width of the cross arms is shown for the range of a/g = 0.075, 0.1, 0.15, 0.2, 0.225 and b/g = 0.05, 0.1, 0.125, 0.15 and 0.175.

The experimentally observed width of resonance ($\Delta\lambda/\lambda$), of cross shaped meshes with different geometries is compiled in Table 3.2. The experiments agree well with the Micro-Stripes calculations and the results of Equation 3.12.

Table 3.2 Values of Width of Resonance $\Delta\lambda/\lambda$, Thin Metal Thick Dielectric (Thin Metal Meshes on Top of Silicon Substrate. First Column Displays the Cross parameters, Second Column Two Displays Experimental Results, Third Column Displays Micro-Stripes Results).

	Experimental ($\Delta\lambda/\lambda$)	Micro-Stripes
Cross g = 26.4 2a = 3.2 2b = 4.8 a/g = 0.06 b/g = 0.09	0.3472	0.3683
Cross g = 16.4 2a = 2.5 2b = 4.8 a/g = 0.0762 b/g = 0.0146	0.39	0.41667
Cross g = 20 2a = 2.4 2b = 3.6 a/g = 0.06 b/g = 0.09	0.3253	0.37
Cross g = 20 2a = 8 2b = 6 a/g = 0.2 b/g = 0.15	0.101	0.097
Cross g = 12.5 2a = 1.5 2b = 2.25 a/g = 0.06 b/g = 0.09	0.3406	0.344

3.3.3 Shift of Resonance Wavelength on Silicon

The resonance wavelength of a free standing cross-shaped mesh shifts on the average by a factor of 2.78 compared to the mesh deposited on silicon substrate. The dependence of this factor on *a/g* and *b/g* is shown in Figure 3.5. The ratio of the calculated resonance wavelengths was plotted of the cross shaped meshes on silicon substrate divided by the resonance wavelength of the free standing mesh(See Ch-2), and is shown in Figure 3.5.

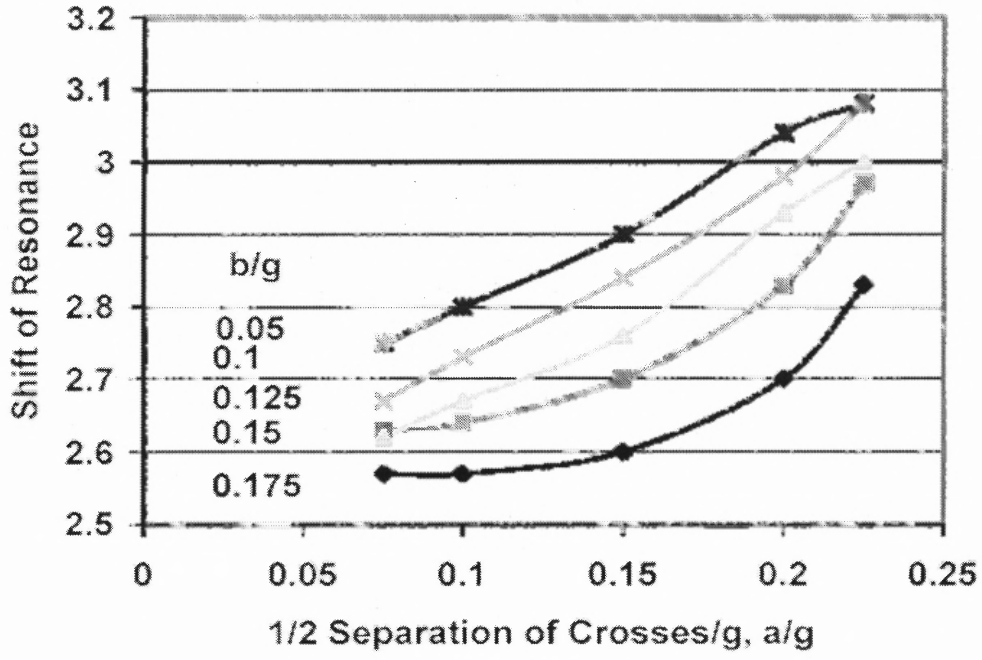

Figure 3.5 Shift of the resonance wavelength of the free standing mesh when deposited on the Silicon substrate. The resonance wavelength, calculated for the mesh on the Silicon substrate, is divided by the resonance wavelength calculated for the freestanding cross-shaped mesh. The dependence on the separation of the crosses and the width of the cross arms is shown for the range of a/g = 0.075, 0.1, 0.15, 0.2, 0.225 and b/g = 0.05, 0.1, 0.125, 0.15 and 0.175.

An empirical best-fit formula[17] was obtained for the presentation of the calculated data.

$$2.26(a/g) + 2.05(b/g) + 0.9 * [(n_1^2 + n_2^2)/2]^{1/2} \qquad (3.13)$$

Whitbourn and Compton[19] have used transmission line theory to study the shift of the wavelength of a metal mesh on a thick dielectric substrate and arrived at a shift factor of $[(n_1^2 + n_2^2)/2]^{1/2}$, where n_1 is the refractive index of the dielectric on the front side of the mesh and n_2 on the back side. For $n_1 = 1$ and $n_2 = 3.4$ the value of $[(n_1^2 + n_2^2)/2]^{1/2}$ is 2.5. Sternberg[17] *et al* arranged the best-fit formula of Equation 3.13 in such a way that the

terms depending on *a/g* and *b/g* appear as correction terms with respect to the result of References 8 and 17.

An interpretation may be given in terms of the mode model, see Figure 3.6. A mode corresponding to the resonance wavelength is composed of surface waves on both sides of the mesh. When one surface wave oscillates in a dielectric its wavelength shifts to longer wavelength. This shift depends not only on the refractive index of the dielectric but also on the thickness of the layer. The resonance wavelength of the mesh shifts for small thicknesses of the dielectric, there is only one peak, and in most cases there remains one peak for larger thicknesses.

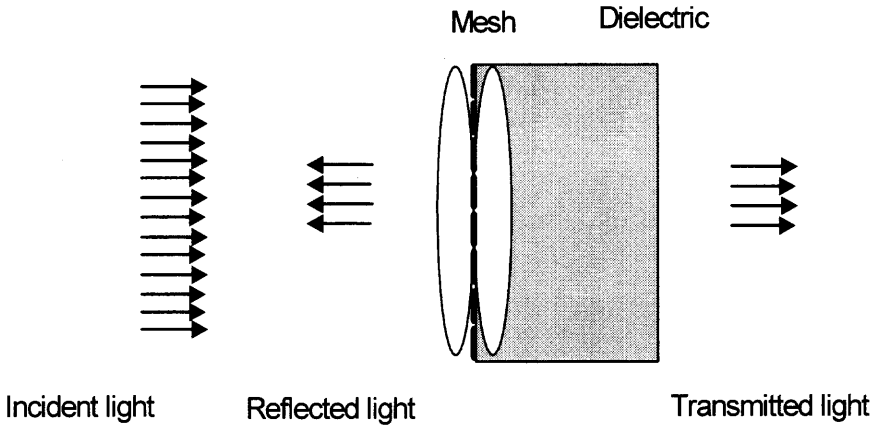

Figure 3.6 The incident light induces a mode of the mesh, consisting of two pairs of surface waves on each side of the mesh. One surface wave oscillates in a dielectric, and the other in air. The modes are not strongly coupled as in the case of the free standing mesh and so the degeneracy is lifted; the resonance wavelength is shifted.

The coupling of the two surface waves depends not only on the geometry of the crosses but also on the thickness of dielectric layer. For fixed thickness of the dielectric layer, the shift factor gets larger with larger a/g values, that is with larger separation of the crosses. The shift factor gets smaller with larger b/g values, that is larger values of the width of the cross arms.

3.4 Single Metal Mesh on Dielectrics and Its Dependence on Thickness of Substrate

The Micro-Stripes program has been used to calculate the resonance wavelength of a single mesh depending on the thickness of a dielectric substrate or embedded in a dielectric for refractive indices 1.5 and 3.4. The parameters of the mesh are g = 20μm, 2a = 1.5μm, 2b = 3μm, and t = 0.2μm, and the thickness of the dielectric was varied from 0.2 to 20 μm, see Figures 3.7 and 3.8. In general, when a thin metal mesh is combined with a dielectric substrate, whether it is embedded in it or mounted on one side of the mesh, the resonance wavelength will shift to a longer wavelength. The shift depends strongly on the configuration and the thickness of the substrate as well as the index of refraction of the material.

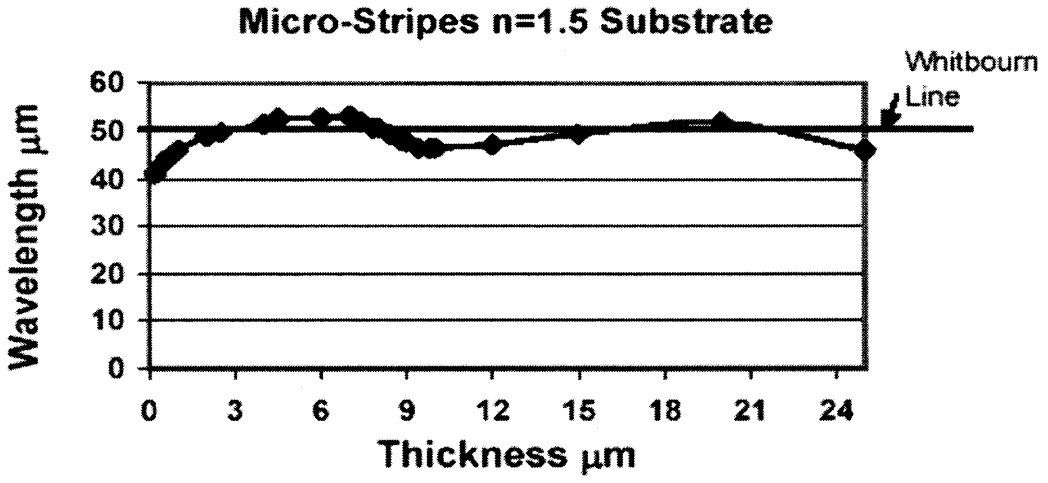

Figure 3.7a Micro-Stripes calculation of a cross shaped mesh. Geometrical parameters: g = 20µm, 2a = 1.5µm, 2b = 3.6µ, t = 0.2µm. Substrate n=1.5, data series varies from 0.2µm to 25µm. Asymmetric configuration (Metal-Dielectric).

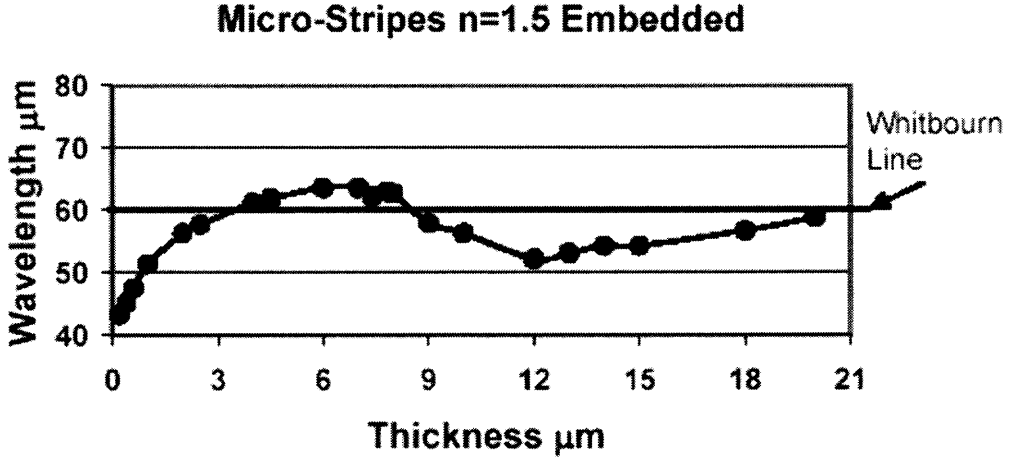

Figure 3.7b Micro-Stripes calculation of a cross shaped mesh. Geometrical parameters: g = 20µm, 2a = 1.5µm, 2b = 3.6µm, t = 0.2µm. . Embedded n=1.5, data series varies from 0.2µm to 25µm. Symmetric configuration (Dielectric-Metal-Dielectric).

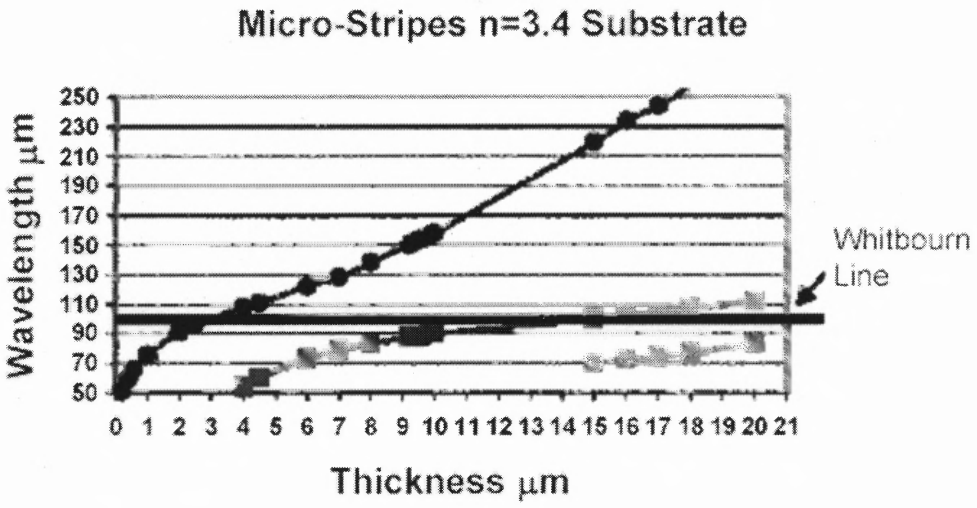

Figure 3.7c Micro-Stripes calculation of a cross shaped mesh. Geometrical parameters: g = 20μm, 2a = 1.5μm, 2b = 3.6μm, t = 0.2μm. Substrate n=3.4, data series varies from 0.2μm to 20μm. Asymmetric configuration (Metal-Dielectric), circles-resonance Pattern, squares- Fabry-Perot modes.

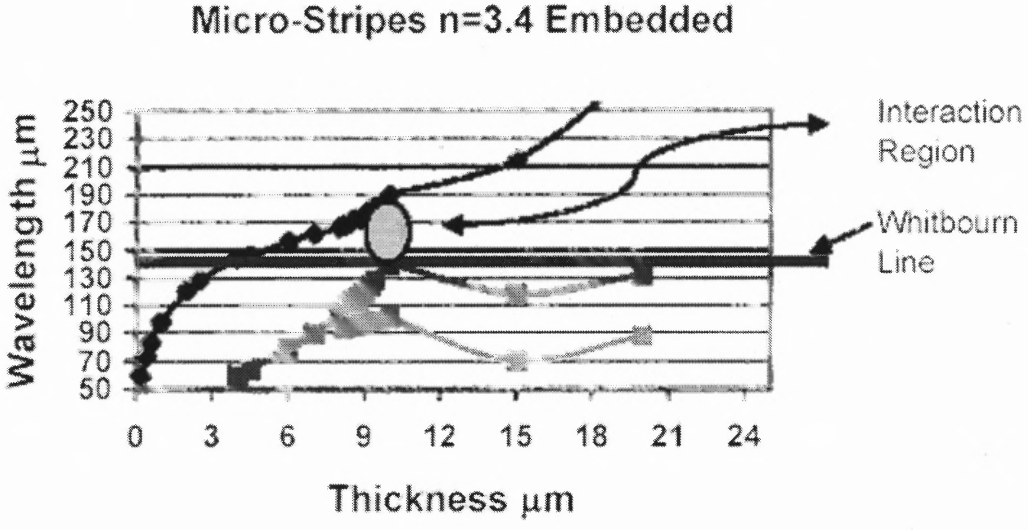

Figure 3.7d Micro-Stripes calculation of a cross shaped mesh. Geometrical parameters: g = 20μm, 2a = 1.5μm, 2b = 3.6μm, t = 0.2μm. Embedded n=3.4, data series varies from 0.2μm to 20μm. Symmetric configuration (Dielectric-Metal-Dielectric), circles-resonance modes, squares-Fabry-Perot modes.

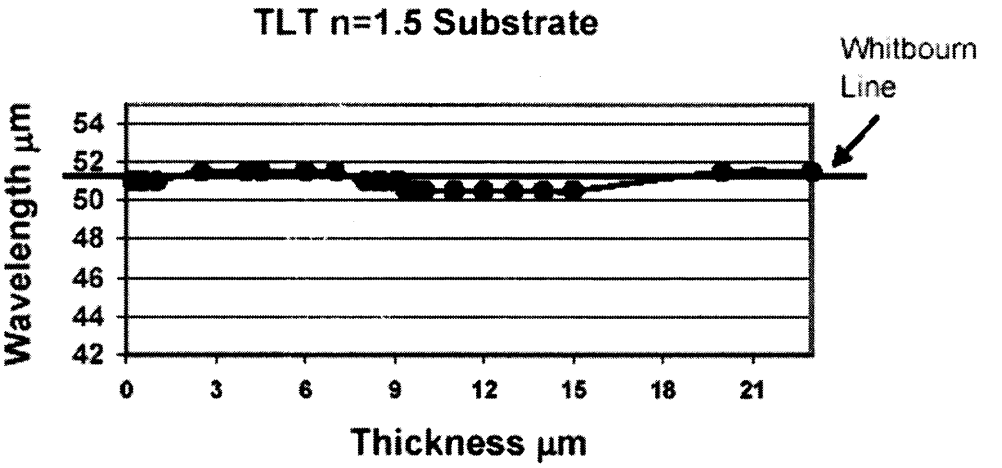

Figure 3.8a TLT calculation of a cross shaped mesh. Geometrical parameters: g = 20µm, 2a = 1.5µm, 2b = 3.6µm, t = 0.2µm. Substrate n=1.5, data series varies from 0.2µm to 25µm. Asymmetric configuration (Metal-Dielectric).

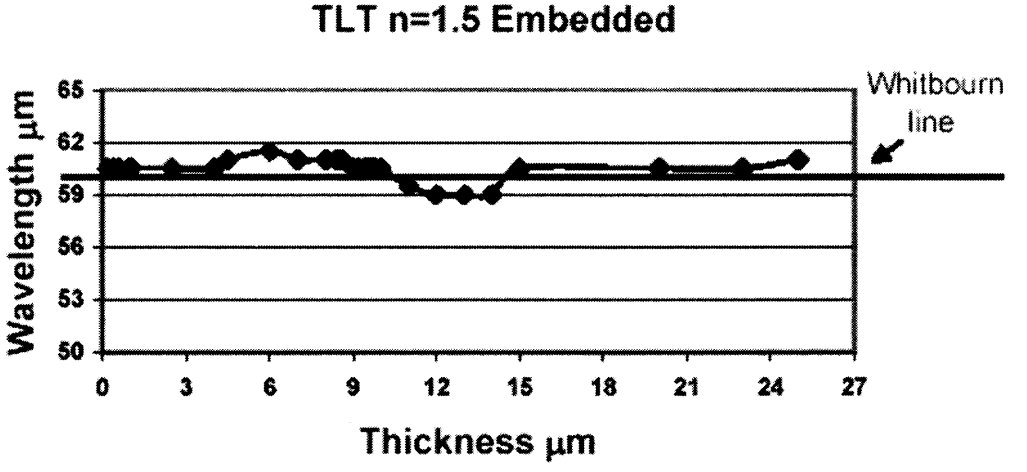

Figure 3.8b TLT calculation of a cross shaped mesh. Geometrical parameters: g = 20µm, 2a = 1.5µm, 2b = 3.6µm, t = 0.2µm. Substrate n=1.5, data series varies from 0.2µm to 25µm. Symmetric configuration (Dielectric-Metal-Dielectric).

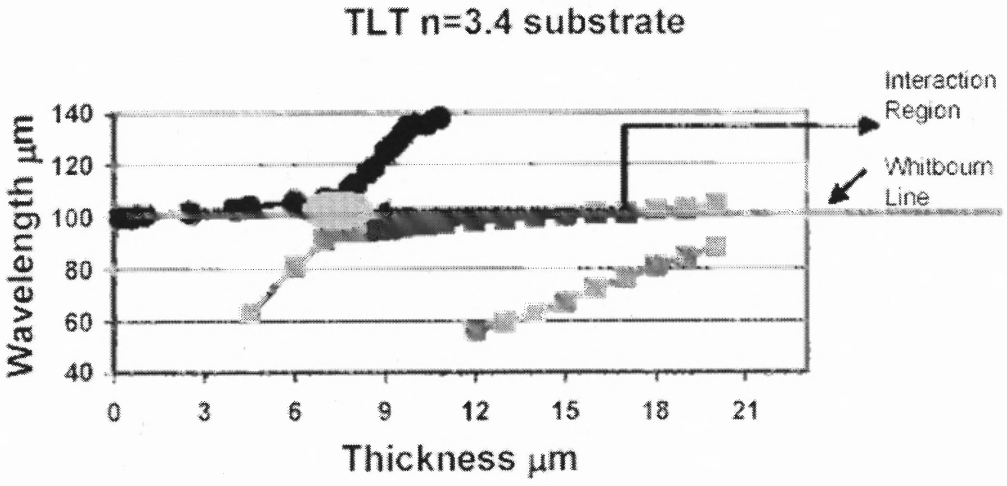

Figure 3.8c TLT calculation of a cross shaped mesh. Geometrical parameters: g = 20µm, 2a = 1.5µm, 2b = 3.6µm, t = 0.2µm. Substrate n=1.5, data series varies from 0.2µm to 25µm. Asymmetric configuration (Metal-Dielectric). circles-resonance pattern, squares-Fabry-Perot modes.

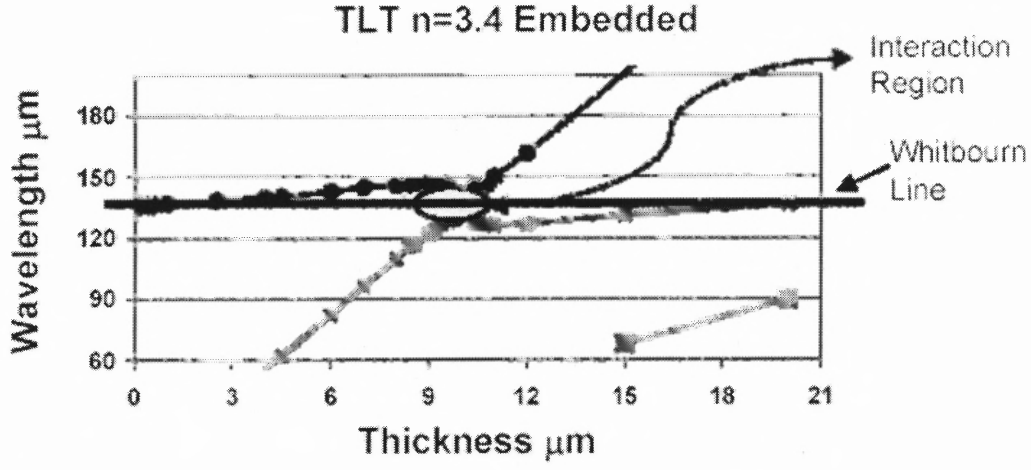

Figure 3.8d TLT calculation of a cross shaped mesh. Geometrical parameters: g = 20µm, 2a = 1.5µm, 2b = 3.6µm, t = 0.2µm. Substrate n=1.5, data series varies from 0.2µm to 25µm. Symmetric configuration (Dielectric-Metal-Dielectric). circles-resonance pattern, squares-Fabry-Perot modes.

The transmittances shown in Figures. 3.7, and 3.8 are interpreted as follows:

(i) n = 1.5 case. In Figure 3.7a, 3.7b, 3.8a, and 3.8b, the material has an index of refraction n = 1.5. The two surface waves and the Fabry-Perot modes constitute a compound mode. Micro-Stripes shows the progression of the compound mode. As the dielectric thickness is increasing, there is not enough interaction for the surface waves to separate from the mode of the dielectric layer; the strongest interaction can be seen around the Whitbourn Compton[19] line. Transmission line theory shows the same effect, that is the peak wavelength of the compound mode of surface waves and dielectric layer mode move back and forth around the Whitbourn Compton line[19].

(ii) n = 3.4 case. In Figures 3.7c, 3.7d, and 3.8c and 3.8d, the material has an index of refraction n = 3.4. Micro-Stripes shows the progression of the compound mode. As the thickness of the dielectric is increasing, initially a pair of surface waves represented by a resonance mode is displayed, whereas the dielectric itself affects the pair of surface wave by a slight shift. As the dielectric thickness reaches to a $\lambda/4*n$ (around 4 μm), a Fabry-Perot mode appears.. The Whitbourn Compton line is at 100μm (Figure 3.7c) for the Substrate case(Metal-Dielectric), and 136μm (Figure 3.8c) for the Embedded case. The surface wave exchanges energy with the Fabry-Perot modes when passing through the thickness region of maximum interaction between the two modes.

3.5 Calculation of Two Metal Meshes with Dielectric Spacer or Embedded in a Dielectric

3.5.1 Single Mesh Parameters

The calculations of two mesh filters are defined by the parameters g=24μm, 2a=9.6μm, 2b=3.6μm, metal thickness t=0.2μm, and surface impedance of 1.635 Ω. The resonance wavelength was calculated by Micro-Stripes and was found to be λ_R=32.4μm with $\lambda_R/4$=8μm. The width of resonance $\Delta\lambda/\lambda$ was found to be 18%, see Reference 22.

3.5.2 Two Meshes and Dielectrics

Two meshes with a spacer and its embedded counterpart are schematically shown in Figure 3.9.

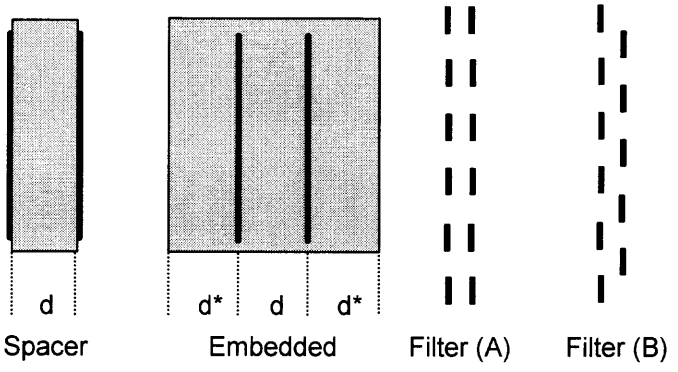

Figure 3.9 Spacer configuration (SP) and Embedded configuration (EM) with spacer thickness d, and thickness d* of layers on the outside of meshes for the embedded case. Black is metal, gray is dielectric. In the filter configuration (A) the openings of both metal meshes are lined up, in configuration (B) the openings of one mesh are between the openings of the other mesh.

The thickness of the dielectric separation of the meshes is defined as d, and the thickness of the layers on each side of the two mesh is called d^*. For the embedded cases the choice of d^* is such that the shift is equal to the Whitbourn Compton[19] shift, see Section 3.4. The chosen values are for $d^* = 10\mu m$ for n=1.5 and $d^* = 5\mu m$ for n=3.4.

3.5.3 Alignment of Two and Four Cross Shaped Meshes Micro-Stripes Calculations

The Micro-Stripes program uses a unit cell for the calculation of the transmittance of a periodic array. An analogy can be made to wave guide with a square shaped cross section, with reflecting walls. There are two different placements of the cross, one with ¼ cross in each corner see Figure 2.1c, and one with a cross at the center Figure 2.1d. Two meshes may have aligned crosses, see Filter (A) in Figures 3.9 and 3.10, or non-aligned crosses, see Filter(B) in Figures 3.9 and 3.10.

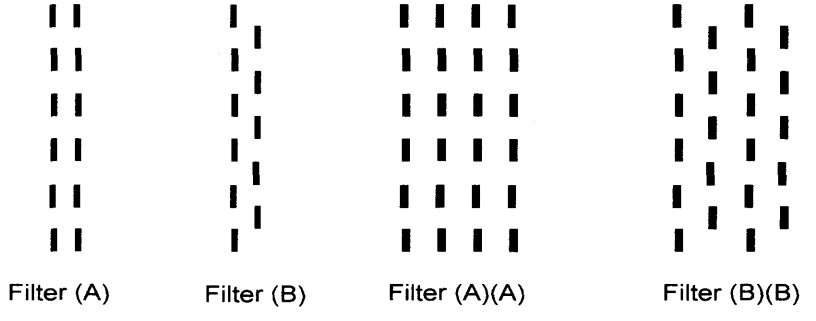

Figure 3.10 Positioning of crosses in two and four mesh filters. Filter (A): crosses of the two meshes are lined-up. Filter (B): crosses in second mesh are shifted with respect to first. Filter (A)(A): crosses of all meshes are lined-up. Filter (B)(B): the crosses of second and fourth mesh are shifted.

3.5.4 Transmission Line Theory

Transmission line theory (TLT), does not take into account the geometrical configuration. However one can calculate the resonance frequency ω_0 by using either Micro-Stripes or an empirical formula[8,17]. Using the parameters for single mesh (See Ch 2, and Appendix B) one can obtained λ_R = 32.4μm. The loss parameter a1 is taken as 0.001, see ref, and the bandwidth parameter is obtained from Micro-Stripes calculation, which is then compared with the TLT calculation. In addition one adjusts the bandwidth of a single mesh using λ_R and a1, see References 1,19, and 20.

3.6 Two Meshes, Micro-Stripes and TLT (Guidance) Calculations for d=4μm and d=8μm, n=1.5

The separation of the meshes was chosen to be d = 4μm to study possible near field effects. Both Micro-Stripes and Transmission line theory calculations were applied. A second distance of 8μm was considered; at that distance free standing meshes show minimum interaction. Transmission line theory shown in Figures 3.11-3.15 will serve as a qualitative guide for the interpretation of the various modes.

Transmission line theory was applied to the calculation of the meshes, representing meshes with non-aligned crosses. The peak transmittances are plotted in Figure 3.11, as (SP) in the range of spacer thickness of d=0 to 18μm. There are two separate resonance peaks for all values of d, and at about 8μm a branch of new peaks appears. These peaks are Fabry-Perot and were generated between the two meshes. The peaks depend on the separation of the meshes[20,22].

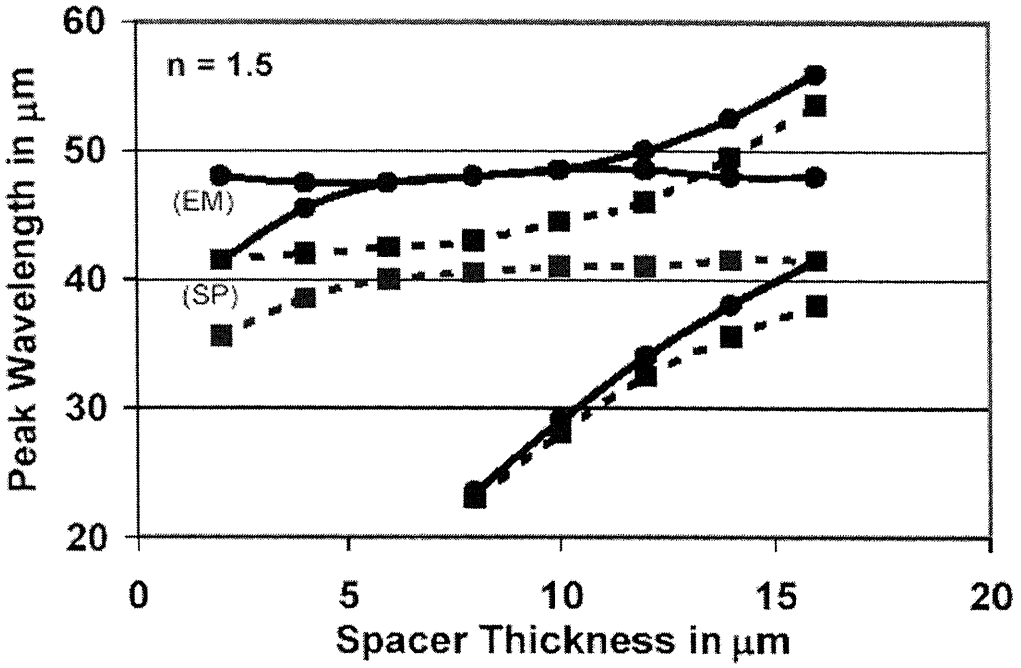

Figure 3.11 Transmission line calculations of peak wavelengths of resonance and Fabry-Perot peaks of two meshes with dielectrics of n=1.5 depending on thickness of spacer d = 2μm to 16μm. Square (SP): Spacer only. Round dots(EM): Embedded. Transmission line parameters λ_0 = 32.4μm, A1 = 0.1, a1 = 0.001 corresponding to g = 24μm, 2a = 9.6μm, 2b = 3.6μm and thickness of 0.2μm. The thickness of the outside layer for the embedded case is d* = 10μm.

3.6.1 Spacer

The appearance of the peaks for (TLT) in Figures 3.12, and 3.13 will be used as a guide for the discussion of Filter (A) and Filter (B). There are two (TLT) resonance peaks for 4μm and 8μm and no Fabry-Perot peaks are shown. For Filter (A), there are two resonance peaks for the distance 4μm and one resonance peak for distance of 8μm. For Filter (B), we have two resonance peaks for the distances of 4μm and 8μm. The shortest wavelength peak for filter (A) and (B) are the "Fabry-Perot peaks".

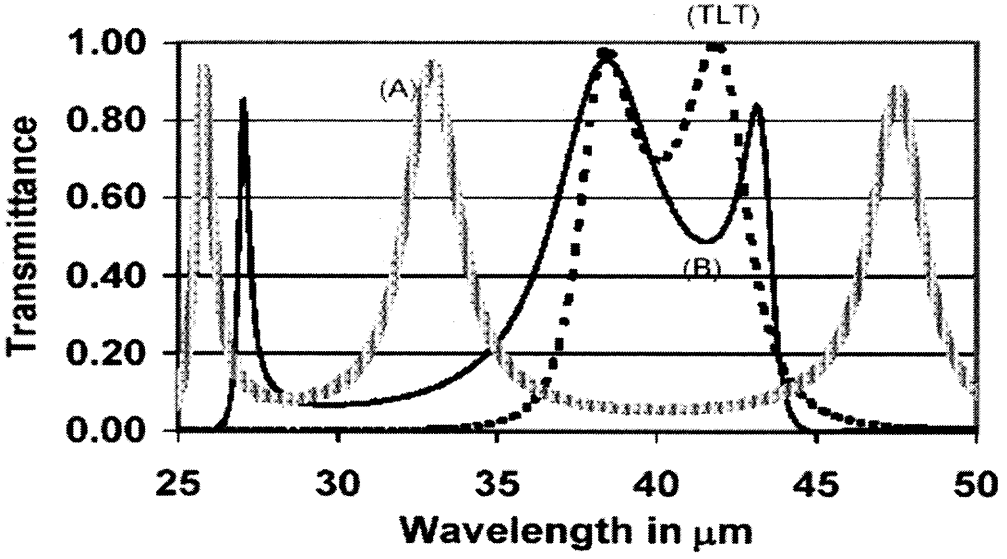

Figure 3.12 Micro-Stripes calculations of two metal meshes with spacer of refractive index n = 1.5 and thickness d = 4 μm. Geometrical parameters of g = 24 μm, 2a = 9.6 μm, 2b = 3.6 μm and thickness of 0.2 μm. Shaded line: Micro-Stripes calculation of filter (A). Solid line: Micro-Stripes calculation of filter (B). Broken line: Transmission line theory calculations, filter (TLT), using parameters λ_o = 32.4 μm, A1 = 0.1, a1 = 0.001.

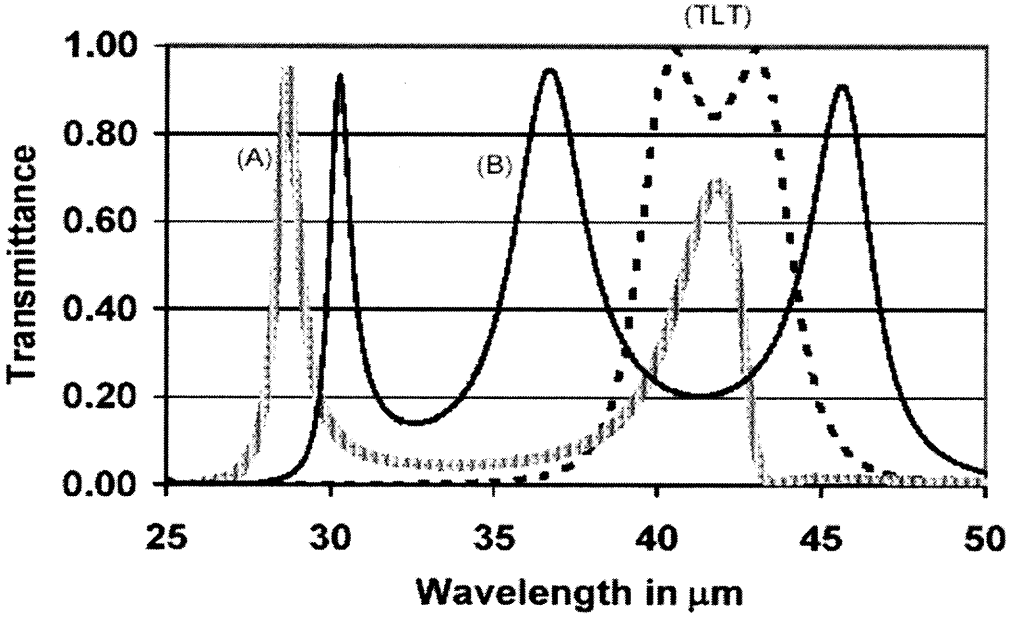

Figure 3.13 Micro-Stripes calculations of two metal meshes with spacer of refractive index n = 1.5 and thickness d = 8 μm. Geometrical parameters of g = 24 μm, 2a = 9.6 μm, 2b = 3.6 μm and thickness of 0.2 μm. Shaded line: Micro-Stripes calculation of filter (A). Solid line: Micro-Stripes calculation of filter (B). Broken line: Transmission line theory calculations, filter (TLT), using parameters λ_o = 32.4 μm, A1 = 0.1, a1 = 0.001.

3.6.2 Embedded

The transmission line calculations are plotted in Figure 3.11 as (EM) for the range of spacing d=0 to 18μm. There are two separate resonance peaks at 4μm, merged into one peak at 8μm. This is different compared to the (SP) case. A branch of new peaks appears at about 8μm. These Fabry-Perot peaks have about the same wavelength as for the (SP) case. The (TLT) peaks in Figures 3.13, and 3.14, will be used for the discussion of Filter (A) and (B).

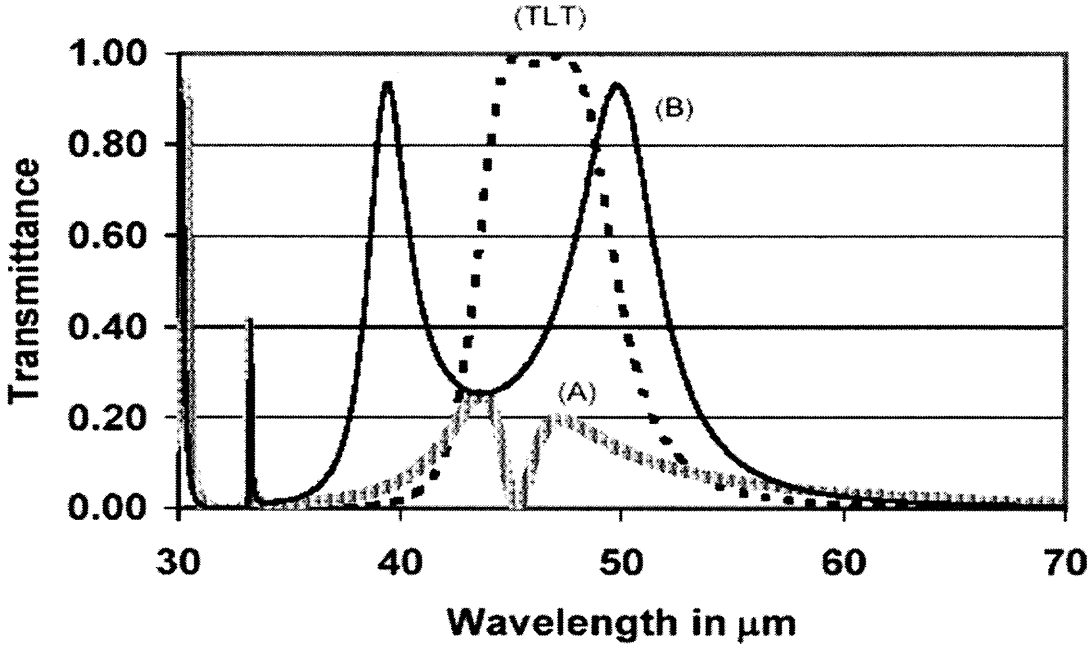

Figure 3.14 Micro-Stripes calculations of two metal meshes embedded in a dielectric of refractive index n = 1.5 and spacer thickness d = 4 μm and outside layer of thickness d* = 10 μm. Geometrical parameters of g = 24 μm, 2a = 9.6 μm, 2b = 3.6 μm and thickness of 0.2 μm. Shaded line: Micro-Stripes calculation of filter (A). Solid line: Micro-Stripes calculation of filter (B). Broken line: Transmission line theory calculations, filter (TLT), using parameters λ_o = 32.4 μm, A1 = 0.1, a1 = 0.001.

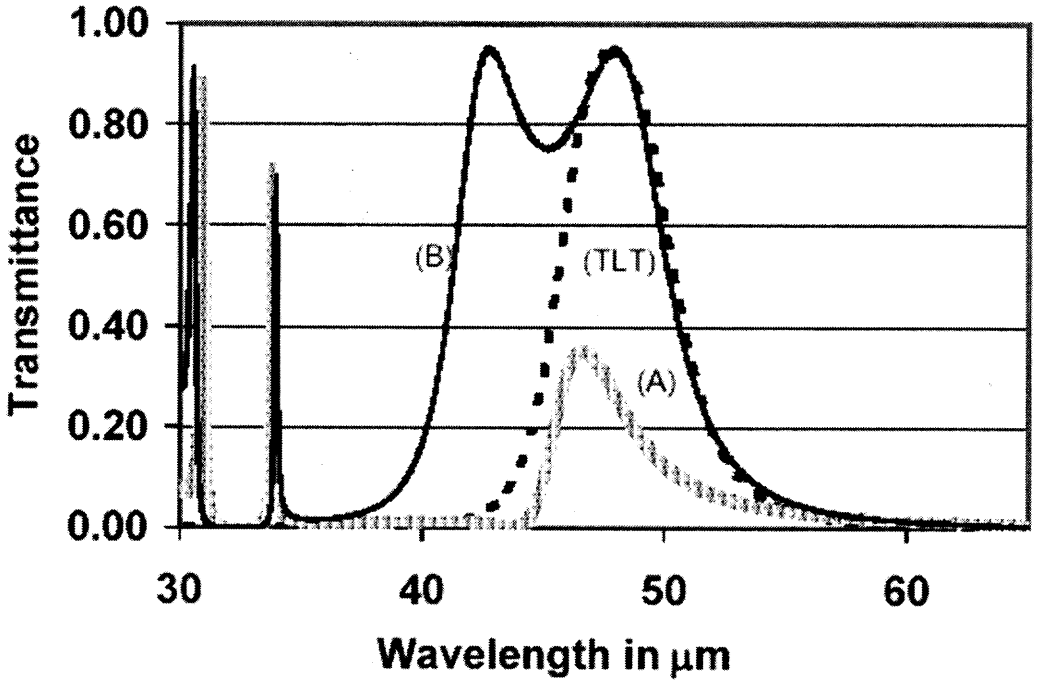

Figure 3.15 Micro-Stripes calculations of two metal meshes embedded in a dielectric of refractive index n = 1.5, spacer thickness of d = 8 μm and outside layer of thickness d* = 10 μm. Geometrical parameters of g = 24 μm, 2a = 9.6 μm, 2b = 3.6 μm and thickness of 0.2 μm. Shaded line (A): Micro-Stripes calculation of filter. Solid line (B): Micro-Stripes calculation of filter. Broken line: Transmission line theory (TLT) using parameters λ_o = 32.4 μm, A1 = 0.1, a1 = 0.001.

There are two (TLT) resonance peaks at distance of 4μm, merged to one at distance of 8μm. The Fabry-Perot peak is not shown (it is below 30μm). For Filter (A), we have two small resonance peaks for distance of 4μm, Figure 3.14, and one small peak for distance of 8μm, Fig.3.15. The shortest wavelength peak is the Fabry-Perot peak. For Filter (B) one has two resonance peaks at the distance of 4μm and 8μm and again the shortest wavelength peak is the Fabry-Perot Peak.

3.7 Two Meshes, Micro-Stripes and TLT Calculations

for d=4μm and d=8μm, n=3.4

3.7.1 Spacer

The Transmission line calculation represents meshes with non-aligned crosses. The peak transmittances are plotted in Figure 3.16 as (SP) in the range of spacer thickness of d=0 to 18μm. There are two separate resonance peaks for all values of d and at about 10μm a branch of new peaks appears. These peaks are Fabry-Perot peaks generated between the two meshes, and the Fabry-Perot peaks depend on the separation of the meshes[9].

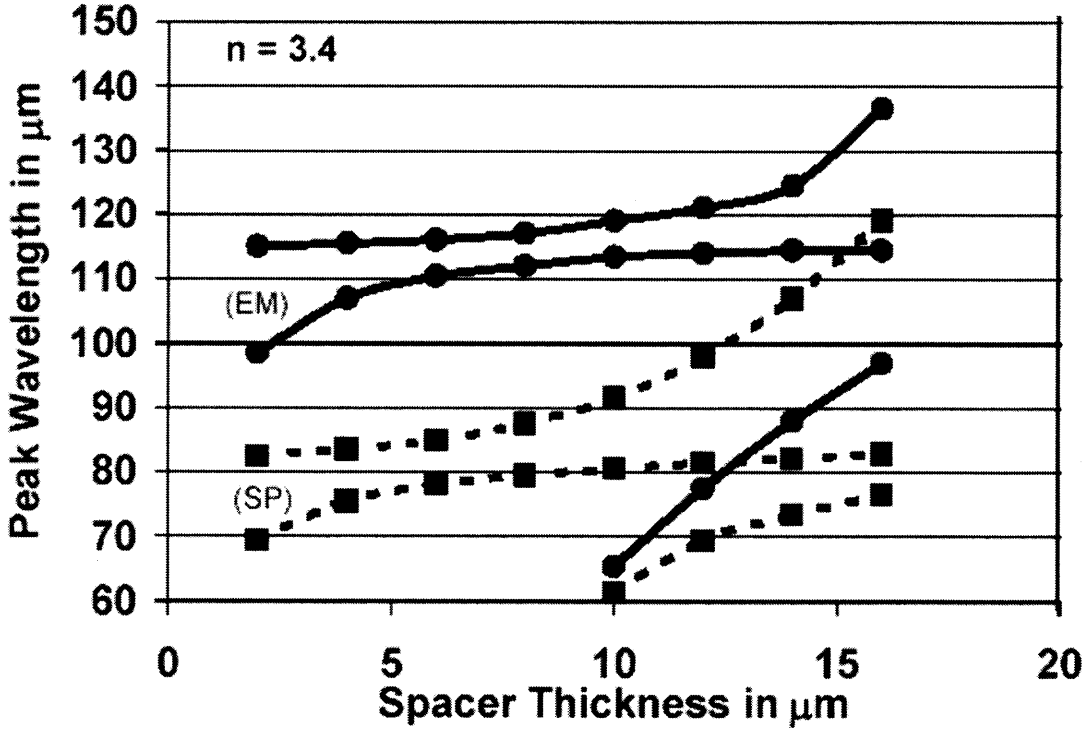

Figure 3.16 Transmission line calculations of peak wavelengths of resonance and Fabry-Perot peaks of two meshes with dielectrics of refractive index n = 3.4 depending on thickness of spacer d = 2 to 16μm. Squares (SP): spacer only. Round dots (EM): embedded. Transmission line parameters λ_0 = 32.4μm, A1 = 0.1, a1 = 0.001 corresponding to g = 24μm, 2a = 9.6μm, 2b = 3.6μm and thickness of 0.2μm The thickness of the outside layer for the embedded case is d* = 5μm.

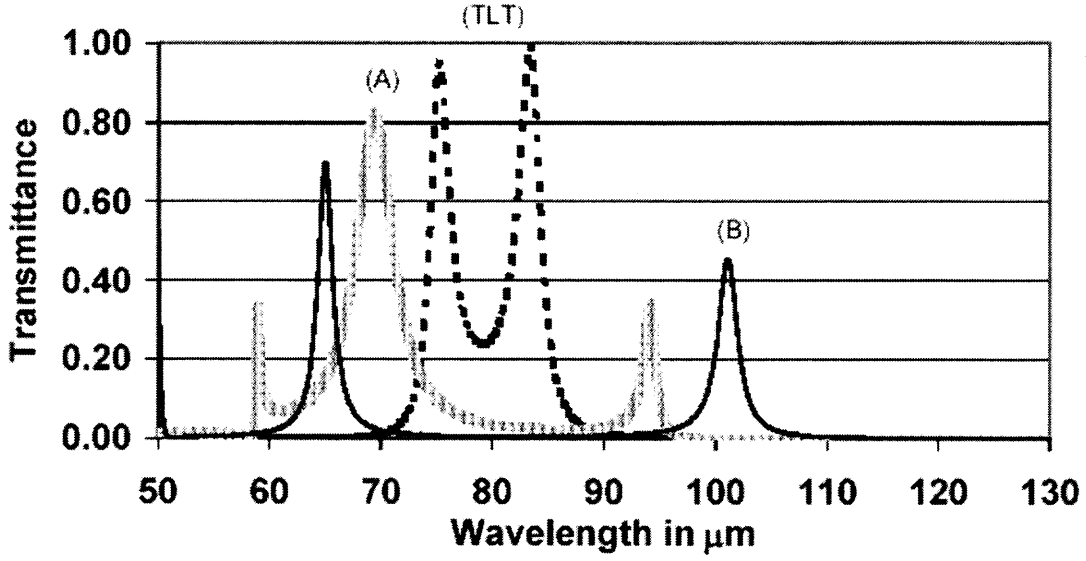

Figure 3.17 Micro-Stripes calculations of two metal meshes embedded in a dielectric of refractive index n = 3.4 and spacer thickness of d = 4 μm. Geometrical parameters of g = 24 μm, 2a = 9.6 μm, 2b = 3.6 μm and thickness of 0.2 μm. Shaded line (A): Micro-Stripes calculation of filter. Solid line (B): Micro-Stripes calculation of filter. Broken line: Transmission line theory (TLT) using parameters λ_o = 32.4 μm, A1 = 0.1, a1 = 0.001.

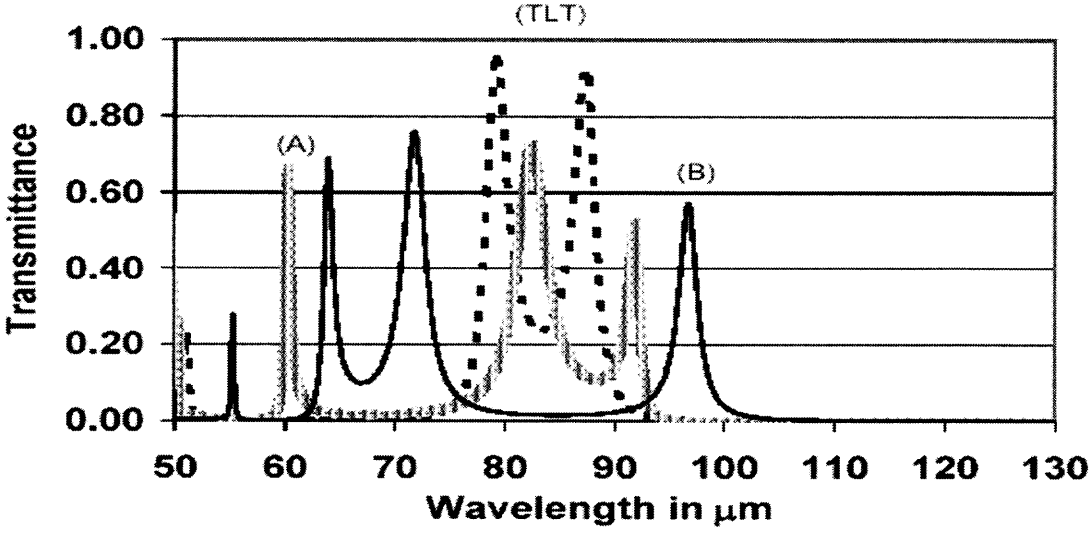

Figure 3.18 Micro-Stripes calculations of two metal meshes with spacer of refractive index n = 3.4 and thickness d = 8 μm. Geometrical parameters of g = 24 μm, 2a = 9.6 μm, 2b = 3.6 μm and thickness of 0.2 μm. Shaded line (A): Micro-Stripes calculation of filter. Solid line (B): Micro-Stripes calculation of filter. Broken line: Transmission line theory (TLT) using parameters λ_o = 32.4 μm, A1 = 0.1, a1 = 0.001.

The appearance of the peaks for TLT in Figure 3.17, and 3.18 will be used as a guide for the discussion of Filter (A) and Filter (B). There are two resonance peaks for 4μm, and 8μm, and the Fabry-Perot peak is shown for 8μm. For Filter (A), there are two resonance peaks for the distance 4μm and one resonance peak for distance of 8μm. The two shortest wavelength peaks are Fabry-Perot peak. For Filter (B) one has two resonance peaks for the distances of 4μm and 8μm. The two shortest wavelength peaks are the Fabry-Perot peaks.

3.7.2 Embedded

The transmission line calculation represents meshes with the non-aligned case of crosses. The peak transmittances are plotted in Figure 3.16, as (EM) for the range of spacing d=0 to 18μm. There are two separate resonance peaks around 10μm, that is when a branch of new peaks appears, the Fabry-Perot peaks are generated between the two meshes. The appearance of the (TLT) peaks in Figure 3.16, will be used as a guide for the discussion of Filter (A) and (B), see Figures 3.19, and 3.20. There are two resonance peaks at the distance of 4μm and 8μm. Only one Fabry-Perot peak is just shown for 8μm, (TLT). For Filter (A), we have small transmission of two resonance peaks at a distance of 4μm and peaks. For Filter (B), one small peak at the distance of 8μm, the shortest wavelength peaks are the Fabry-Perot has two resonance peaks at the distance of 4μm and 8μm and at shorter wavelengths the Fabry-Perot peak.

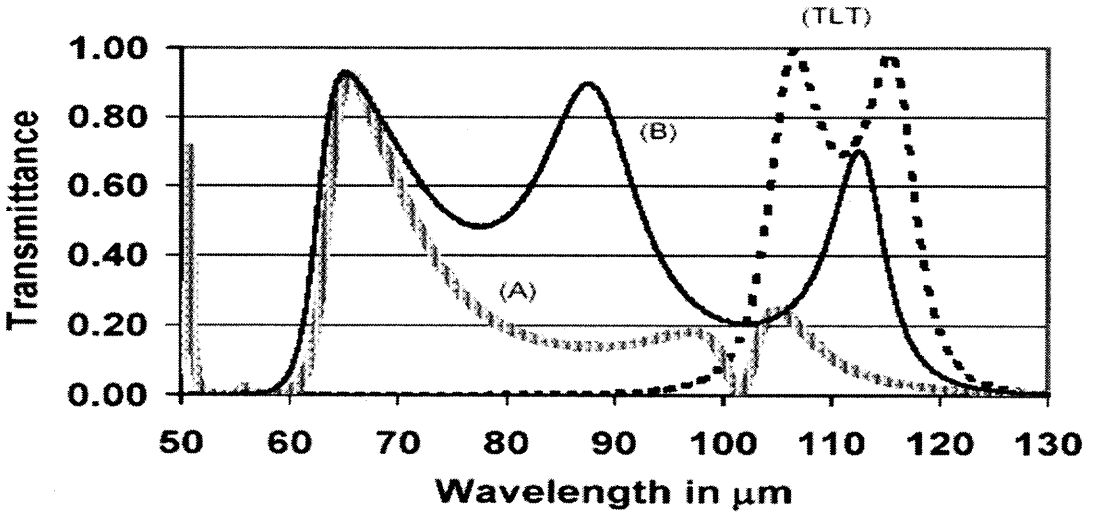

Figure 3.19 Micro-Stripes calculations of two metal meshes embedded in a dielectric of refractive index n = 3.4 and spacer thickness d = 4 μm and outside layer of thickness d* = 5 μm. Geometrical parameters of g = 24 μm, 2a = 9.6 μm, 2b = 3.6 μm and thickness of 0.2 μm. Shaded line: Micro-Stripes calculation of filter (A). Solid line: Micro-Stripes calculation of filter (B). Broken line: Transmission line theory (TLT) using parameters λ_o = 32.4 μm, A1 = 0.1, a1 = 0.001.

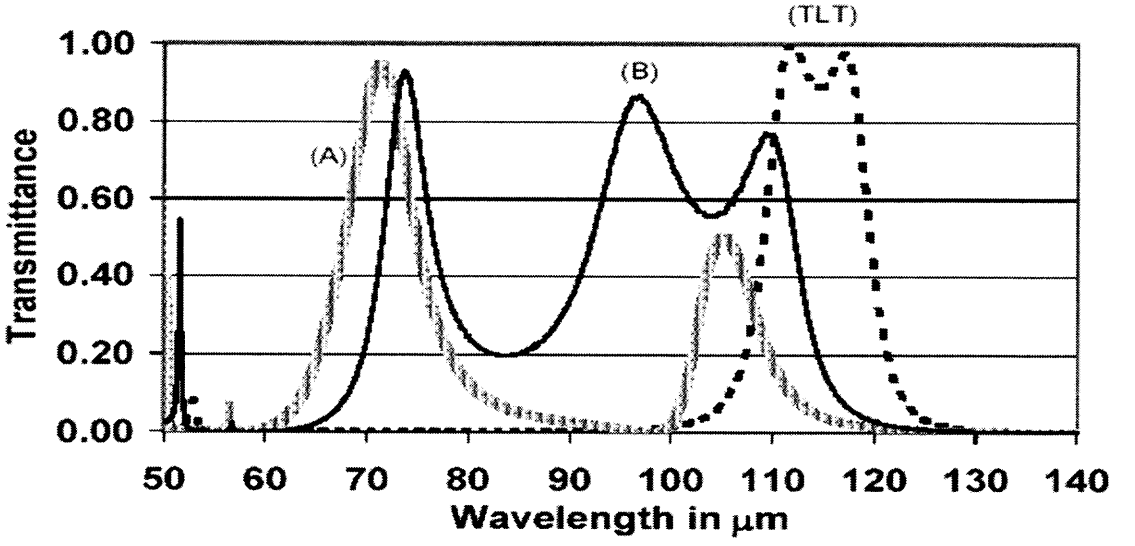

Figure 3.20 Micro-Stripes calculations of two metal meshes embedded in a dielectric of refractive index n = 3.4 and spacer thickness d = 8 μm and outside layer of thickness d* = 5 μm. Geometrical parameters of g = 24 μm, 2a = 9.6 μm, 2b = 3.6 μm and thickness of 0.2 μm. Shaded line: Micro-Stripes calculation of filter (A). Solid line: Micro-Stripes calculation of filter (B). Broken line: Transmission line theory (TLT) using parameters λ_o = 32.4 μm, A1 = 0.1, a1 = 0.001.

3.8 Application to Filter Design

If one were to design a filter, ideally one would wish the filter to have close to 100% transmittance. For a cross with g = 24μm, 2a = 9.6μm, 2b = 3.6, the investigation leads to the conclusion that the ideal condition can be approached. In order to accomplish that condition, one can use a substrate material with index of refraction of n = 1.5, with an embedded configuration and with a distance of 8μm, see Figure 3.11, and Figure 3.15. A similar results can be reached by taking two free standing meshes at this distance, see Reference [18]. Filter(A) shows in Figure 3.13, 3.15, and 3.24 only one peak, but the referred figures all have undesirable low transmittance, Filter(B) shows more than one peak for all cases. If one were to accept for a filter two narrowly spaced peaks, one can use a configuration of Filter (TLT), for index of refraction of n=1.5 and spacing of 4μm, and for index of refraction n=3.4 spacing of 8μm. Changing the spacer thickness can change the contour to the desired shape.

At spacing of 8μm = $\lambda_R/4$, where λ_R is the resonance wavelength of the free standing mesh, oscillators show minimum interaction. There is a compensation of the effect of the shift by the dielectric layers to longer wavelength and the effect of the dielectric constant on the wavelength in the dielectric spacer. Therefore, the value of the spacing of $\lambda_R/4$ for two free standing meshes is about the same as for dielectric spacer. While the resonance wavelength is shifted when using dielectric layers, the width of resonance remains about the same, see Figure 21. The width of resonance at 8μm for two free standing meshes (F) is about 10%, for a spacer of refractive index n=1.5 (SP) is 10% and embedded in the dielectric of n=1.5 (EM) is 12%.

The use of transmission line theory to predict the peak wavelength of two-mesh filter with dielectric spacer is not possible for small thicknesses. The reason for that is the corresponding shift depending on the thickness of the dielectric. To avoid the "Thickness" issue, the Micro-Stripes program can be used to calculate the correct peak wavelength shift of a single mesh on a dielectric substrate as thin as one chooses. Then a two mesh filter is to be assembled with the metal meshes facing each other, having the dielectric substrate on the outside of the spacing area. The desired spacing may be determined with the transmission line theory since one has an index of refraction of n = 1 for the spacer.

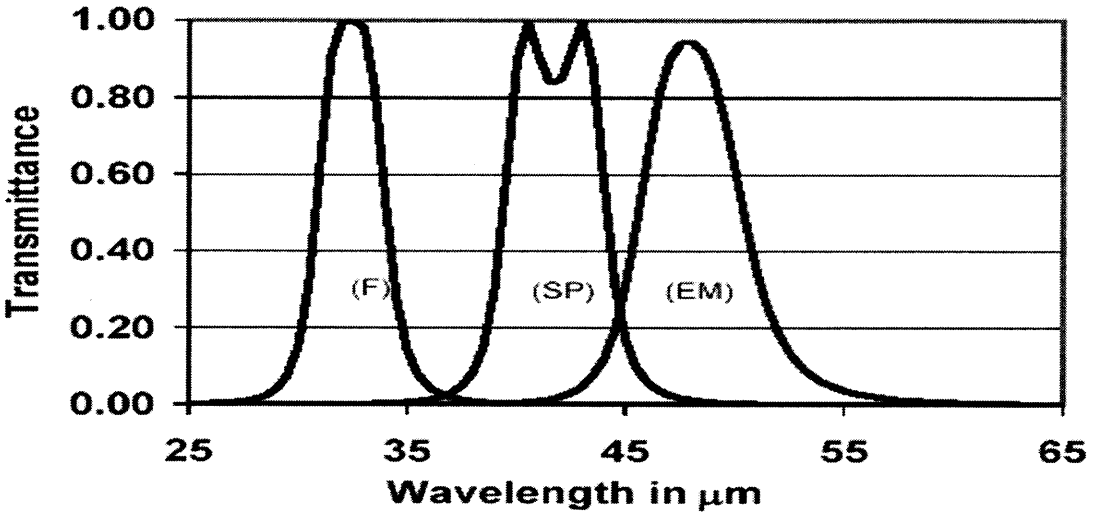

Figure 3.21 Transmittance of two meshes with spacer of thickness 8μm. Transmission line parameters λ_o = 32.4 μm, A1 = 0.1, a1 = 0.001. Free standing meshes (F), spacer of refractive index n = 1.5 (SP) and embedded in dielectrics of refractive index n = 1.5 with d* = 10 μm (EM). The ratio of bandwidth at half height to peak wavelength BW is for (F) equal to10%, for (SP) equal to10% and for (EM) equal to 12%.

3.9 Summary

The resonance wavelength and bandwidth of a single mesh in contact with dielectric layers was calculated with electromagnetic theory using as input parameters the geometrical configuration, the surface impedance of the metal, and the refractive index of the dielectric layers. An empirical non-linear relation was given for the experimental results, for both the resonance and the bandwidth. Using Micro-Stripes calculations, the resonance wavelength of two metal meshes was studied for two specified alignments of the crosses and the dependences of the resonance peaks on the thickness and refractive index of the spacing. Transmission line theory was used to study the transmittance of two non-aligned cross-shaped meshes and the limitations of the spacer thickness. Filter with non-aligned crosses show desirable filter characteristics for quarter wavelength spacing and low refractive index. A special configuration may be used for meshes on thin meshes.

The interpretation of the study was done with the oscillator mode model. In simple terms, the incident light excites a compound mode of mesh and dielectric and this mode transfers the energy to the reflected and transmitted light. The compound mode consist of modes of the meshes with $k = 0$ and Fabry-Perot modes with wavevectors parallel to the incident light and their interaction.

CHAPTER 4

THICK METAL MESHES

4.1 Inductive Metal Meshes - Introduction

In Chapters 2 and 3 thin inductive metal meshes were discussed, free standing and in contact with dielectrics. The metal thickness of most of the meshes was assumed to be 0.2μm and a periodicity constant of 20μm was used. Thick metal meshes with thickness of 11, 20 and 29μm and periodicity constant of g = 20μm have been produced by Ruprecht *et al.*[11]; these meshes have been manufactured with high accuracy and have been used to adjust the surface impedance of the metal in the Micro-Stripes simulation program. The transmittance of these free standing cross shaped metal meshes shows a resonance peak and an additional peak at shorter wavelength, both show dependence on the thickness of the mesh. Whitbourn *et al.*[19] have predicted such peaks for thick free standing cross shaped metal meshes and Möller *et al.*[8,23] have given an interpretation in terms of coupling of the k vectors of resonance and thickness peak.

In the short wavelength region Ebbesen *et al.*[24] and Grupp *et al.*[25] have presented experimental studies of metal meshes with round holes and thicknesses of ¼ of the periodicity constant. Martin-Moreno *et al.*[26] have calculated similar meshes with square shaped openings. Möller *et al.*[8,22,23] have calculated meshes with cross shaped openings. All these metal meshes in the short and long wavelength region have similar transmittances with identical peak dependence on the thickness. A rudimentary model, expressed in transmission line theory, describes very well all resonance peaks of these meshes.

4.2 Free Standing Thick Inductive Metal Meshes

4.2.1 Inductive Metal Meshes with Periodicity Constant of g = 20μm

The transmittance of inductive cross shaped meshes with g = 20μm, $2a$ = 1.5μm, $2b$ = 3μm has been calculated for thicknesses of 0.2, 1.0, 3.2,6.4, 9.6, 12.8, 16, 19.2, 22.4 and 25.6μm, and are shown in Figure 4.1 to 4.3. In Figure 4.4, the peak wavelength transmittance of all peaks is plotted depending on the thickness t of the meshes.

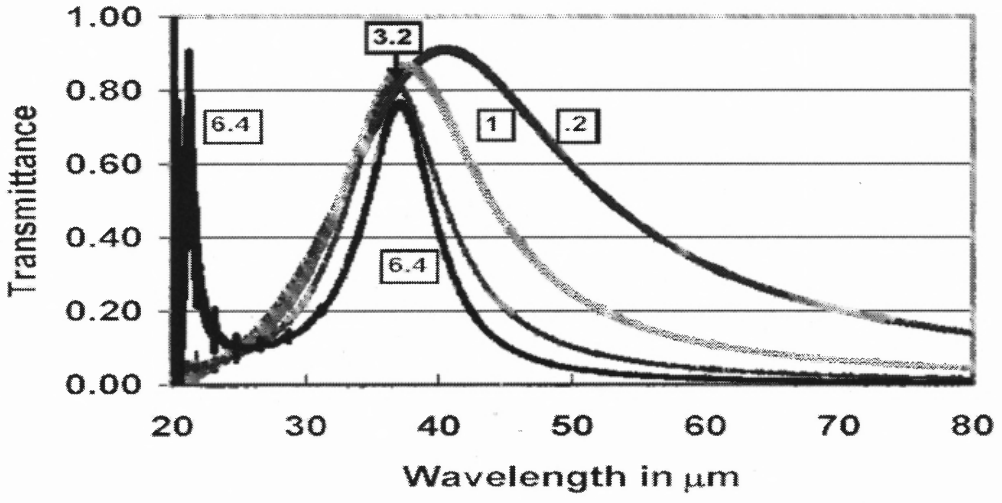

Figure 4.1 Transmittance of inductive cross shaped meshes calculated with Micro-Stripes program. Geometrical parameters g = 20μm, $2a$ = 1.5μm, $2b$ = 3μm. The metal thicknesses of 0.2, 1, 3.2, and 6.4μm are indicated in the graph area. The resonance peaks shift to shorter wavelength with increasing metal thickness, (see also Figure 4.4).

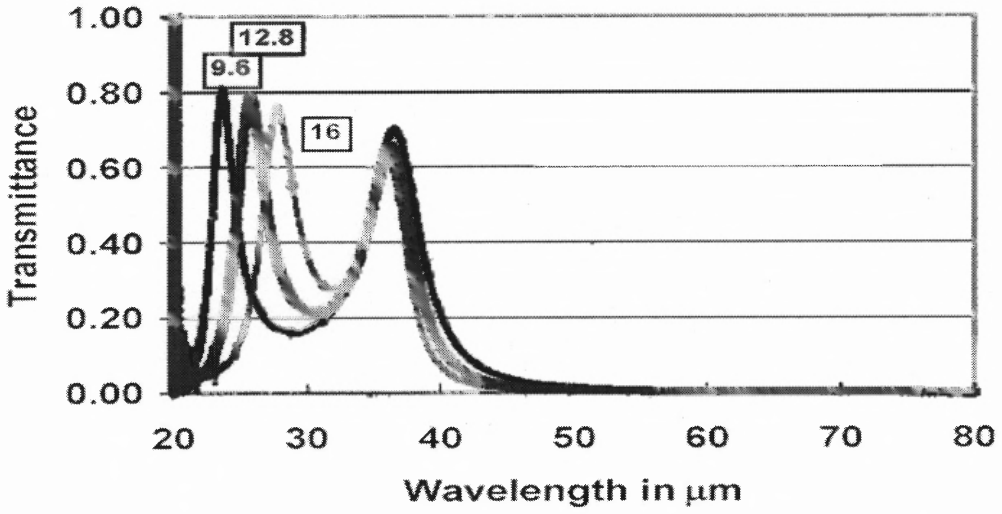

Figure 4.2 Transmittance of inductive cross shaped meshes calculated with Micro-Stripes program. Geometrical parameters g = 20μm, $2a$ = 1.5μm, $2b$ = 3μm. The metal thicknesses 9.6, 12.8 and 16μm are indicated in the graph area. The long wavelength peaks are resonance peaks, the short wavelength peaks are the first series of thickness peaks, (see also Figure 4.4).

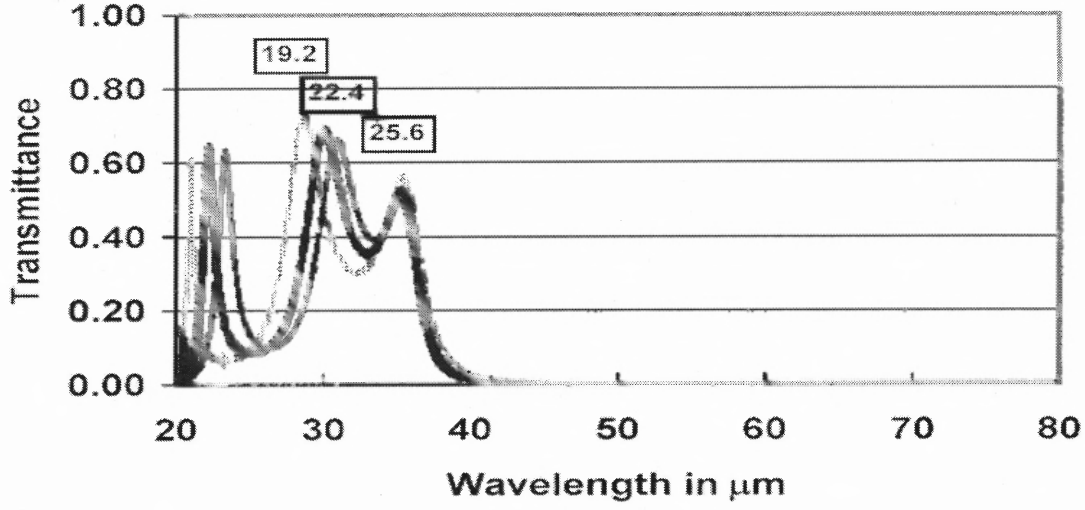

Figure 4.3 Transmittance of inductive cross shaped meshes calculated with Micro-Stripes program. Geometrical parameters g = 20μm, $2a$ = 1.5μm, $2b$ = 3μm. The metal thicknesses 19.2, 22.4 and 25.6μm are indicated in the graph area. The longest wavelength peaks are resonance peaks. At shorter wavelengths, the first series of thickness peaks appear, and at even shorter wavelengths, the second series of thickness peaks, (see also Figure 4.4).

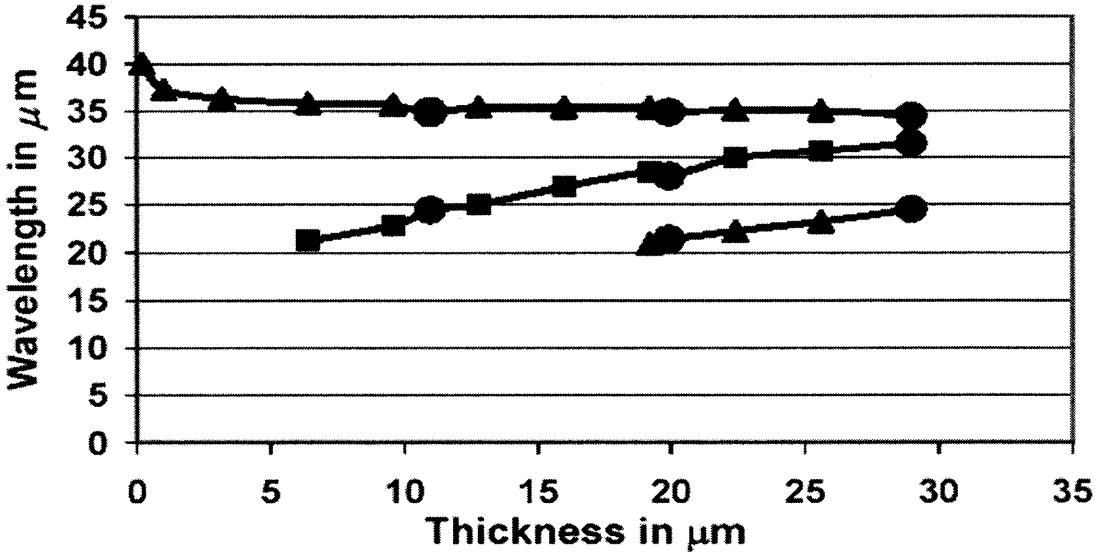

Figure 4.4 Graph of wavelengths of resonance and thickness peaks depending on metal thickness t of the meshes. Upper curve: Resonance wavelengths. Triangles calculated with Micro-Stripes program. Round dots are experimental data. Next lower curve: Thickness peaks. Squares calculated with Micro-Stripes program. Round dots are experimental data. Lowest curve: Thickness peaks. Triangles calculated with Micro-Stripes program. Round dots are experimental data.

4.2.2 Experiments

Ruprecht *et al.*[11] have manufactured free standing metal meshes of excellent quality with the same geometrical parameters as used above of g = 20μm, $2a$ = 1.5μm, $2b$ = 3μm and for thickness' of 11, 20 and 29μm. Micro-Stripes calculations are shown in Figure 4.5 and agree with the experimental data of Reference [11] within a few percent. All calculated peaks and the experimental observed data of Reference [11] are shown in Figure 4.4.

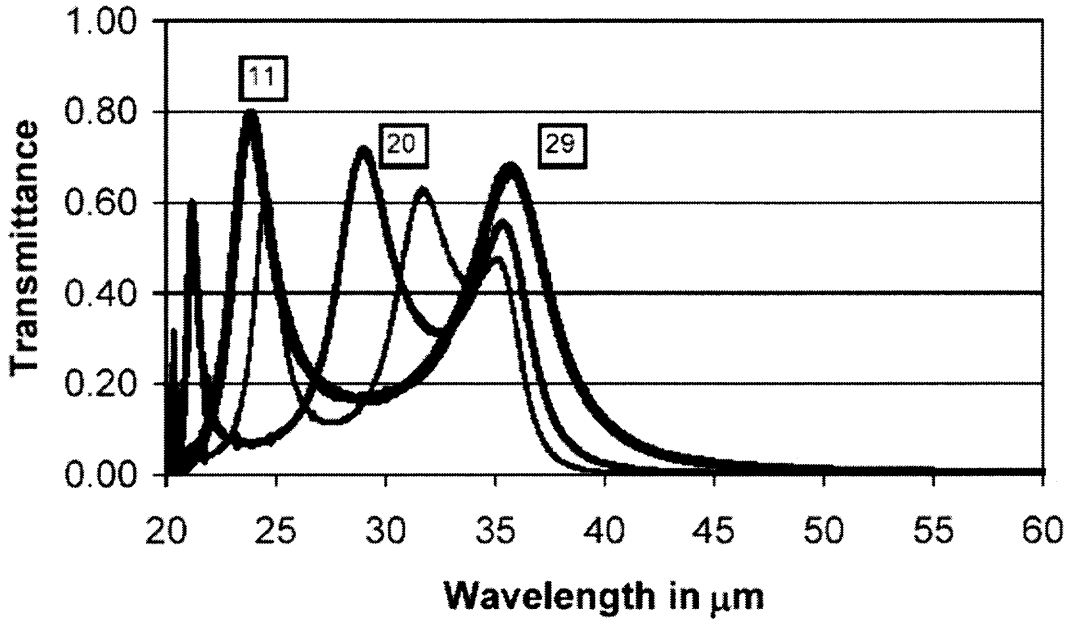

Figure 4.5 Micro-Strips calculations of the transmittance of free standing metal meshes of thicknesses 11, 20 and 29μm. The parameters of the cross are $g = 20$, $2a = 1.5$ and $2b = 3$μm, (see Reference [11]).

4.2.3 Resonance Peaks

From Figure 4.4, one can observe that the wavelength of the resonance peaks shifts to shorter wavelength with increasing thickness, while the wavelength of the thickness peaks shift from the region of $\lambda=g$ to a longer wavelength. For larger thicknesses a new series of thickness peaks is generated. The linear formula, see Equation 2.1a , for free standing inductive metal meshes gives the resonance wavelength for $t = 0.2$μm, while the empirical formula of Equation 2.1b gives approximately the resonance wavelength for all thicknesses larger than $t = 3$μm.

4.2.4 Thickness Peaks

The thickness peaks appear first at a wavelength close to the periodicity constant g and shift with increasing thickness towards the resonance peak. After a certain thickness of the mesh, a new series of thickness peaks appear with its first peak having again a wavelength close to the periodicity constant. An empirical formula has been suggested (see Reference 23) for the wavelength of the thickness peaks λ_T based on the interaction of a surface wave with wave vector k_S and a wave traveling in the opening with wave vector k_F. Since the two wave vectors are perpendicular, the resulting wave vector of the thickness peak is obtained as

$$k_T^2 = k_S^2 + k_F^2 \tag{4.1}$$

Taking for the wavelength of the surface wave $\lambda_S = 2g$ and for the wavelength of the wave in the openings $\lambda_F = g + t$, the wavelength of the thickness peak λ_T was calculated from

$$1/(\lambda_T)^2 = 1/(2g)^2 + 1/(g+t)^2 \tag{4.2}$$

The wavelengths of the experimental thickness peaks for thicknesses of 11, 20 and 29 μm agreed well with the wavelength calculated with Equation 4.2. A similar approach was taken to represent the Micro-Stripes program calculations of the thickness peaks with an empirical formula. In a slightly different approach the resonance wavelength λ_R was used instead of 2g and two coefficients were used for the term with g and t.

$$1/(\lambda_T)^2 = 1/(\lambda_R)^2 + 1/(c_1 g + c_2 t)^2 \quad (4.3)$$

A good fit was obtained using c_1 =0.82 and c_2 =1.30, calculations are shown in Appendix C.

4.3 Cross Shaped Inductive Meshes with Periodicity Constant g = 1 μm

The Fourier modal method[23,27] was applied to calculate the transmittance of free standing cross shaped metal meshes in the short wavelength region. The geometrical parameters were g = 1μm, *2a* = 0.2μm, *2b* = 0.11μm, for thickness' of 0.2, 0.4, 0.8, 1, 1.6, and 2μm. The calculations are shown in Figure 4.6 and 4.7. and are similar to the long wavelength calculations for g = 20μm. There are "resonance peaks" shifting to shorter wavelength, and shorter wavelength peaks, "thickness peaks", with an appearance depending on the thickness of the metal mesh. The peak wavelength of all peaks depending on the thickness is plotted in Figure 4.8 for the range 0 to 2μm. Such calculations have been repeated for cross shaped metal meshes with similar ratios of a/g and b/g for periodicity constants of g = 2.14μm and g = 3μm. The results of the dependence on thickness of resonance and thickness peaks is very similar for much larger periodicity constants in the longer wavelength region, as shown in Figure.4.4

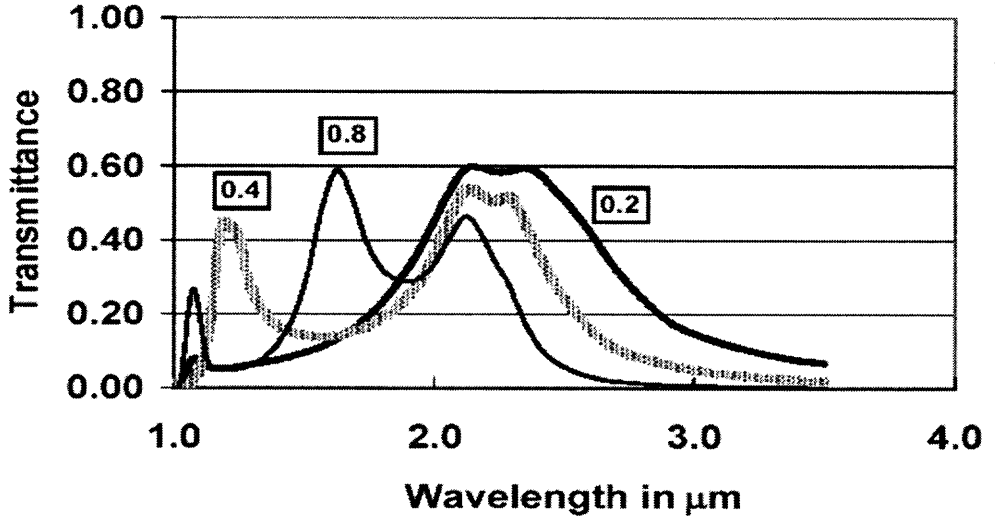

Figure 4.6 Transmittance of inductive cross shaped meshes calculated with the Fourier Modal Method. Geometrical parameters g = 1μm, $2a$ = 0.2μm, $2b$ = 0.11μm. The metal thicknesses 0.2μm, 0.4μm, and 0.8μm are indicated in the graph area. The long wavelength peaks are resonance peaks, the short wavelength peaks are the first series of thickness peaks, (see also Figure 4.8).

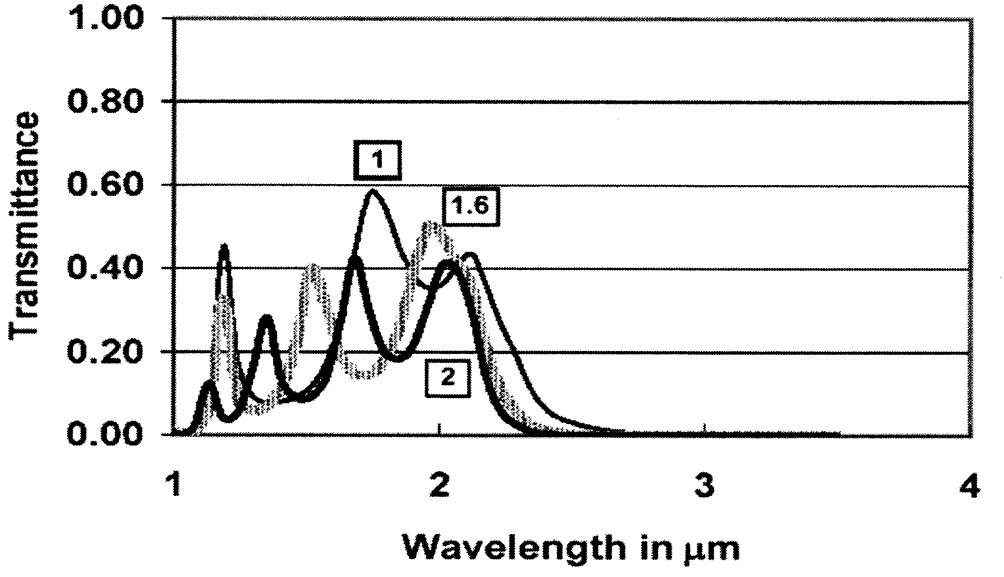

Figure 4.7 Transmittance of inductive cross shaped meshes calculated with the Fourier Modal Method. Geometrical parameters g = 1μm, $2a$ = 0.2μm, $2b$ = 0.11μm. The metal thicknesses 1μm, 1.6μm, and 2μm are indicated in the graph area. The longest wavelength peaks are resonance peaks. At shorter wavelengths the first series of thickness peaks show up, and at even shorter wavelengths the second series of thickness peaks (see also Figure 4.8).

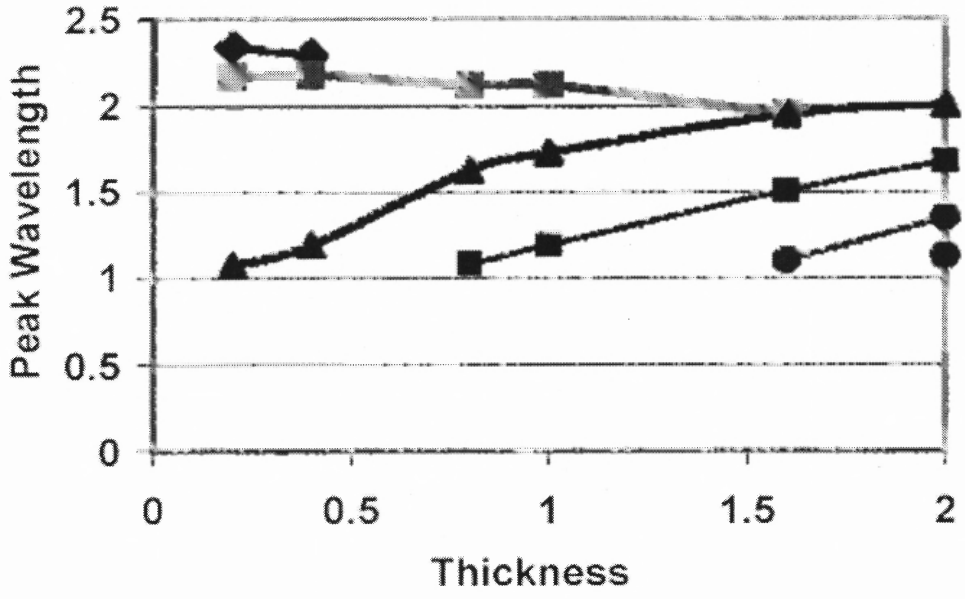

Figure 4.8 Graph of wavelengths of resonance and thickness peaks plotted depending on the metal thickness *t*. Upper curves: Squares and diamonds are resonance wavelengths. Next lower curve: Triangles are first series of thickness peaks. Two lowest curves: Second and third series of thickness peaks.

4.4 The Oscillator Model and Transmission Line Theory

4.4.1 Oscillator Model

Ulrich[1] has analyzed the modes of thin square shaped inductive metal meshes. The modes are composed of pairs of surface waves on each side of the mesh. The corresponding wavelengths are the resonance wavelengths of a thin metal mesh. The thin mesh model is extended to thick meshes and it is assumed that the surface waves on each side of the thick mesh are described by an oscillator having the same resonance wavelength as the surface waves of a thin mesh with the same geometrical parameters. The oscillators on both sides of the thick mesh are coupled by wave guide modes of the openings, depending on the thickness t of the mesh. For a qualitative description of this simple model of two interacting oscillators one can use transmission line theory[1,20,23] and calculate the peaks of the transmitted waves.

4.4.2 Transmission Line Theory

4.2.2.1 Oscillator. TLT used in this section is similar to that described in the previous chapters, but is repeated for completeness. The oscillator is described by a shunt impedance.

$$Y(\lambda) = 1/[a1 - i(\omega_o A1)/\Omega(\lambda)] \tag{4.4}$$

where

$$\Omega(\lambda) = (g/\lambda\omega_o) - (\lambda\omega_o/g). \tag{4.5}$$

The periodicity constant of the mesh is g, the normalized resonance frequency ω_o, the bandwidth parameter A1 and the loss parameter a1. The input parameters ω_o, A1, and a1 may be obtained from observations, simulations such as the Micro-Strips program or empirical formulas.

4.2.2.2 Cascading Matrices. The cascading matrix of each element of the transmission line is presented by a 2 by 2 matrix. The waves on the left side of the impedance Y, are related by a matrix M to the waves on the right side as

$$b_1 = m_{11}\, a_2 + m_{12}\, b_2$$
$$a_1 = m_{21}\, a_2 + m_{22}\, b_2 \qquad (4.6)$$

For $a_2 = 0$, that is no backwards traveling wave on the right side, one has for the ratio of the reflected wave b_1 to incident wave a_1

$$b_1/a_1 = m_{12}/m_{22} \qquad (4.7)$$

and for the ratio of the transmitted wave b_2 to the incident wave a_1

$$b_2/a_1 = 1/m_{22}. \qquad (4.8)$$

The transmitted intensity is calculated from the (2,2) element of the resulting matrix presenting all elements in the transmission line.

The matrix M1 of the impedance Y has the elements

$$m1_{11} = (-Y/2 + 1) \qquad m1_{12} = -Y/2 \qquad (4.9)$$

$$m1_{21} = Y/2 \qquad m1_{22} = (Y/2 + 1)$$

and the matrix M2 of the separation of length t in the medium with refractive index 1 is

$$m2_{11} = \exp(-i2\pi t)/\lambda \qquad m2_{12} = 0 \qquad (4.10)$$

$$m2_{21} = 0 \qquad m2_{22} = \exp(i2\pi t)/\lambda$$

4.4.3 Calculations

The two oscillators of the model are separated by the distance *t* and described by the matrix product M = M1M2M1, where the separation of the oscillators corresponds to the thickness t of the metal mesh. For the input data, one has for the resonance frequency $\omega_o = g/\lambda_R$, where λ_R is obtained from the resonance formula of a thin free standing metal mesh as discussed in Chapter 2. The bandwidth parameter is assumed similar to what has been done in Chapter 2 and Chapter 3, and the loss parameter a1 is taken as 0.001. In Figure 4.9 the calculated peak wavelengths are plotted depending on the thickness of the mesh for the range of 0 to 45μm.

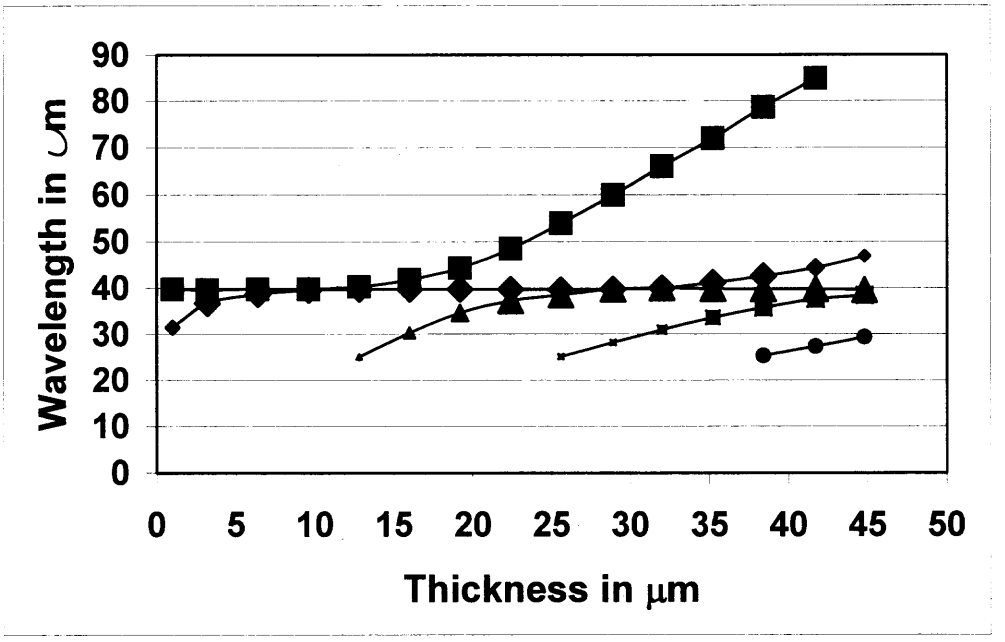

Figure 4.9 Transmission line theory calculations of resonance and thickness peaks of two oscillators at distance t. The peak wavelength of resonance and thickness peaks are plotted depending on the thickness of the mesh. At small values of t, the resonance peaks (squares and diamonds) show interaction and at t = 10μm the interaction of the resonance peaks has vanished and at t = 12μm the first branch of thickness peaks (triangles) appears. At t = 25μm the first peak of the second series of thickness peaks appears and at t = 40μm interacts strongly with the resonance peaks.

For small values of t, the two oscillators interact and show a "splitting", which decreases for increasing values of t. The splitting is observed in Figure 4.9; at around t = 12μm a new peak appears, shifting for larger values of t towards the wavelength of the oscillators. The "new peaks" are the "thickness peaks" and are interpreted as compound modes composed of oscillator resonance and waveguide modes. The wave guide modes are "Fabry-Perot" modes, as they appear between two reflecting plates, similar as described in Reference [26] for narrow slots in thick gratings. The second and third series are also "thickness peaks" composed of resonance and higher order wave guide modes. The appearance of resonance and thickness peaks are plotted for thicknesses of 4, 10 and

18μm in Figure 4.10 on a logarithmic scale for better visibility. It is observed that a splitting occurs at 4μm, at 10μm the splitting disappears, while one thickness peak is present. At 18μm, three thickness peaks occur with one thickness peak close to the resonance peak that shows a splitting. The interaction of the oscillators with one another and the wave guide mode is small and therefore the resulting wavelength of the resonance wavelength is close to the resonance wavelength of the thin mesh. In the interaction regions, the resonance and thickness peaks for thicknesses of 16, 20 and 24μm are plotted in Figure 4.11. All three branches of "thickness peaks" appear with their first peak at a wavelength about equal to the periodicity constant g. Interaction occurs when the thickness t is in the range of the periodicity constant.

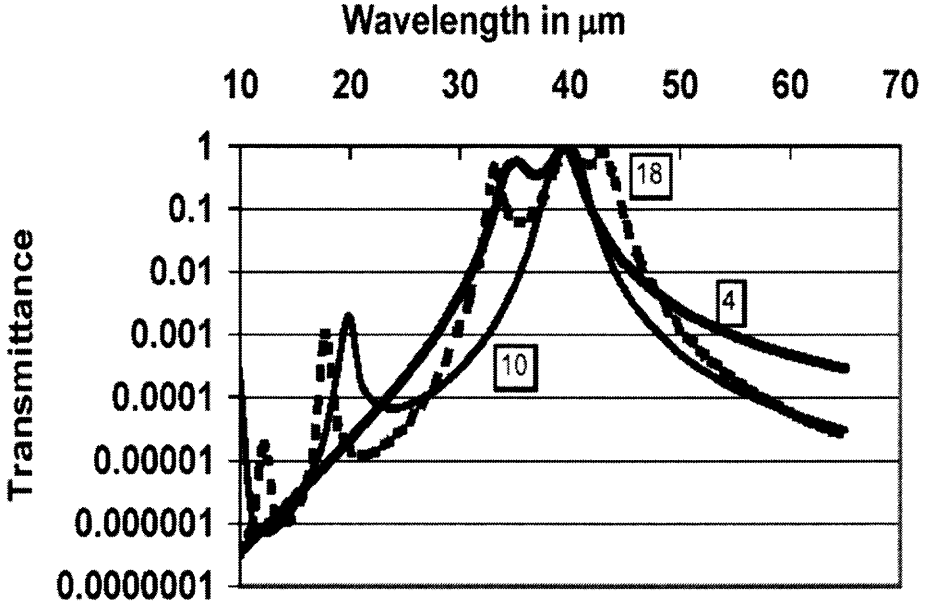

Figure 4.10 Transmission line theory calculations of two oscillators of the same resonance wavelength as used in Figure 4.4, for separation distances of 4, 10 and 18 μm. With increasing distance, the resonance wavelengths show splitting, no splitting and again splitting around 40μm. Waveguide modes appear first at short wavelength and then move to longer wavelength.

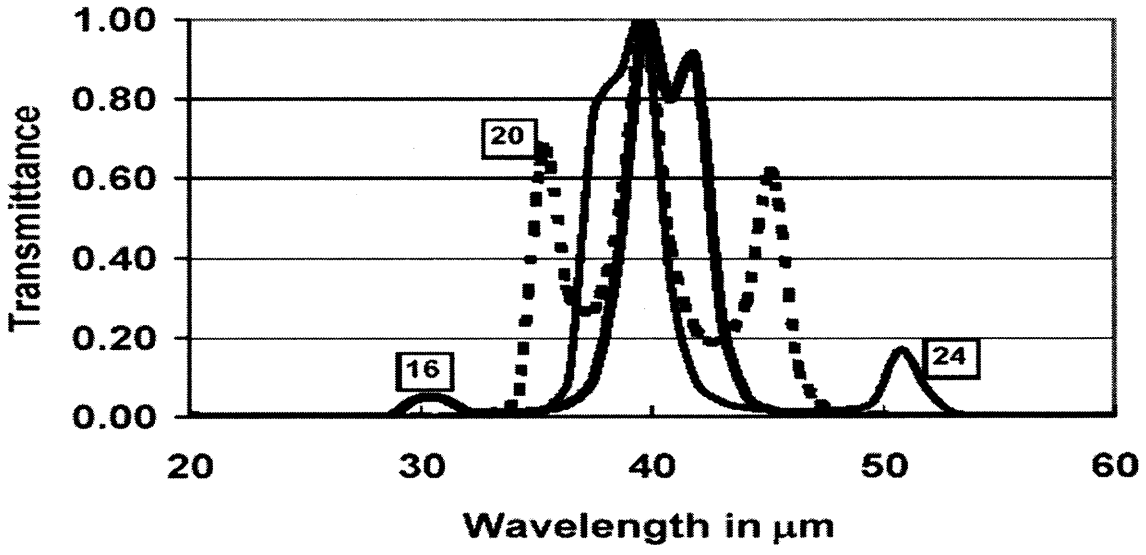

Figure 4.11 The resonance and thickness peaks for thicknesses of 16, 20 and 24μm.

4.5 Discussion

The oscillator model describes the transmittance of the mesh by interaction of the oscillator resonance mode and the waveguide mode. The incident light at normal incidence induces a standing wave mode within the mesh. The mode couples energy of the incident light to the transmitted and reflected light. This induced resonance mode is composed of two standing surface waves, one on each side of the mesh. When the surface waves interact through the openings, the degeneracy is lifted and the resonance is split into two. As the metal thickness increases, the coupling decreases and the resonance peaks are merged into one peak. This is shown in simulations for the short wavelength region as a splitting disappearing for larger thickness, see Figures 4.6 to 4,8, and simulations and experiments in the long wavelength region as a broad peak decreasing in

width, see Figure 4.2. With increasing metal structure thickness, the interaction of the two surface waves deceases and the energy transfer is now accomplished by wave guide modes. The simulations in both spectral regions and the experiments in the long wavelength region show series of new peaks with peak wavelength depending on the thickness of the mesh and shifting to longer wavelength.

The oscillator model has been applied to the interpretation of the transmittance data of cross shaped meshes. The geometrical property of crosses is contained in the input data of the oscillators used in transmission line theory. These input data will be different for square or hole apertures, but the qualitative result will not change much. Martin-Moreno *et al*[26] have calculated thick periodic structures with square shaped openings in the short wavelength region. Transmission data are reported for free standing meshes with periodicity constant g = 750nm, square length of 280nm and five thickness' with t/g values of 0.13, 0.26, 0.4, 0.53, 0.67. The transmittances depending on thickness of these meshes show a resonance and a thickness peak, very similar to our results for crosses and expected from the oscillator model. A thickness peak appears first for t/g = 0.13 at a wavelength close to g. For increasing thickness, the thickness peaks shift to longer wavelength while the resonance peak shifts to shorter wavelength, and both appear together in the range of t/g = 0.4 to 0.67.

The results of Reference [22] have been applied to the interpretation of experimental data on round holes, studied by Ebbesen *et al.*[24] on substrates, and by Grupp *et al.*[25] as free standing structures. Unfortunately, these experimental investigations are done only for a narrow range of t/g values. In Reference [24](Figure 2), one peak is shown, perhaps with an additional shoulder, at t/g of about 0.4 for round holes of

diameter of 400 nm and g = 750nm. For the same *t/g* values and the same g, at shorter wavelength, in Reference 10 though a broad peak with a dip is exhibited for squares of length of 280nm.

There is no extraordinary transmission enhancement in the short wavelength region. In order to normalize the transmittance properly, one needs to take the ratio of the area of the aperture to the unit cell area. The percentage transmittance of the experimental data in the short and long wavelength regions is about 2 to 3 times larger than this ratio. These transmittance enhancements occur via resonance modes, as mentioned for the short wavelength region in Reference [23] and follows from Reference [13] for the long wavelength region.

4.6 Free Standing Thick Capacitive Metal Meshes

4.6.1 Introduction

Capacitive grids may not be realized as free standing grids. However, in the far infrared, one has found[4] that a 2.5 microns thick Mylar substrate has little or no effect on the transmissivity of the metal grids. Babinet's principle in electromagnetic formulation[12,13] tells us that thin metal meshes with complementary pattern will result in complementary transmittances. This is not true for thick metal meshes and important difference will appear for thick capacitive meshes in comparison to thick inductive meshes.

4.6.2 Resonance Wavelength, Transition Region and Thickness Peaks

Using the Micro-Stripes program, the transmittance of thick capacitive cross shaped meshes were calculated for meshes with geometrical parameters g = 20μm, *2a* = 1.5μm,

2b = 3μm, and thicknesses 0.2, 1.0, 3.2,6.4, 9.6, 12.8, 16, 19.2, 22.4 and 25.6 μm , see Figure 4.12 to 4.14. The transmittance shows a stop band for small thicknesses, as expected for capacitive meshes. After a thickness of 6.4μm there appear narrow transmittance regions at shorter wavelength. In Figure 4.15 a graph is shown of the transition from minimum to maximum for thicknesses 11, 12, and 12.8μm. In Figure 4.16 the minima of the stop bands are plotted for thicknesses up to 10μm. The resonance wavelength of these minima have about the same values as the maxima of the corresponding inductive mesh, and exactly the same value for thin meshes. For thicknesses larger than around 10μm, that is to longer wavelength from the transition region, there are maxima and thickness peaks, similar as one has for thick inductive meshes.

The thickness peaks for capacitive meshes are interpreted similarly to as has been done for thick inductive meshes. After a thickness of about g/2 has been passed, Fabry-Perot modes are generated in the openings and the capacitive mesh makes a transition to an inductive mesh. The resonance wavelengths, that are now maxima, of thick capacitive meshes from 16 to 25.6 microns, may be calculated from an empirical formula $\lambda_{Rt} = g/6 + 2t$.

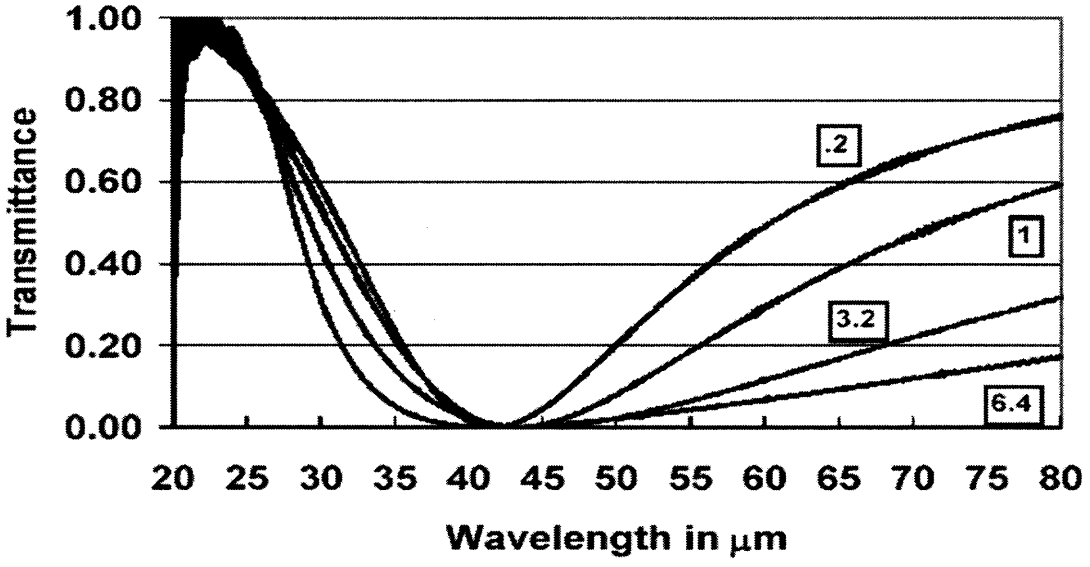

Figure 4.12 Micro-Stripes calculations of the transmittance as function of wavelength for four free standing capacitive cross shaped metal grids with g = 20μm, $2a$ = 1.5μm, $2b$ = 3μm. Thickness in μm are indicated.

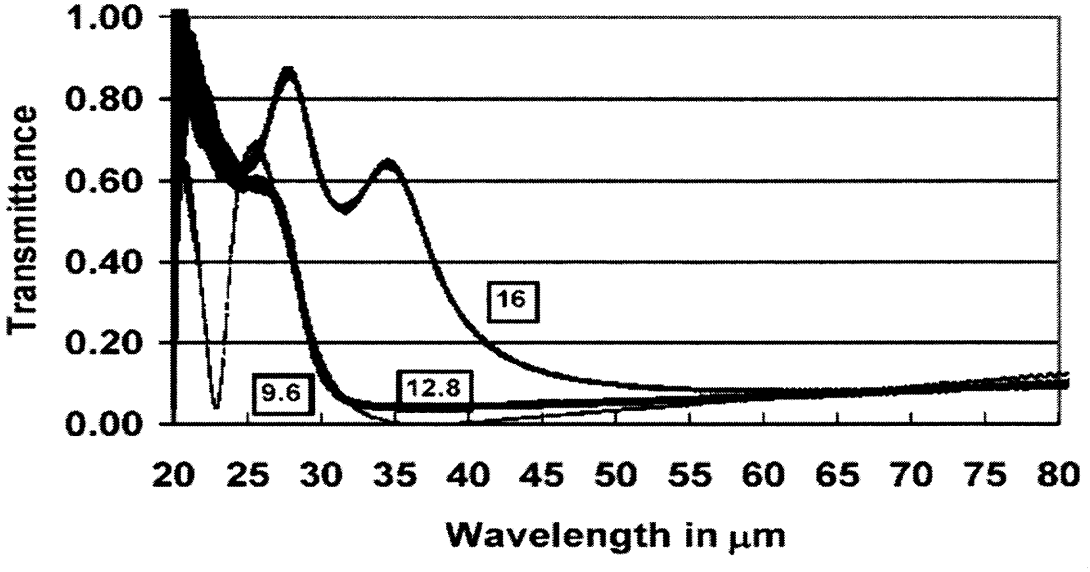

Figure 4.13 Micro-Strips calculation of the transmittance as function of wavelength for three free standing capacitive cross shaped metal grids with g = 20μm, $2a$ = 1.5μm, $2b$ = 3μm. Thicknesses in μm are indicated.

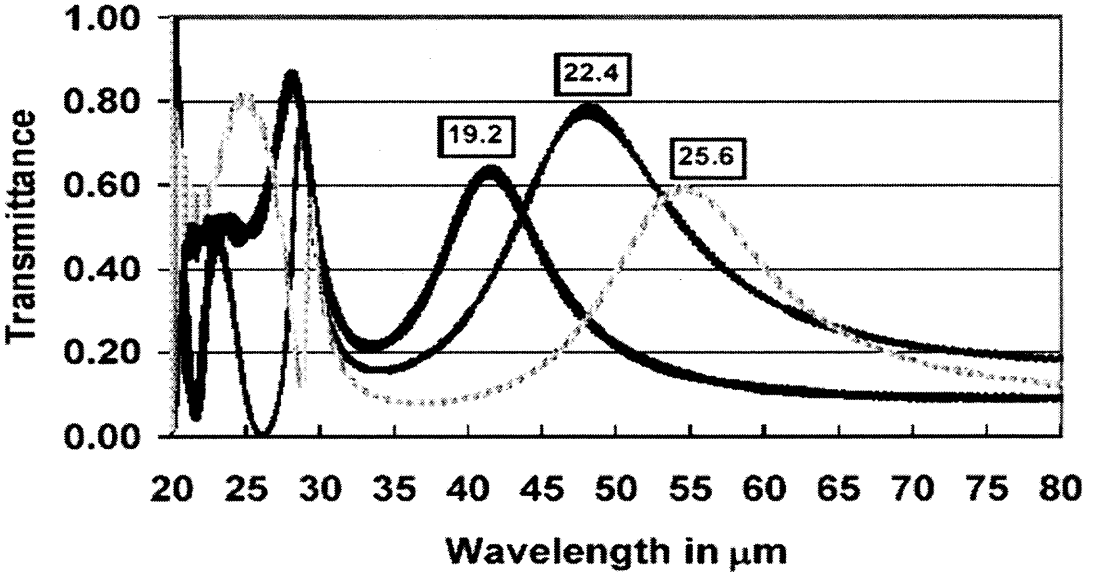

Figure 4.14 Micro-Strips calculation of the transmittance as function of wavelength for three free standing thick capacitive cross shaped metal grids with g = 20μm, $2a$ = 1.5μm, $2b$ = 3μm. Thicknesses in microns are indicated.

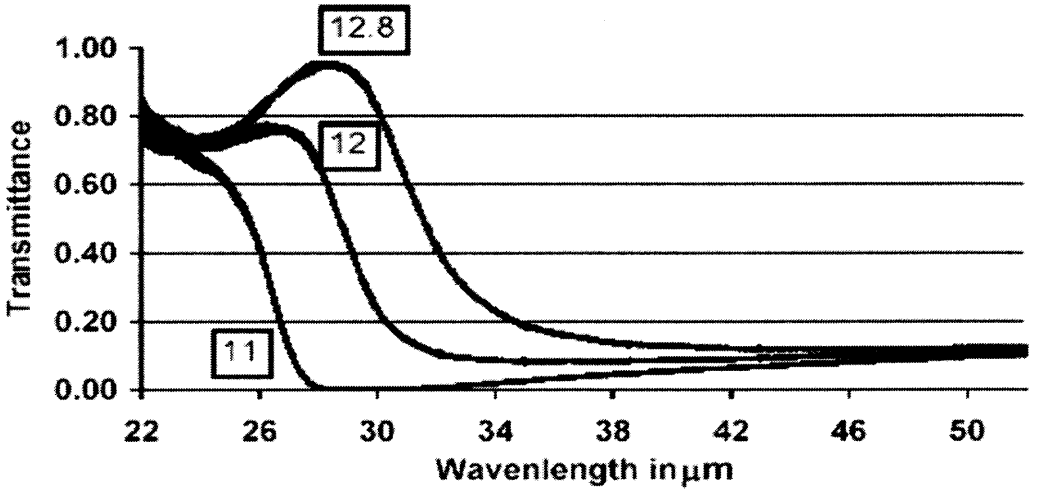

Figure 4.15 Micro-Strips calculation of the transmittance as function of wavelength for three free standing thick capacitive cross shaped metal grids with g = 20μm, $2a$ = 1.5μm, $2b$ = 3μm. The transition from capacitive to inductive mesh is seen for thicknesses of 11, 12, and 12.8 μm.

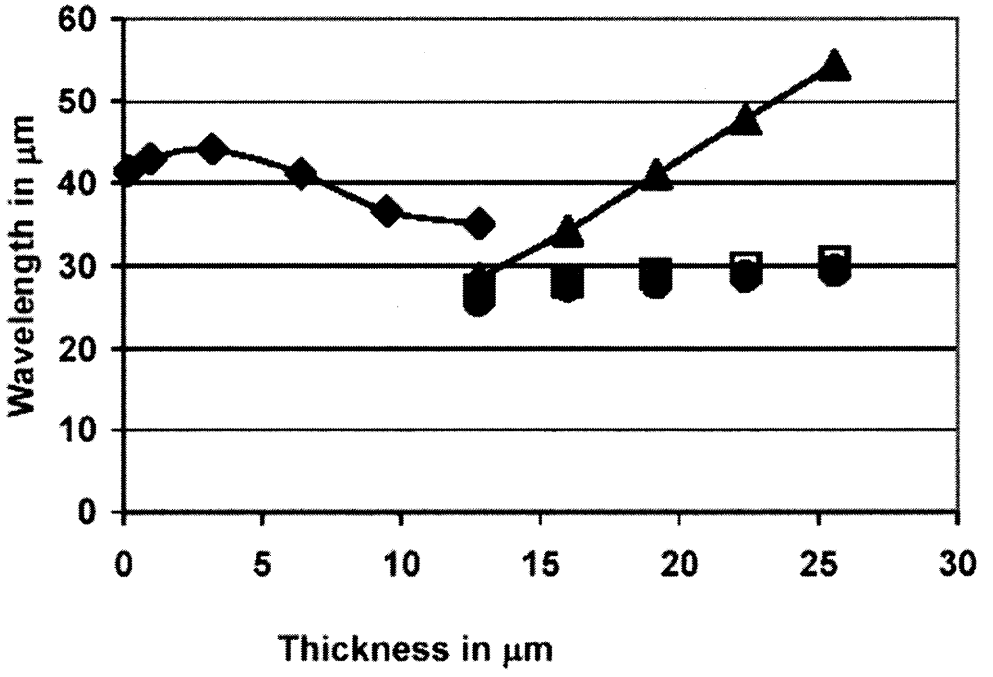

Figure 4.16 Micro-Stripes, graph of wavelengths of resonance and thickness peaks plotted depending on the metal thickness t. Diamonds: Resonance of capacitive meshes (minima). Triangles: Resonance of inductive meshes after transition. Round holes: Thickness peaks. Open squares: Best fit data of thickness peaks with Equation 4.11.

The thickness peaks are again considered as compound mode of resonance and Fabry-Perot mode. Similar to the discussion for inductive meshes, the coupling is described by wave vector addition and the wavelength of the thickness peak is calculated from

$$1/(\lambda_T)^2 = 1/(\lambda_R)^2 + 1/(c_1 g + c_2 t)^2 \qquad (4.11)$$

where λ_R is the resonance wavelength and $\lambda_F = c_1 g + c_2 t$ was taken for the Fabry-Perot mode. A good fit was obtained using $c_1 = 1.15$ and $c_2 = 0.82$, see Figure 4.16 One notes that the coefficients c_1 and c_2 have almost the same values as c_2 and c_1, respectively, for the inductive mesh. The good agreement of this formula for large thicknesses of

capacitive cross shaped meshes with the same g, a, and b values is taken as strong support for the compound mode model described by the interaction of two modes with perpendicular k vectors.

4.6.3 The Oscillator Model for Capacitive grid

The oscillator model describes the transmittance of thick metal meshes by interaction of the oscillator resonance modes, corresponding to the pair of standing surface waves on front and back side of the thick mesh and coupling to wave guide mode. Inductive thick metal meshes have been discussed by assuming that the incident light induces the pair of standing waves on both surfaces and that waveguide modes are generated to transport energy from the incident light to the transmitted and reflected light, increasing the transmittance for certain wavelength regions. Similarly for capacitive meshes, after a certain thickness of the metal meshes has been obtained, waveguide modes are generated and the transmittance in increased in certain wavelength regions.

CHAPTER 5

PHOTONIC CRYSTALS

5.1 Introduction

Stacks of inductive and capacitive metal meshes have recently been considered as photonic band gap structures. Inductive metal layers have been studied by McCalmont *et al.*[28] as multi-layer square shaped metal meshes separated by dielectric layers in the mm spectral region. Fleming *et al*[29] studied in the near infrared layers of metal rod gratings with the rods in a crossed arrangement from layer to layer and separated by dielectric material. An arrangement of metal spheres, which can be considered as a layered structure of capacitive meshes has been experimentally investigated in the millimeter region by Serpenguzel[30].

In Chapter 2 and 3 multi-mesh filters were studied and in particular free standing inductive cross shaped metal meshes at various spacer distances, both free standing and with dielectric spacers. All of the studies in the previous chapters were done for normal incidence and the photonic crystals considered in this chapter are stacks of inductive or capacitive meshes. The coupled oscillator model was applied for the interpretation of the simulations in Chapter 2 and 3. The compound mode, consists of the modes of the metal meshes via a pair of surface waves on both sides on the mesh, and the Fabry-Perot modes which depends distance between the metal meshes, as well as the coupling between Fabry-Perot modes and the surface waves.

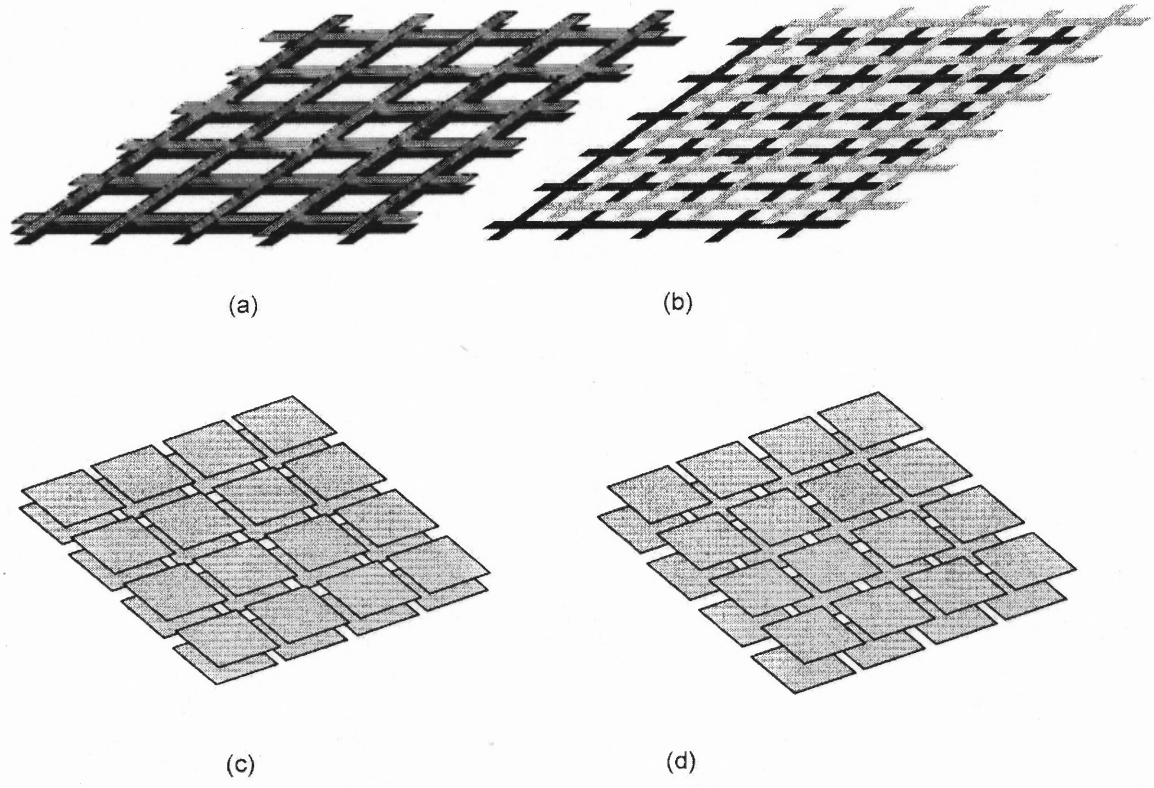

Figure 5.1 Two layers of inductive meshes; aligned (a) and shifted (b). Capacitive meshes; aligned (c) and shifted (d).

5.2 Inductive Cross Shaped Metal Meshes

The Micro-Stripes program allows for one to study the metal meshes of the layers lined up or not aligned configurations, see Figure 5.1a and Figure 5.1b. In contrast, transmission line theory calculations do not include alignment specification.

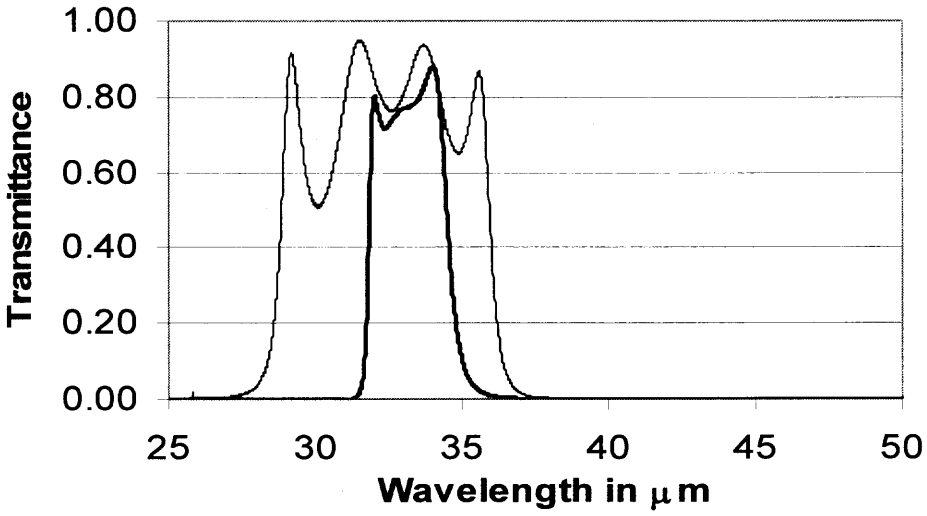

Figure 5.2 Micro-Stripes calculations of four free standing inductive meshes at ¼ λ_R spacing. Bold: aligned, thin: shifted.

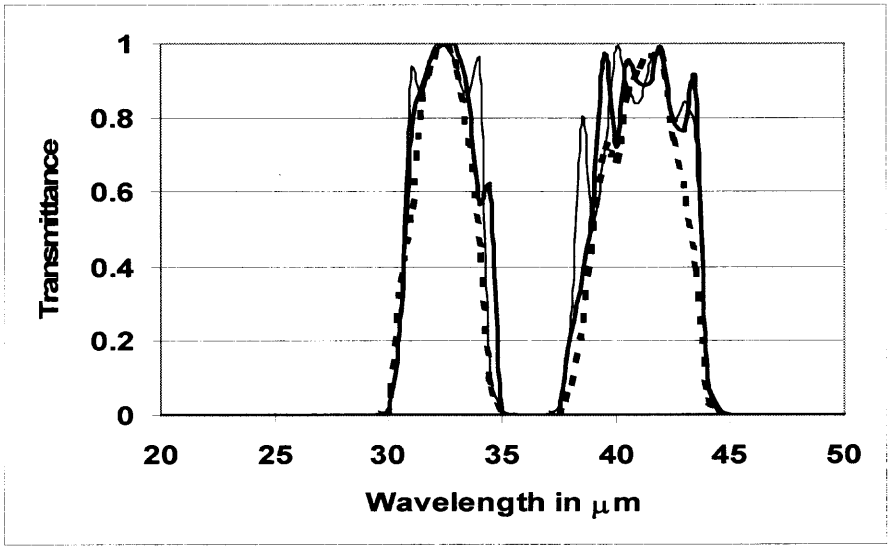

Figure 5.3 Transmission line theory calculations of four inductive meshes with spacing at ¼ λ_R, where the resonance wavelength is taken in the medium. Short wavelength peak, free standing, long wavelength peak, medium of spacers is n = 1.5. Thin: 4 meshes, Bold: 10 meshes, Bold broken: 100 meshes.

5.2.1 Free Standing Inductive Meshes

The transmittance of four free standing inductive cross shaped meshes, aligned and non aligned, at distance of ¼ of the resonance wavelength is shown in Figure 5.2. In Figure 5.3 the transmittance of 4, 10, and 100 layers is shown, calculated using transmission line theory.

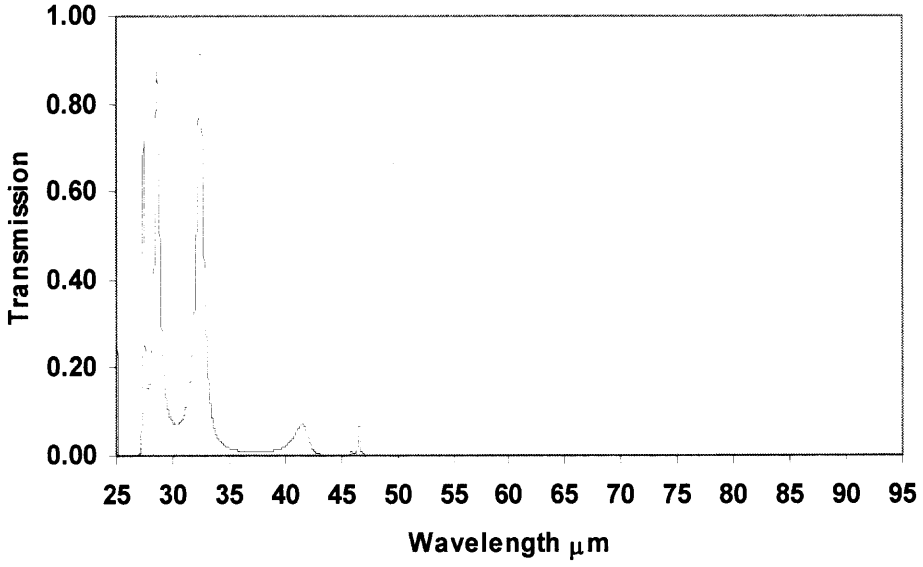

Figure 5.4 Micro-Stripes calculations of four aligned inductive meshes with spacer of n = 1.5 and thickness of ¼ λ_R.

5.2.2 Inductive Meshes with Spacers of Refractive Index n = 1.5

The transmittance of four inductive cross shaped meshes at distance of ¼ of the resonance wavelength in the dielectric is shown for the aligned case in Figure 5.4, and the non aligned case in Figure 5.5, it is observed that there is a greater interaction between all modes. In Figure 5.3 the transmittance of 4, 10, and 100 are shown for layers for dielectric spacers with index n = 1.5, calculated using transmission line theory.

A very narrow transmittance band and very broad gap of no transmittance is shown in Figure 5.2 for four free stranding meshes at distance of ¼ λ_R, for the aligned

case. Each mode of a mesh is composed of a degenerate set of two surface waves on each side of the mesh and together using the placement at a distance of ¼ λ_R, there is minimum interaction of the meshes. The transmission line calculation assumes non-alignment of the meshes but agrees very well with this aligned case and shows also a very narrow transmittance for 4, 10 and 100 layers, see Figure 5.3.

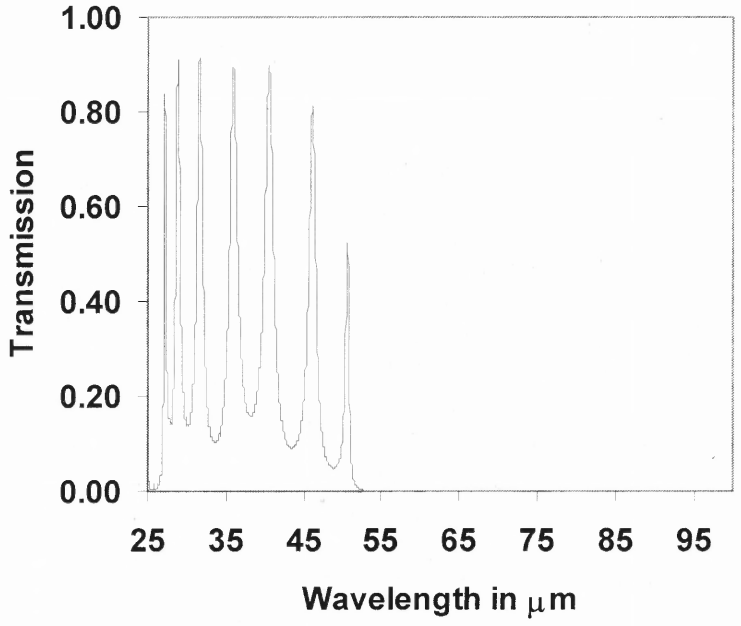

Figure 5.5 Four non aligned inductive meshes with spacer of n = 1.5 and thickness of ¼ λ_R.

The free standing case of non aligned meshes is shown in Figure 5.2, and meshes with dielectric layers in Figure 5.4 and Figure 5.5, all have broader transmittance regions. The appearance of additional peaks indicates stronger interaction of the mesh modes of non aligned meshes and when dielectrics are present with Fabry-Perot modes. As result, for a photonic crystal with a narrow transmittance region, one should use aligned inductive metal meshes at spacing of ¼ λ_R.

5.3 Capacitive Cross Shaped Metal Meshes

The Micro-Stripes program may be used to calculate metal meshes of layers lined up or not aligned, see Figure 1c and Figure 1d and transmission line theory calculations do not include any such specific alignments. While inductive meshes may be used without dielectric support, capacitive meshes need always a substrate. For comparison with the free standing inductive mesh of four layers, capacitive meshes are considered.

5.3.1 Free Standing Capacitive Meshes

The transmittance of four free standing capacitive cross shaped meshes, aligned and non aligned, at distance of ¼ λ_R is shown in Figure 5.6. In Figure 5.7 transmission line theory is used for the calculation of the transmittance of 4, 10, and 100 layers.

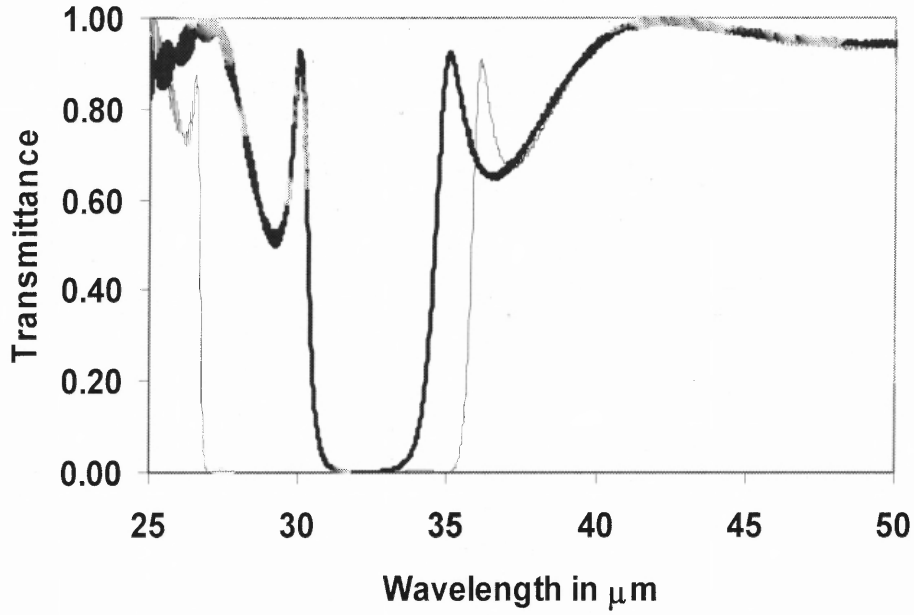

Figure 5.6 Micro-Stripes calculations of four free standing capacitive meshes at ¼ λ_R spacing. Bold: aligned, thin: shifted.

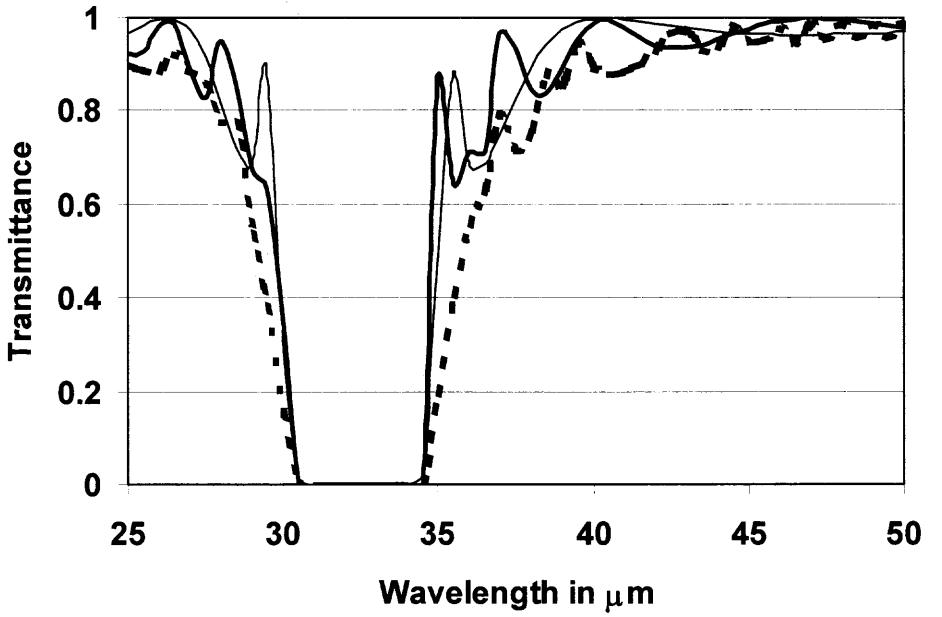

Figure 5.7 Transmission line theory calculations of four free standing capacitive meshes with spacing at ¼ λ_R. Thin: 4 meshes, Bold: 10 meshes, Bold broken: 100 meshes.

5.3.2 Capacitive Meshes with Spacers of Refractive Index n = 1.5

The transmittance of four capacitive cross shaped meshes at distance of the resonance wavelength in the dielectric is shown for the aligned case in Figure 5.8. Transmission line calculations of the transmittance of 4, 10, and 100 layers are shown in Figure 5.9, using dielectric spacers of refractive index n = 1.5 and thickness of ¼ λ_R in the medium.

Comparing the free standing case of non aligned meshes, shown in Figure 5.6, and meshes with dielectric layers, Figure 5.8, one observes that the shifted free standing and the unshifted(aligned) meshes in medium of n = 1.5 have broader bandstop regions. The broadening indicates stronger interaction of the mesh modes for the non aligned meshes and with the Fabry-Perot modes in the dielectric.

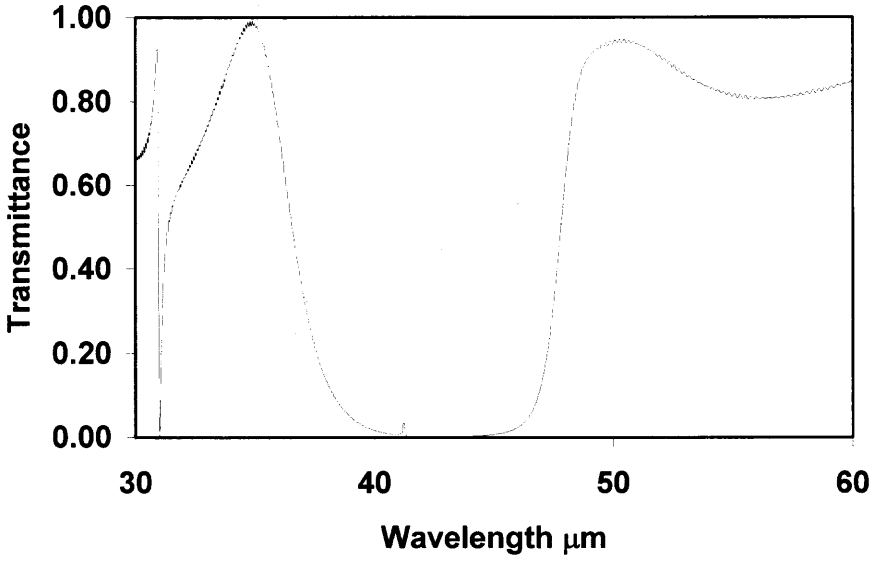

Figure 5.8 Micro-Strips calculations of four capacitive meshes, aligned, with dielectric spacers of ¼ resonance wavelength in the medium n = 1.5.

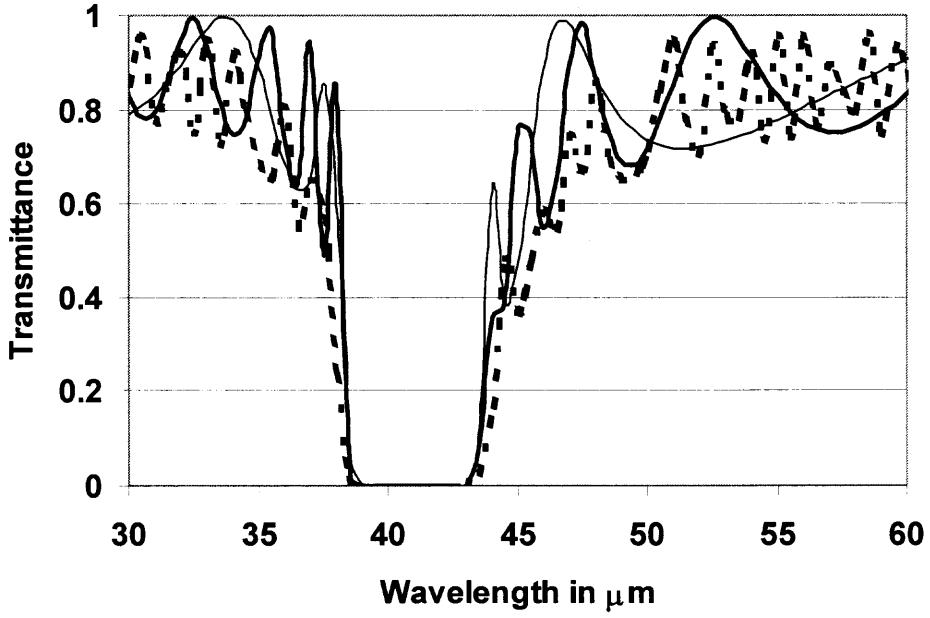

Figure 5.9 Transmission line theory calculations of capacitive meshes with dielectric spacers of ¼ resonance wavelength in the medium. Thin: 4 meshes, Bold: 10 meshes, Bold broken: 100 meshes.

A similar result was found for inductive meshes. The transmittance region was narrow for aligned inductive metal meshes at spacing of ¼ λ_R. However, for practical purposes (capacitive grids cannot be suspended in air), capacitive meshes need a thin substrate.

In Figure 5.10 a comparison is shown for free standing capacitive meshes at spacing of 1/4 and 1/2 resonance wavelength. One observes that the bandstop region is narrower for ¼ of the resonance wavelength.

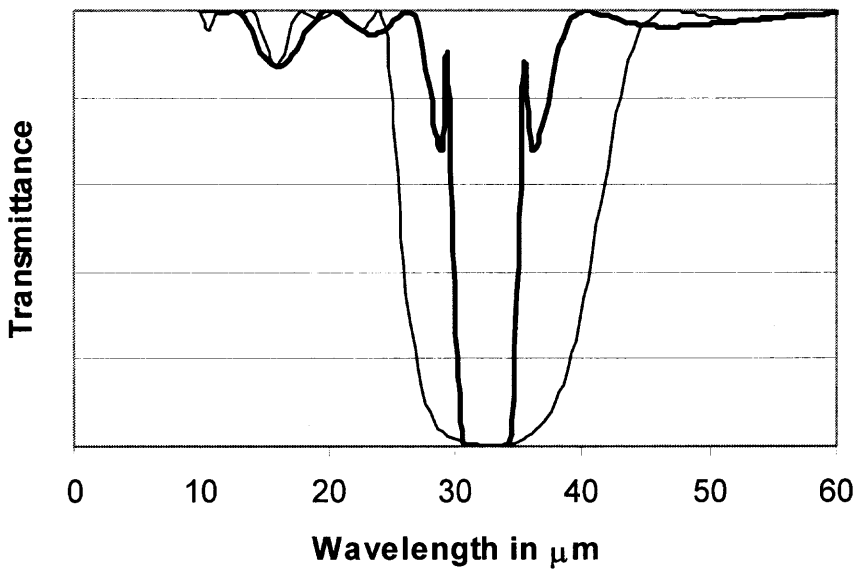

Figure 5.10 Transmittance of 2 freestanding capacitive meshes at distance of λ/4 (bold) and λ/2 (thin solid).

5.4 Metal Meshes and Photonic Crystals

One should recall that all calcuations are done for normal incidence. The transmission line theory calculations are in good agreement with the result obtained for the aligned meshes of four layers. A cubic photonic crystal may be considered to be made of a large set of aligned layers. Transmission line theory predicts that the width of the transmittance is about the same for small and large numbers of layers. The layers are presented by oscillator modes with resonance wavelength depending on the geometry of the metal mesh structure. Therefore the position of the transmission or stop band can be calcualted from the geometrical structure of the metal mesh. The smaller width of transmittance or bandstop regions is obtained for a spacing of ¼ λ_R, and in contrast for 1/2 λ_R the width is much larger, see Figure 5.10. The use of the Bragg condition for the determination of reflection maxima uses only the concept of optical path difference in interference from the reflecting layers. The description using resonance oscillators for the layers and their interaction determines the wavelength of transmitted or reflected maxima by the resonance wavelength of the layer and interaction between them.

CHAPTER 6

SUMMARY AND CONCLUSION

6.1 Thin Free Standing Meshes

A single free standing metal mesh is well described by a resonance mode with oscillation dependence of the resonance wavelength on the geometrical parameters of the mesh. The intensity depends on the surface impedance of the metal and does not show in the long wavelength region much of difference for good conductors.

A set of n meshes at equal separation shows n resonance modes and (n-1) first order Fabry-Perot modes, generated between the planes of the resonance modes, however the latter not appearing for very small separations. All modes show interaction depending on the separation of the meshes, and minimum interaction is at a value of separation equal to ¼ of the resonance wavelength. In stacks of meshes with crosses aligned in their position with respect to next neighbor meshes, there is little interaction of the resonance modes for a large range of spacing around the ¼ resonance wavelength spacing. For the non-aligned case strong interaction exist, even at around ¼ resonance wavelength spacing.

6.2 Thin Free Standing Meshes and Dielectrics

The resonance wavelength of the mode of a single free standing mesh on a thick substrate shifts to longer wavelength by an amount smaller than the refractive index of the substrate. Reduction of thickness of a thin substrate reduces the shift of the resonance wavelength and demonstrates the extent of the surface wave in normal direction. At a

very small value of the substrate the resonance wavelength is approaching the resonance wavelength of the free standing mesh.

The resonance wavelength of the mode of a single free standing mesh embedded in thick dielectric layers shifts to longer wavelength by an amount equal to the refractive index of the dielectric. The behavior-extent of the surface waves into normal direction is similar as for the metal mesh on a substrate.

A set of n meshes at equal separation shows n resonance modes and (n-1) first order Fabry-Perot modes, generated between the planes of the resonance modes, however they do not appear for very small separations. All modes show interaction depending on separation and value of the refractive index and have minimum interaction at a value of separation equal to ¼ of the resonance wavelength.

In stacks of meshes with crosses aligned in their position with respect to next neighbor meshes, there is little interaction of the resonance modes for spacing around ¼ wavelength for refractive index n = 1.5 and 3.4, while one has large interaction for meshes with non aligned crosses.

The Wood anomaly appears at a wavelength equal to the product of the refractive index and the periodicity constant. It is interpreted as the value of the wavelength for which the diffraction angle is 90^{o}, diffraction is not any longer possible and an evanescent wave appears. The wavelength of the Wood anomaly does not depend on the geometrical parameters of different periodic structures for a number of meshes[17]. The dependence on the refractive index of the Wood anomaly of the periodic metal structure could be confirmed by simulations, and experiments[17].

6.3 Thick Metal Meshes

Thick inductive metal meshes are described by compound modes consisting of resonance modes corresponding to surface waves on each side of the metal mesh and waveguide modes of the openings. These two modes interact and appear as two transmission peaks. The resonance mode shows little interaction with the waveguide mode and has about the same wavelength as one has for thin meshes. The waveguide modes of the openings interact with the resonance modes depending on the thickness of the metal. Their wavelength is obtained by vector addition of the perpendicular k vectors of both modes. Calculations using the Fourier modal method showed similar results in the 1 microns region, deducing that the analysis for meshes for the longer wavelength in general can be applied to the near infrared region. Extraordinary transmittance reported[24] of inductive metal meshes in this spectral region could be referred to as a simple resonance phenomenon.

According to Babinet's principle in electromagnetic formulation, thick capacitive metal meshes are not complementary to thick inductive metal meshes. They have transmission minima at the resonance wavelength but also show waveguide peaks at larger thickness. The interaction of the waveguide peaks with the resonance wavelength is so strong that the transmittance of a thick capacitive mesh is similar to an inductive thick mesh.

6.4 Thin and Thick Metal Meshes as Photonic Crystals

Metal dielectric photonic crystals have been constructed by stacks of aligned inductive meshes with dielectric spacers, See Reference [28]. These photonic crystals are considered to be made of identical layers and all have the same distance from one another. The resonance wavelength of one layer depends on the geometrical parameters of the metal structure. They are described similarly as done for four inductive metal meshes with dielectric spacers, as discussed in Chapter 3, and the extension to 10 or 100 layers, as discussed in Chapter 5.

6.5 Thin and Thick Metal Meshes as Filters for the Astrophysical Community

The astrophysical community needs for space missions in the infrared region, filters with a fixed resonance wavelength and a width of the transmission band of about 10%. Emission measurements are conducted on astro-physical objects, such as galaxies. Filters using metal meshes, as a Fabry-Perot type filter, are used in the far infrared, from 60 to 1000 microns. These filters can not be made in the 20 to 60 micron region because of the increasing manufacturing difficulties of the small geometrical pattern required as reflector plates and critical spacer thickness in the shorter wavelength region. In the 20 to 60 micron region, inductive cross shaped meshes can be used as two coupled oscillator filters at distance of ¼ wavelength for minimum interaction. The geometrical pattern may well be fabricated and the spacing of the meshes is considerable less critical to change the resonance wavelength as in a Fabry-Perot filter. Cross shaped meshes on polyimide or polypropylene may be manufactured and the geometrical design parameters can be

assumed from a study using Micro-Stripes calculations. In a special geometrical arrangement, with metal meshes facing one another, the final resonance wavelength can be determined by transmission line theory. Free standing inductive metal meshes show an advantage. They have a smaller width of band for the same design parameters used for the thin meshes on dielectric substrates. The question which of the two mesh filters, the meshes on substrate or the free standing meshes, are better has to be determined form experimental manufacturing of such filters and studying the conduction losses of the meshes.

APPENDIX A

MICRO-STRIPES OVERVIEW

Micro-Stripes[10] is a powerful software program ideal for the design of waveguide components, non-planar circuit structures, and variety of antennae. Micro-Stripes provide 3D electromagnetic analysis of arbitrary geometries yielding results in time/frequency domain. The simulator uses the Transmission Line method (TLM). The TLM method is based on establishing a network of transmission lines that represents the physics of the problem, and finding equivalence between the electrical solutions of that network and the physical parameters of the problem.

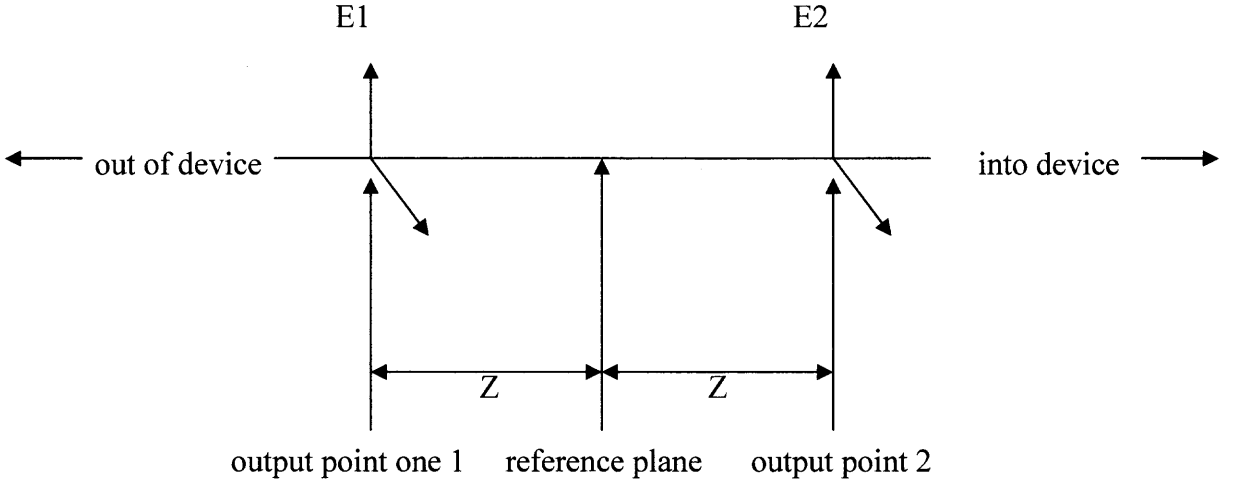

Figure A.1 The data required of the 3D-simulater by resolve wave consists of a record of two field components at two points in each port of the simulated device. The analysis is done in the time domain at each output point and then is transformed to the frequency domain.

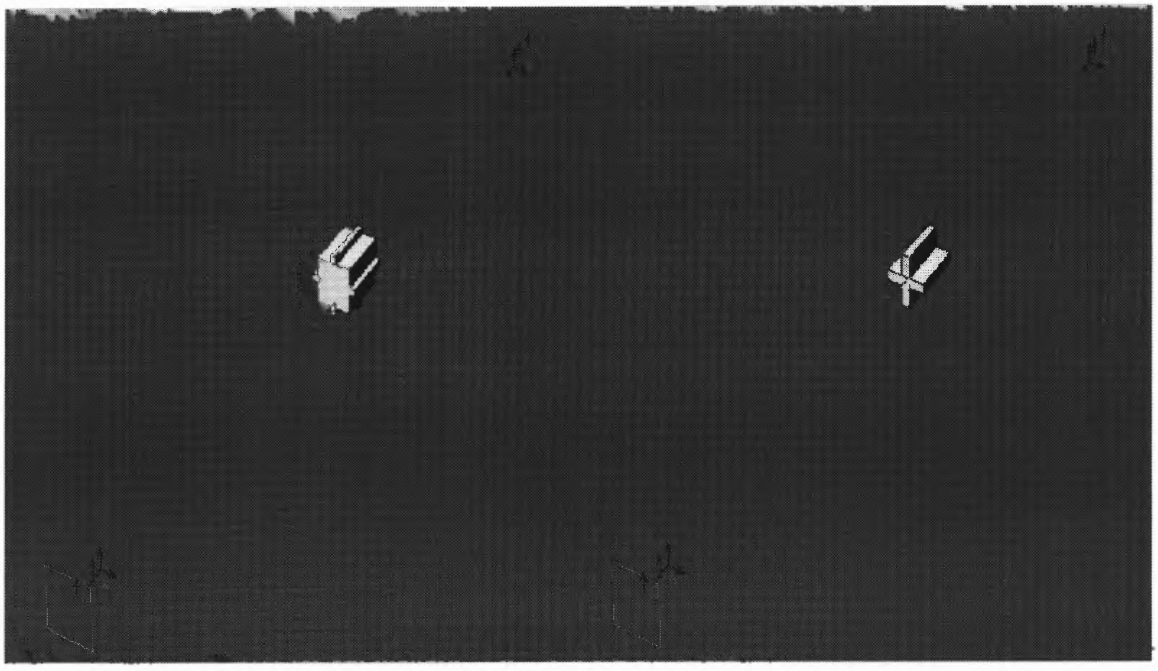

Figure A.2 Inductive /Capacitive Grid 3d-View.

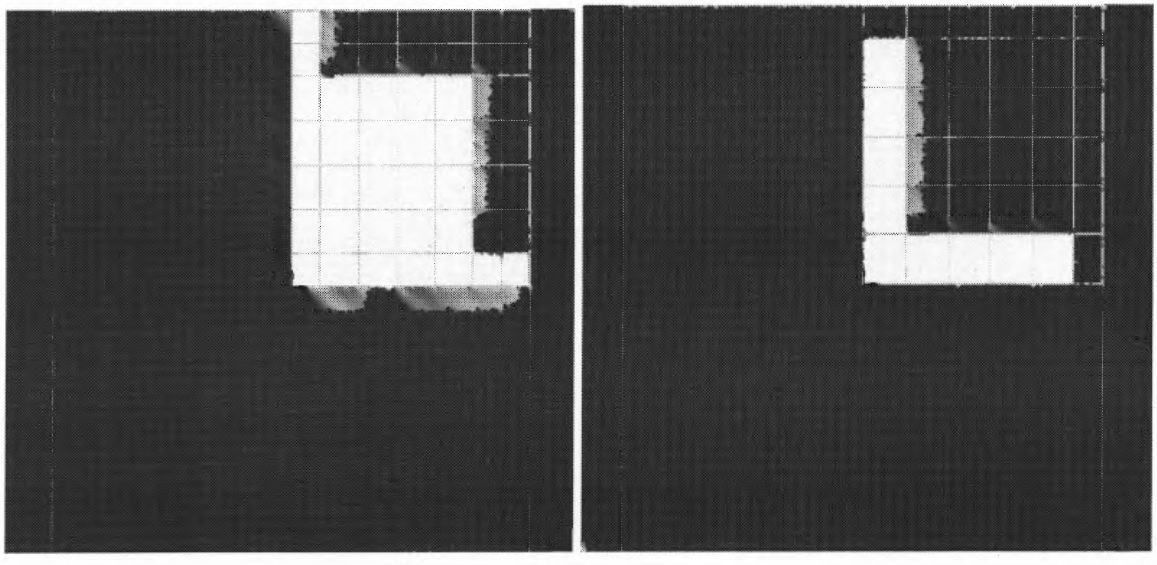

Figure A.3 Inductive/Capacitive grid front elevation profile.

The directional output shown in Figure A.1 is simply a record of the ingoing and outgoing signals at the port. These signals are resolved by comparing E and H fields at two points, one on each side of the reference plane. The arrangement is closely analogous to monitoring the signals in a waveguide by attaching a directional coupler. To get a directional output in a waveguide, it is only necessary to place two time-domain output points on a line parallel to the waveguide axis.

In order to construct the computational mesh, a workspace needs to be defined, followed by the construction of the mesh. Each mesh is actually defined by a small rectangular homogenized cell and each cell is entirely empty or entirely filled with the same metal or dielectric. Accuracy is improved with a greater amount of cells(greater accuracy means longer calculation time) . Micro-Stripes simulator works in the time domain. Depending on the size of the problem, it can take as much as several seconds of computer run- time to simulate each nano-second in real time. The duration of the simulation is the length of time simulated – it is proportional to the computer run-time, and is consequently limited by the patience of the user.

APPENDIX B

FABRICATION OF METAL DIELECTRIC HYBRID

Since the invention of the first integrated circuit in 1960's there has been an ever-increasing density of devices manufactured on semiconductor substrates. Silicon technology has remained the dominant force in integrated fabrication and is likely to retain this position in the foreseeable future. There are two main steps in the course of manufacturing integrated circuits. These steps can be grouped into two phases: 1) design phase, and 2) fabrication phase. The standard fabrication phase for some of the meshes in this thesis is outlined below[31]

Step 1-Wafer Preparation

In order to prevent/remove an array of contamination it is necessary to remove organic/metallic contaminant on bare Silicon, proper cleaning is necessary. The "Cleaning" is often referred to as an RCA clean. The typical solvent for an RCA clean consists of very aggressive solvents. The most commonly used mixture is 7 parts sulfuric acid H_2SO_4(98%) and 3 parts 30% H_2O_2. This solution has earned (rightly so) the name of "pirrhana clean", because it attacks organic materials so aggressively. Wafers are immersed in piranha at 100-130^{0}C for about 10 minutes. Upon removal the wafers are vigorously rinsed in de-ionized water.

Step 2- Sputter Deposition

Sputtering is a term used to describe the mechanism in which atoms are ejected from the surface of a material when that surface is struck by sufficiently energetic particles. It has become the dominant technique for depositing a variety of metallic films in VLSI and ULSI fabrication, including aluminum alloys, titanium, titanium: tungsten, titanium nitride, tantalum, and cobalt.

Step 3- Wet cleaning of metal-Coated wafers

Once metal is deposited on a wafer, the aggressive acids and alkali solutions used in the RCA clean can no longer be used. Instead, cleaning must be done with less reactive solvents. The most common solvent used is n-methly-pyrrolidone (NMP). In some case this step might be omitted.

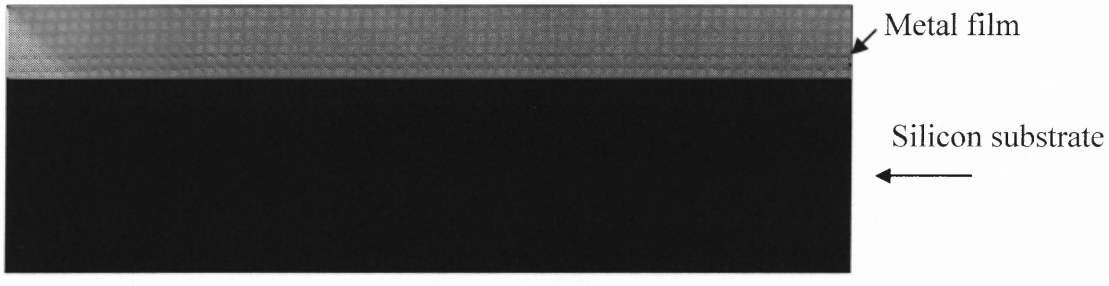

Figure B.1 Sputtered metal film on top of a silicon wafer.

Step 4- Resist Processing: Spin Coating

Following cleaning, drying, and priming, the wafers are ready to be coated with the photoresist. The goal of the coating step is to produce a uniform, adherent, defect-free polymeric film of a desired thickness over the entire wafer which adheres well to the substrate. This procedure is carried out by dispensing the resist solution onto the wafer surface, and then rapidly spinning the wafer until the resist is almost dry.

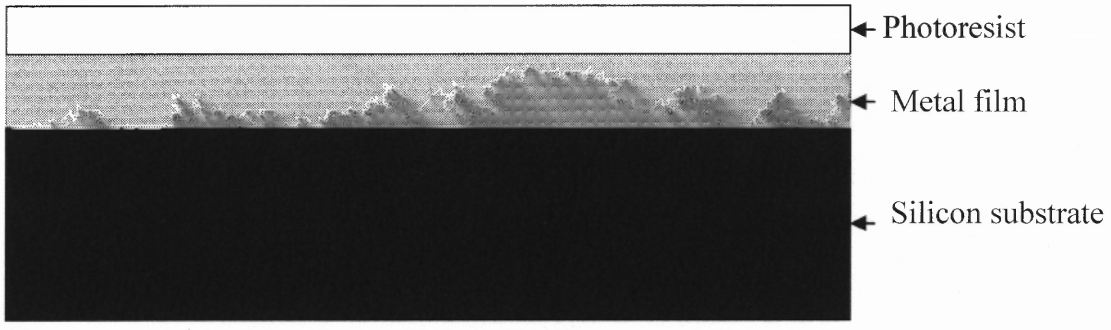

Figure B.2 A spun photoresist film on top of a metallic film, mounted on top of a Silicon Wafer. (Figure not to scale).

Step 5 Resist Processing: Soft-Bake

After the wafers are coated with the resist, they are subjected to a baking step called soft-bake (or pre-bake or post-apply bake). Several important functions are accomplished by this step. First, solvent is driven out of the spun-on resist, reducing its level in the film to about 5%, and the liquid-cast film is converted into solid form. Second, soft-baking improves the adhesion of the resist by relieving film stress that arises from the shear forces encountered in the spinning process. If not relieved, such stresses could enhance the tendency of the resist to delaminate. The standard technique for soft-baking ULSI resists used vacuum hot-plate-baking, in most standard cases hot plates provide better

temperature and uniformly control than that of ovens. In hot-plate baking, one wafer at a time is processed, with the heat being conducted to the wafer through its backside. In this step the resist is heated quickly to the desired temperatures, and the soft bake cycle can be short.

Step 6- Resist Processing: Exposure

After a wafer has been coated with resist and suitably soft-baked, it is ready to be exposed to some form of radiation in order to create a latent image in the resist. The degree of exposure is adjusted by controlling the energy impinging on the resist. An energy integrator is used to detect the total energy striking a unit area of a resist, and automatically adjusts the time of exposure to compensate for aging variation in the source.

Step 7- Resist Processing: Post-Exposure Bake (PEB)

The post-exposure (and pre-develop) bake step subjects the resist to a temperature 5-15^{0}C higher than the soft-bake step. This step causes an unexposed region to diffuse through the resist an averaging effect across the exposed/unexposed boundary.

Step 8- Resist Processing: Development

Following exposure and post-exposure-baking, the resist film must undergo development to turn the latent image in the resist into the final resist image. The resist image, which results after development serves as the mask in a subsequent etching, steps. Development

is another of the critical steps in the photo resist process, and often entails both extensive process development efforts and stringent control after it put into production.

Step 9- Resist-Processing: Post-Development-Bake

Post-Development-bake, or hard baking is a process that subjects the resist to an elevated temperature after completion of development, and it performed prior to etching or implant. Its chief functions are to remove the residue solvents, to improve adhesion, and to increase the etch resistance of the resists. Hard baking, like soft baking are normally done using vacuum hot plates. After soft baking the resist contains about 5% solvent, and hard baking reduces this value even further

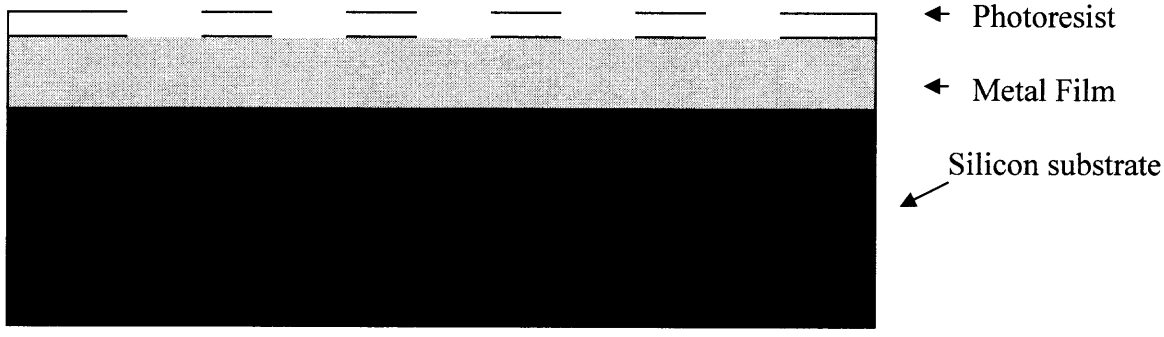

Figure B.3 Developed photoresist prior to etching. Metal spunned mesh on top of a silicon substrate (Figure not up to scale).

Etching in microelectronics is a process by which material is removed from the silicon substrate (or from thin films on the substrate surface) by chemical reaction with a reagent material (etching solution). When a mask layer is used to protect specific regions of the

wafer surface, the main goal of etching is to precisely transfer the pattern created by the mask onto the wafer surface by removing the material not covered by the resist.

Wet chemical etching was the standard pattern transfer technique when early generation of integrated circuits were fabricated. Its widespread use was based upon two factors. First wet etching technology was well-established from its long use in the printing industry. Second, liquid etchent systems are available which selectively remove only the material to be etched (and not the materials beneath them), and most of these do not attack photoresist. However, wet chemical process typically etches in all directions at the same rate.

Step 10- Photo-Resist Removal

Photoresist must be removed following a variety of processing steps, such as etching, and high temperature post-baking. And simple removal of misaligned resist patterns for re-imaging after development and inspection. The main objective in resist stripping is to insure that all the photoresist is removed as quickly as possible without attacking any underlying surface materials. Cleaning is typically done with NMP.

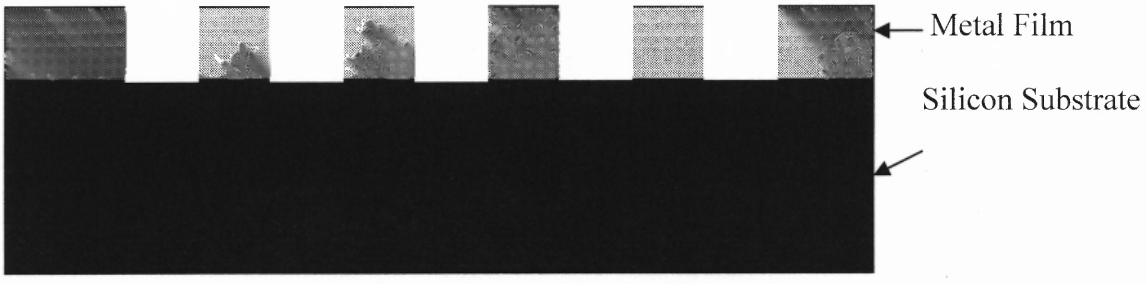

Figure B.4 Patterned, and etched metal mesh on top of a silicon substrate (Figure not up to scale).

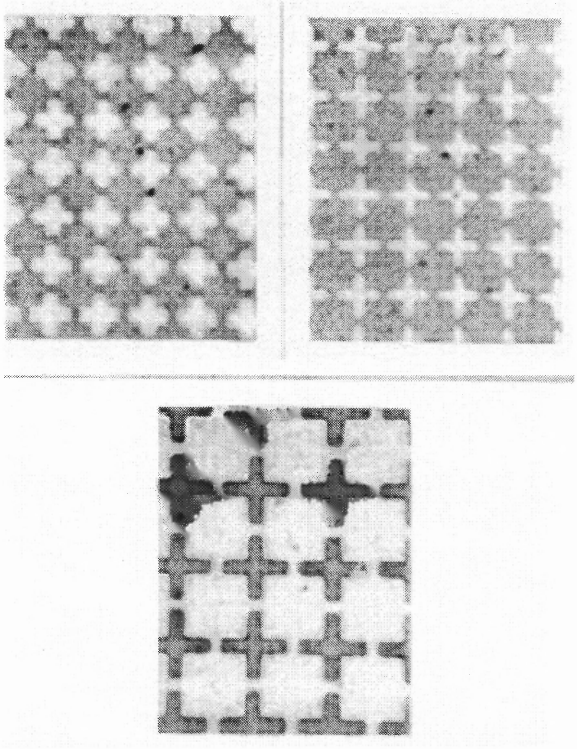

Figure B.5 Photograph of experimental Inductive and capacitive cross shaped metal meshes on silicon substrate.

APPENDIX C

TRANSMISSION LINE THEORY AND MATHCAD

There are three important parameters used in transmission line theory of metal meshes. The parameters are the resonance wavelength, bandwidth and the loss parameter. The transmittance of a mesh with resonance wavelength λ_R of a single mesh, corresponding to the normalized frequency $\omega_0 = g/\lambda_R$, is obtained from Micro-Stripes calculations and used as a parameter.

A shift of the resonance wavelength factor $((n_1^2 + n_2^2)/2)^{1/2}$ is implemented for the case of a metal meshes with an interface of two dielectrics of refractive index n_1 and n_2. The width of resonance band parameter A1 is obtained by adjusting the transmission line transmittance curve to the Micro-Stripes transmittance curve. The loss parameter a1 is taken as 0.001 from Reference [18] and [19].

Inductive Configuration

One mesh, substrate or embedded

$g := 24 \qquad i := \sqrt{-1} \qquad \omega o := \frac{g}{\lambda o} \qquad \lambda := 10, 10.5 .. 180$

$$\omega 23 := \omega o \cdot \sqrt{\frac{2}{(n2^2 + n3^2)}}$$

$$\Omega 23(\lambda) := \left[\frac{g}{\lambda} \cdot (\omega 23)^{-1} - \frac{\omega 23 \cdot \lambda}{g} \right]$$

$$Y23(\lambda) := \frac{1}{a1 - \frac{i \cdot \omega 23 \cdot A1}{\Omega 23(\lambda)}}$$

Matrix for interface of first dielectrics, M1

$$M111(\lambda) := \frac{n1 + n2}{2 \cdot n1} \qquad M121(\lambda) := \frac{(n1 - n2)}{2 \cdot n1}$$

$$M112(\lambda) := \frac{(n1 - n2)}{2 \cdot n1} \qquad M122(\lambda) := \frac{n1 + n2}{2 \cdot n1}$$

$$M1(\lambda) := \begin{pmatrix} M111(\lambda) & M112(\lambda) \\ M121(\lambda) & M122(\lambda) \end{pmatrix}$$

Matrix of first dielectric n2, thickness d1, M2

$$M211(\lambda) := e^{\frac{-i \cdot 2 \cdot \pi \cdot n2 \cdot d1}{\lambda}} \quad M212(\lambda) := 0 \quad M221(\lambda) := 0 \quad M222(\lambda) := e^{\frac{i \cdot 2 \cdot \pi \cdot n2 \cdot d1}{\lambda}}$$

$$M2(\lambda) := \begin{pmatrix} M211(\lambda) & M212(\lambda) \\ M221(\lambda) & M222(\lambda) \end{pmatrix}$$

Figure C.1a Page 1, MATHCAD output of an inductive mesh, substrate/embedded configuration. ω23, shifted frequency, g the periodicity constant, M1 Matrix (Interface, from n1 to n2), M2 Second Matrix (Propagation Inside dielectric n2), Y Shut Impedance.

Matrix of first mesh, M3

$$Ma311(\lambda) := \frac{-Y23(\lambda)}{2 \cdot n2} + \frac{n2 + n3}{2 \cdot n2} \qquad Ma312(\lambda) := \frac{-Y23(\lambda)}{2 \cdot n2} + \frac{n2 - n3}{2 \cdot n2}$$

$$Ma321(\lambda) := \frac{Y23(\lambda)}{2 \cdot n2} + \frac{(n2 - n3)}{2 \cdot n2} \qquad Ma322(\lambda) := \frac{Y23(\lambda)}{2 \cdot n2} + \frac{n2 + n3}{2 \cdot n2}$$

$$M3(\lambda) := \begin{pmatrix} Ma311(\lambda) & Ma312(\lambda) \\ Ma321(\lambda) & Ma322(\lambda) \end{pmatrix}$$

Matrix for thickness d2 and n3, M4

$$M411(\lambda) := e^{\frac{-i \cdot 2 \cdot \pi \cdot n3 \cdot d2}{\lambda}} \quad M412(\lambda) := 0 \quad M421(\lambda) := 0 \qquad M422(\lambda) := e^{\frac{i \cdot 2 \cdot \pi \cdot n3 \cdot d2}{\lambda}}$$

$$M4(\lambda) := \begin{pmatrix} M411(\lambda) & M412(\lambda) \\ M421(\lambda) & M422(\lambda) \end{pmatrix}$$

Matrix to get from third dielectric to outside, M5

$$M511(\lambda) := \frac{n3 + n4}{2 \cdot n3} \qquad M512(\lambda) := \frac{(n3 - n4)}{2 \cdot n3}$$

$$M521(\lambda) := \frac{(n3 - n4)}{2 \cdot n3} \qquad M522(\lambda) := \frac{n3 + n4}{2 \cdot n3}$$

$$M5(\lambda) := \begin{pmatrix} M511(\lambda) & M512(\lambda) \\ M521(\lambda) & M522(\lambda) \end{pmatrix}$$

$$Mf(\lambda) := M1(\lambda) \cdot M2(\lambda) \cdot M3(\lambda) \cdot M4(\lambda) \cdot M5(\lambda)$$

$$tf(\lambda) := \frac{1}{Mf(\lambda)_{1,1}}$$

$$Tf(\lambda) := tf(\lambda) \cdot \overline{tf(\lambda)} \qquad \textbf{Transmittance}$$

Figure C.1b Page 2, inductive mesh, substrate/embedded configuration. M3 Matrix (n2 to n3,Y), M4 Matrix (Propagation Inside dielectric n3), M5 Matrix (Interface, from n3 to n4). Mf Final Matrix product; Tf- final transmittance.

$A1 \equiv .1 \qquad n1 \equiv 1 \quad n2 \equiv 1.5 \quad n3 \equiv 1.5 \qquad n4 \equiv 1$

$a1 \equiv .001 \qquad d1 \equiv 50 \qquad d2 \equiv 50 \qquad \lambda o \equiv 32.4$

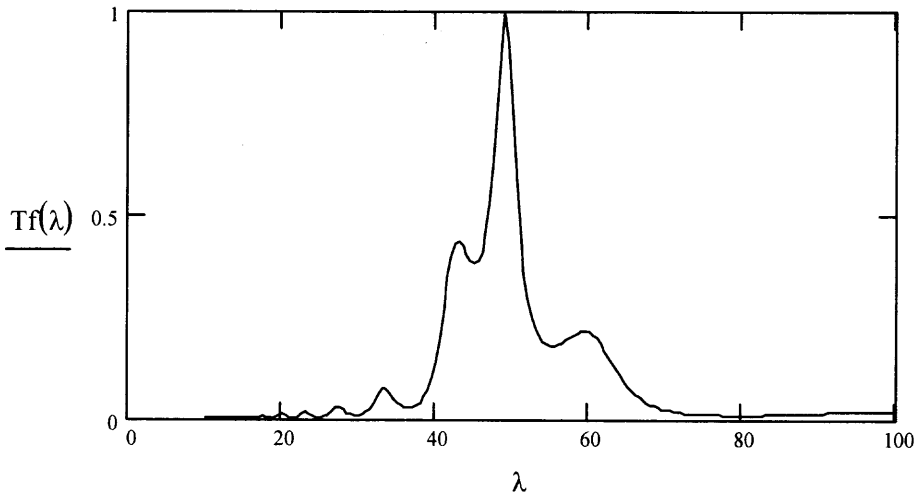

Figure C.1c Page 3, MATHCAD output Inductive mesh, substrate/embedded configuration. A1-the bandwidth Parameter, a1- the loss parameter, λ_0- the resonance wavelength (free standing), d1, d2- dielectric thickness, Tf- Transmittance.

N+2 inductive meshes, same index and distance for all spacings.
2 different indices

$$i := \sqrt{-1} \qquad \lambda := 10, 10.5 .. 200$$

$$\omega 1o := \frac{g1}{\lambda 1} \qquad \omega 3o := \frac{g3}{\lambda 3}$$

$$\omega 1 := \omega 1o \cdot \sqrt{\frac{2}{(n1^2 + n2^2)}} \qquad \omega 3 := \omega 3o \cdot \sqrt{\frac{2}{(n1^2 + n3^2)}}$$

$$\Omega 1(\lambda) := \left[\frac{g1}{\lambda} \cdot (\omega 1)^{-1} - \frac{\omega 1 \cdot \lambda}{g1} \right] \qquad \Omega 3(\lambda) := \left[\frac{g3}{\lambda} \cdot (\omega 3)^{-1} - \frac{\omega 3 \cdot \lambda}{g3} \right]$$

$$Y1(\lambda) := \frac{1}{a1 - \frac{i \cdot \omega 1 \cdot A1}{\Omega 1(\lambda)}} \qquad Y3(\lambda) := \frac{1}{a1 - \frac{i \cdot \omega 3 \cdot A1}{\Omega 3(\lambda)}}$$

Mesh from n1 to n2, M12

$$M111(\lambda) := \frac{-Y1(\lambda)}{2 \cdot n1} + \frac{n1 + n2}{2 \cdot n1} \qquad M112(\lambda) := \frac{-Y1(\lambda)}{2 \cdot n1} + \frac{n1 - n2}{2 \cdot n1}$$

$$M121(\lambda) := \frac{Y1(\lambda)}{2 \cdot n1} + \frac{(n1 - n2)}{2 \cdot n1} \qquad M122(\lambda) := \frac{Y1(\lambda)}{2 \cdot n1} + \frac{n1 + n2}{2 \cdot n1}$$

$$M12(\lambda) := \begin{pmatrix} M111(\lambda) & M112(\lambda) \\ M121(\lambda) & M122(\lambda) \end{pmatrix}$$

Distance in n2 thickness d2 M2d2

$$M211(\lambda) := e^{\frac{-i \cdot 2 \cdot \pi \cdot n2 \cdot d2}{\lambda}} \qquad M212(\lambda) := 0 \qquad M221(\lambda) := 0 \qquad M222(\lambda) := e^{\frac{i \cdot 2 \cdot \pi \cdot n2 \cdot d2}{\lambda}}$$

$$M2d2(\lambda) := \begin{pmatrix} M211(\lambda) & M212(\lambda) \\ M221(\lambda) & M222(\lambda) \end{pmatrix}$$

Figure C.2a Page 1, MATHCAD output: N+2 inductive meshes configuration. ω1, ω3 shifted frequencies, g the periodicity constant, M12 First Matrix (from n1 to n2), M2d2 Second Matrix (Propagation Inside dielectric n2), Y1 Shut Impedance.

Mesh from n2 to n1, M21

$$M311(\lambda) := \frac{-Y1(\lambda)}{2\cdot n2} + \frac{n2 + n1}{2\cdot n2} \qquad M312(\lambda) := \frac{-Y1(\lambda)}{2\cdot n2} + \frac{n2 - n1}{2\cdot n2}$$

$$M321(\lambda) := \frac{Y1(\lambda)}{2\cdot n2} + \frac{(n2 - n1)}{2\cdot n2} \qquad M322(\lambda) := \frac{Y1(\lambda)}{2\cdot n2} + \frac{n2 + n1}{2\cdot n2}$$

$$M21(\lambda) := \begin{pmatrix} M311(\lambda) & M312(\lambda) \\ M321(\lambda) & M322(\lambda) \end{pmatrix}$$

Mesh from n2 to n2, M22

$$M411(\lambda) := \frac{-Y1(\lambda)}{2\cdot n2} + \frac{n2 + n2}{2\cdot n2} \qquad M412(\lambda) := \frac{-Y1(\lambda)}{2\cdot n2}$$

$$M421(\lambda) := \frac{Y1(\lambda)}{2\cdot n2} \qquad M422(\lambda) := \frac{Y1(\lambda)}{2\cdot n2} + \frac{n2 + n2}{2\cdot n2}$$

$$M22(\lambda) := \begin{pmatrix} M411(\lambda) & M412(\lambda) \\ M421(\lambda) & M422(\lambda) \end{pmatrix}$$

Mesh from n1 to n3, M13

$$M511(\lambda) := \frac{-Y3(\lambda)}{2\cdot n1} + \frac{n1 + n3}{2\cdot n1} \qquad M512(\lambda) := \frac{-Y3(\lambda)}{2\cdot n1} + \frac{n1 - n3}{2\cdot n1}$$

$$M521(\lambda) := \frac{Y3(\lambda)}{2\cdot n1} + \frac{(n1 - n3)}{2\cdot n1} \qquad M522(\lambda) := \frac{Y3(\lambda)}{2} + \frac{n1 + n3}{2\cdot n1}$$

$$M13(\lambda) := \begin{pmatrix} M511(\lambda) & M512(\lambda) \\ M521(\lambda) & M522(\lambda) \end{pmatrix}$$

Figure C.2b Page 2, MATHCAD output: N+2 inductive meshes configuration. M21 Matrix (from n2 to n1, Y1), M22 Matrix (Propagation Inside dielectric n2, Y1), M13 Matrix (from n1 to n3, Y3).

Distance in n3 thickness d3, M3d3

$$M611(\lambda) := e^{\frac{-i\cdot 2\cdot\pi\cdot n3\cdot d3}{\lambda}} \qquad M612(\lambda) := 0 \qquad M621(\lambda) := 0 \qquad M622(\lambda) := e^{\frac{i\cdot 2\cdot\pi\cdot n3\cdot d3}{\lambda}}$$

$$M3d3(\lambda) := \begin{pmatrix} M611(\lambda) & M612(\lambda) \\ M621(\lambda) & M622(\lambda) \end{pmatrix}$$

Mesh from n3 to n1, M31

$$M711(\lambda) := \frac{-Y3(\lambda)}{2\cdot n3} + \frac{n3 + n1}{2\cdot n3} \qquad M712(\lambda) := \frac{-Y3(\lambda)}{2\cdot n3} + \frac{n3 - n1}{2\cdot n3}$$

$$M721(\lambda) := \frac{Y3(\lambda)}{2\cdot n3} + \frac{(n3 - n1)}{2\cdot n3} \qquad M722(\lambda) := \frac{Y3(\lambda)}{2\cdot n3} + \frac{n3 + n1}{2\cdot n3}$$

$$M31(\lambda) := \begin{pmatrix} M711(\lambda) & M712(\lambda) \\ M721(\lambda) & M722(\lambda) \end{pmatrix}$$

Mesh from n3 to n3, M33

$$M811(\lambda) := \frac{-Y3(\lambda)}{2\cdot n3} + \frac{n3 + n3}{2\cdot n3} \qquad M812(\lambda) := \frac{-Y3(\lambda)}{2\cdot n3}$$

$$M821(\lambda) := \frac{Y3(\lambda)}{2\cdot n3} \qquad M822(\lambda) := \frac{Y3(\lambda)}{2\cdot n3} + \frac{n3 + n3}{2\cdot n3}$$

$$M33(\lambda) := \begin{pmatrix} M811(\lambda) & M812(\lambda) \\ M821(\lambda) & M822(\lambda) \end{pmatrix}$$

Dielectric Interface n1 to n2, Mde12

$$Mde11(\lambda) := \frac{n1 + n2}{2\cdot n1} \qquad Mde12(\lambda) := \frac{n1 - n2}{2\cdot n1}$$

$$Mde21(\lambda) := \frac{(n1 - n2)}{2\cdot n1} \qquad Mde22(\lambda) := \frac{n1 + n2}{2\cdot n1}$$

$$Mde12(\lambda) := \begin{pmatrix} Mde11(\lambda) & Mde12(\lambda) \\ Mde21(\lambda) & Mde22(\lambda) \end{pmatrix}$$

Figure C.2c Page 3, MATHCAD Output: N+2 inductive meshes configuration. M3d3 Matrix (Propagation Inside dielectric n3). M31 (from n3 to n1, Y3), M33 Matrix (Propagation Inside dielectric n3, Y3), Mde12 Matrix (Interface-from n1 to n2).

Dielectric Interface n2 to n1,Mde21

$$Mde11a(\lambda) := \frac{n2 + n1}{2 \cdot n2} \qquad Mde12a(\lambda) := \frac{n2 - n1}{2 \cdot n2}$$

$$Mde21a(\lambda) := \frac{(n2 - n1)}{2 \cdot n2} \qquad Mde22a(\lambda) := \frac{n2 + n1}{2 \cdot n2}$$

$$Mde21(\lambda) := \begin{pmatrix} Mde11a(\lambda) & Mde12a(\lambda) \\ Mde21a(\lambda) & Mde22a(\lambda) \end{pmatrix}$$

Examples: Mcf1 with N =2 is: Four meshes, separation of d2 and n2, outside n1

Mcf2 with N =2 is: Four meshes, separation of d3 and n3, outside n1

$$Mf1(\lambda) := M12(\lambda) \cdot M2d2(\lambda) \cdot (M22(\lambda) \cdot M2d2(\lambda))^{N} \cdot M21(\lambda)$$

$$Mf2(\lambda) := M13(\lambda) \cdot M3d3(\lambda) \cdot (M33(\lambda) \cdot M3d3(\lambda))^{NN} \cdot M31(\lambda)$$

$$tf1(\lambda) := \frac{1}{Mf1(\lambda)_{1,1}} \qquad tf2(\lambda) := \frac{1}{Mf2(\lambda)_{1,1}}$$

$$Tf1(\lambda) := tf1(\lambda) \cdot \overline{tf1(\lambda)} \qquad Tf2(\lambda) := tf2(\lambda) \cdot \overline{tf2(\lambda)}$$

Figure C.2d Page 4, MATHCAD output: N+2 inductive meshes. Mde21 Matrix (Interface-from n2 to n1). Mf1, Mf2 Final Matrix products (two sets of independent and different filters, N+2 Filters); Tf1 – Transmittance (one set), Tf2 Transmittance (second set).

Mesh constants

A1 ≡ .1 a1 ≡ .001 g1 ≡ 24 λ1 ≡ 32.40 g3 ≡ 24 λ3 ≡ 32.40

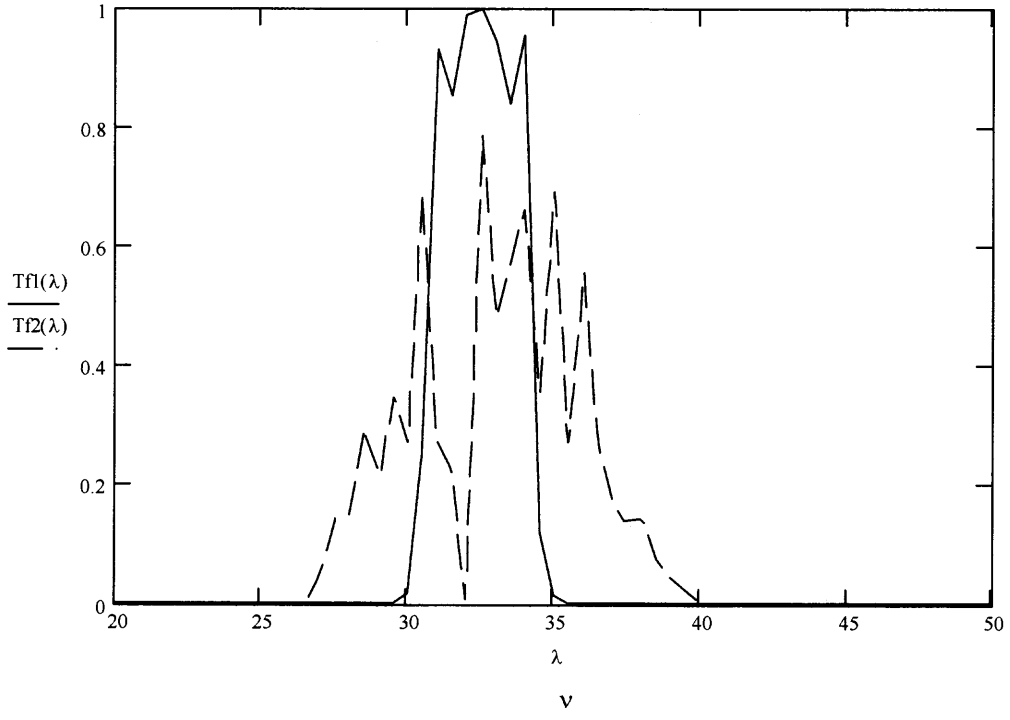

n1 ≡ 1

number of meshes 2+N

n2 ≡ 1	spacing in 2	d2 ≡ 8	N ≡ 2
n3 ≡ 1	spacing in 3	d3 ≡ 16	NN ≡ 98

Figure C.2e Page 5, MATHCAD output: N+2 inductive meshes. A1-the bandwidth Parameter, a1- the loss parameter, λ_1, λ_3- the resonance wavelengths (resonances are independent), d1, d2, d3- dielectric thickness (distances are independent). Tf1, and Tf2- Transmittances (two different sets), N=2 First set (4 filters), NN=98 Second set (100 filters).

N+2 capacitive meshes, same index and distance for all spacings.
2 different indices

$$i := \sqrt{-1} \qquad \lambda := 10, 10.5 .. 150$$

$$\omega 1oc := \frac{g1c}{\lambda 1c} \qquad \omega 3oc := \frac{g3c}{\lambda 3c}$$

$$\omega 1c := \omega 1oc \cdot \sqrt{\frac{2}{(n1^2 + n2^2)}} \qquad \omega 3c := \omega 3oc \cdot \sqrt{\frac{2}{(n1^2 + n3^2)}}$$

$$\Omega 1c(\lambda) := \left[\frac{g1c}{\lambda} \cdot (\omega 1c)^{-1} - \frac{\omega 1c \cdot \lambda}{g1c} \right] \qquad \Omega 3c(\lambda) := \left[\frac{g1c}{\lambda} \cdot (\omega 3c)^{-1} - \frac{\omega 3c \cdot \lambda}{g1c} \right]$$

$$Y1c(\lambda) := \frac{1}{a1c + \frac{i \cdot \Omega 1c(\lambda)}{2 \cdot (n1^2 + n2^2) \cdot \omega 1c \cdot A1c}} \qquad Y3c(\lambda) := \frac{1}{a1c + \frac{i \cdot \Omega 3c(\lambda)}{2 \cdot (n1^2 + n3^2) \cdot \omega 3c \cdot A1c}}$$

Mesh from n1 to n2, Mc12

$$Mc111(\lambda) := \frac{-Y1c(\lambda)}{2 \cdot n1} + \frac{n1 + n2}{2 \cdot n1} \qquad Mc112(\lambda) := \frac{-Y1c(\lambda)}{2 \cdot n1} + \frac{n1 - n2}{2 \cdot n1}$$

$$Mc121(\lambda) := \frac{Y1c(\lambda)}{2 \cdot n1} + \frac{(n1 - n2)}{2 \cdot n1} \qquad Mc122(\lambda) := \frac{Y1c(\lambda)}{2 \cdot n1} + \frac{n1 + n2}{2 \cdot n1}$$

$$Mc12(\lambda) := \begin{pmatrix} Mc111(\lambda) & Mc112(\lambda) \\ Mc121(\lambda) & Mc122(\lambda) \end{pmatrix}$$

Distance in n2 thickness dc2, Mc2d2

$$1c211(\lambda) := e^{\frac{-i \cdot 2 \cdot \pi \cdot n2 \cdot dc2}{\lambda}} \qquad Mc212(\lambda) := 0 \qquad Mc221(\lambda) := 0 \qquad Mc222(\lambda) := e^{\frac{i \cdot 2 \cdot \pi \cdot n2 \cdot dc2}{\lambda}}$$

$$Mc2d2(\lambda) := \begin{pmatrix} Mc211(\lambda) & Mc212(\lambda) \\ Mc221(\lambda) & Mc222(\lambda) \end{pmatrix}$$

Figure C.3a Page 1, MATHCAD output: N+2 capacitive meshes configuration. ω1c, ω3c shifted frequency, g the periodicity, Mc12 First Matrix elements(from n1 to n2), Mc2d2 matrix Element(Propagation Inside dielectric n2), Y1 Shut Impedance.

Mesh from n2 to n1, Mc21

$$Mc311(\lambda) := \frac{-Y1c(\lambda)}{2\cdot n2} + \frac{n2 + n1}{2\cdot n2} \qquad Mc312(\lambda) := \frac{-Y1c(\lambda)}{2\cdot n2} + \frac{n2 - n1}{2\cdot n2}$$

$$Mc321(\lambda) := \frac{Y1c(\lambda)}{2\cdot n2} + \frac{(n2 - n1)}{2\cdot n2} \qquad Mc322(\lambda) := \frac{Y1c(\lambda)}{2\cdot n2} + \frac{n2 + n1}{2\cdot n2}$$

$$Mc21(\lambda) := \begin{pmatrix} Mc311(\lambda) & Mc312(\lambda) \\ Mc321(\lambda) & Mc322(\lambda) \end{pmatrix}$$

Mesh from n2 to n2, Mc22

$$Mc411(\lambda) := \frac{-Y1c(\lambda)}{2\cdot n2} + \frac{n2 + n2}{2\cdot n2} \qquad Mc412(\lambda) := \frac{-Y1c(\lambda)}{2\cdot n2}$$

$$Mc421(\lambda) := \frac{Y1c(\lambda)}{2\cdot n2} \qquad Mc422(\lambda) := \frac{Y1c(\lambda)}{2\cdot n2} + \frac{n2 + n2}{2\cdot n2}$$

$$Mc22(\lambda) := \begin{pmatrix} Mc411(\lambda) & Mc412(\lambda) \\ Mc421(\lambda) & Mc422(\lambda) \end{pmatrix}$$

Mesh from n1 to n3, Mc13

$$Mc511(\lambda) := \frac{-Y3c(\lambda)}{2\cdot n1} + \frac{n1 + n3}{2\cdot n1} \qquad Mc512(\lambda) := \frac{-Y3c(\lambda)}{2\cdot n1} + \frac{n1 - n3}{2\cdot n1}$$

$$Mc521(\lambda) := \frac{Y3c(\lambda)}{2\cdot n1} + \frac{(n1 - n3)}{2\cdot n1} \qquad Mc522(\lambda) := \frac{Y3c(\lambda)}{2} + \frac{n1 + n3}{2\cdot n1}$$

$$Mc13(\lambda) := \begin{pmatrix} Mc511(\lambda) & Mc512(\lambda) \\ Mc521(\lambda) & Mc522(\lambda) \end{pmatrix}$$

Figure C.3b Page 2, MATHCAD output: N+2 capacitive meshes configuration. Mc21 Matrix (from n2 to n1, Y1 – metal contribution), Mc22 Matrix (Propagation Inside dielectric n2, Y1), Mc13 Matrix (from n1 to n3, Y3).

Distance in n3 thickness dc3 Mc3d3

$$Mc611(\lambda) := e^{\frac{-i\cdot 2\cdot\pi\cdot n3\cdot dc3}{\lambda}} \qquad Mc612(\lambda) := 0 \qquad Mc621(\lambda) := 0 \qquad Mc622(\lambda) := e^{\frac{i\cdot 2\cdot\pi\cdot n3\cdot dc3}{\lambda}}$$

$$Mc3d3(\lambda) := \begin{pmatrix} Mc611(\lambda) & Mc612(\lambda) \\ Mc621(\lambda) & Mc622(\lambda) \end{pmatrix}$$

Mesh from n3 to n1, Mc31

$$Mc711(\lambda) := \frac{-Y3c(\lambda)}{2\cdot n3} + \frac{n3 + n1}{2\cdot n3} \qquad Mc712(\lambda) := \frac{-Y3c(\lambda)}{2\cdot n3} + \frac{n3 - n1}{2\cdot n3}$$

$$Mc721(\lambda) := \frac{Y3c(\lambda)}{2\cdot n3} + \frac{(n3 - n1)}{2\cdot n3} \qquad Mc722(\lambda) := \frac{Y3c(\lambda)}{2\cdot n3} + \frac{n3 + n1}{2\cdot n3}$$

$$Mc31(\lambda) := \begin{pmatrix} Mc711(\lambda) & Mc712(\lambda) \\ Mc721(\lambda) & Mc722(\lambda) \end{pmatrix}$$

Mesh from n3 to n3, Mc33

$$Mc811(\lambda) := \frac{-Y3c(\lambda)}{2\cdot n3} + \frac{n3 + n3}{2\cdot n3} \qquad Mc812(\lambda) := \frac{-Y3c(\lambda)}{2\cdot n3}$$

$$Mc821(\lambda) := \frac{Y3c(\lambda)}{2\cdot n3} \qquad Mc822(\lambda) := \frac{Y3c(\lambda)}{2\cdot n3} + \frac{n3 + n3}{2\cdot n3}$$

$$Mc33(\lambda) := \begin{pmatrix} Mc811(\lambda) & Mc812(\lambda) \\ Mc821(\lambda) & Mc822(\lambda) \end{pmatrix}$$

Dielectric Interface n1 to n2,Mde12

$$Mde11(\lambda) := \frac{n1 + n2}{2\cdot n1} \qquad Mde12(\lambda) := \frac{n1 - n2}{2\cdot n1}$$

$$Mde21(\lambda) := \frac{(n1 - n2)}{2\cdot n1} \qquad Mde22(\lambda) := \frac{n1 + n2}{2\cdot n1}$$

$$Mde12(\lambda) := \begin{pmatrix} Mde11(\lambda) & Mde12(\lambda) \\ Mde21(\lambda) & Mde22(\lambda) \end{pmatrix}$$

Figure C.3c Page 3, MATHCAD output: N+2 capacitive meshes configuration Mc3d3 Matrix (Propagation Inside dielectric n3). Mc31 (from n3 to n1, Y3), Mc33 Matrix (Propagation Inside dielectric n3, Y3- metal mesh contribution), Mde12 Matrix (Interface-from n1 to n2).

Dielectric Interface n2 to n1,Mde21

$$Mde11a(\lambda) := \frac{n2 + n1}{2 \cdot n2} \qquad Mde12a(\lambda) := \frac{n2 - n1}{2 \cdot n2}$$

$$Mde21a(\lambda) := \frac{(n2 - n1)}{2 \cdot n2} \qquad Mde22a(\lambda) := \frac{n2 + n1}{2 \cdot n2}$$

$$Mde21(\lambda) := \begin{pmatrix} Mde11a(\lambda) & Mde12a(\lambda) \\ Mde21a(\lambda) & Mde22a(\lambda) \end{pmatrix}$$

Examples: Mcf1 with N =2 is: Four meshes, separation of d2 and n2, outside n1
Mcf2 with N=2 is: Four meshes, separation of d3 and n3, outside n1

$$Mcf1(\lambda) := Mc12(\lambda) \cdot Mc2d2(\lambda) \cdot (Mc22(\lambda) \cdot Mc2d2(\lambda))^{N} \cdot Mc21(\lambda)$$

$$Mcf2(\lambda) := Mc13(\lambda) \cdot Mc3d3(\lambda) \cdot (Mc33(\lambda) \cdot Mc3d3(\lambda))^{NN} \cdot Mc31(\lambda)$$

$$tcf1(\lambda) := \frac{1}{Mcf1(\lambda)_{1,1}} \qquad tcf2(\lambda) := \frac{1}{Mcf2(\lambda)_{1,1}}$$

$$Tcf1(\lambda) := tcf1(\lambda) \cdot \overline{tcf1(\lambda)} \qquad Tcf2(\lambda) := tcf2(\lambda) \cdot \overline{tcf2(\lambda)}$$

Figure C.3d Page 4, MATHCAD output: N+2 capacitive meshes configuration. Mde21 Matrix (Interface-from n2 to n1). Mcf1, Mcf2 Final Matrix products (two sets of independent and different filters, N+2 Filters); Tcf1 – Transmittance (first set), Tcf2 Transmittance (second set).

Mesh constants

A1c ≡ .1 a1c ≡ .001 g1c ≡ 24 λ1c ≡ 32.40 g3c ≡ 24 λ3c ≡ 32.40

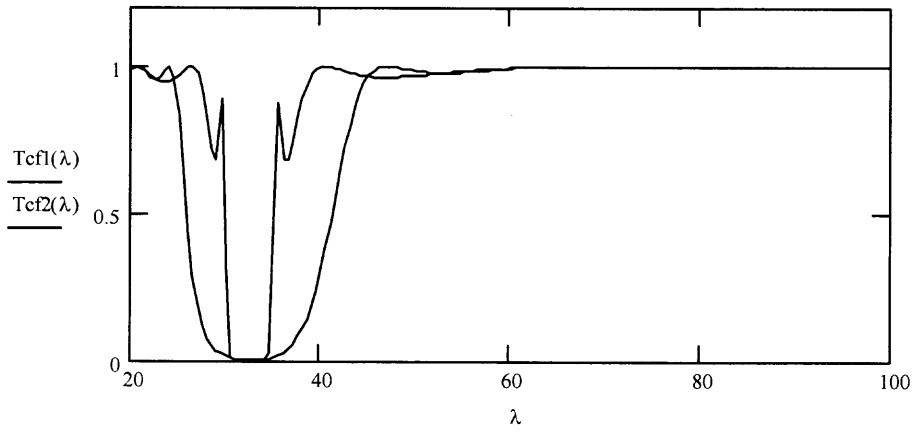

n1 ≡ 1 number of meshes 2+N

n2 ≡ 1 spacing in 2 dc2 ≡ 8 N ≡ 2

n3 ≡ 1 spacing in 3 dc3 ≡ 16 NN ≡ 2

Figure C.3e Page 5, MATHCAD output: N+2 capacitive meshes. A1-the bandwidth Parameter, a1- the loss parameter, λ_1, λ3- the resonance wavelengths (resonances are independent), d1, d2, d3- dielectric thickness (distances are independent). Tcf1, and Tcf2-Transmittances (two different sets), N=2 First set (4 filters), NN=2 Second set (4 filters).

Karlsruhe Inductive Thickness peaks

$$T1 := \begin{pmatrix} 21.2 \\ 22.8 \\ 25 \\ 26.9 \\ 28.5 \\ 29.9 \\ 30.7 \end{pmatrix} \qquad t1 := \begin{pmatrix} 6.4 \\ 9.6 \\ 12.8 \\ 16 \\ 19.2 \\ 22.4 \\ 25.6 \end{pmatrix}$$

$$T2 := \begin{pmatrix} 20.9 \\ 22.2 \\ 23.2 \end{pmatrix} \qquad t2 := \begin{pmatrix} 19.2 \\ 22.4 \\ 25.6 \end{pmatrix}$$

$t := 6, 7 .. 26$

$tt := 18, 19 .. 26$

$\lambda R := 40 \qquad g := 20$

$f1 := .6 \qquad f2 := .65$

$c1 := .85 \qquad c2 := 1.2$

$$F1(t) := \sqrt{\frac{1}{\frac{1}{(2 \cdot g)^2} + \frac{1}{(g + t)^2}}}$$

$$F2(tt) := \sqrt{\frac{1}{\frac{1}{(2 \cdot g)^2} + \frac{1}{\left(\frac{g}{4} + tt\right)^2}}}$$

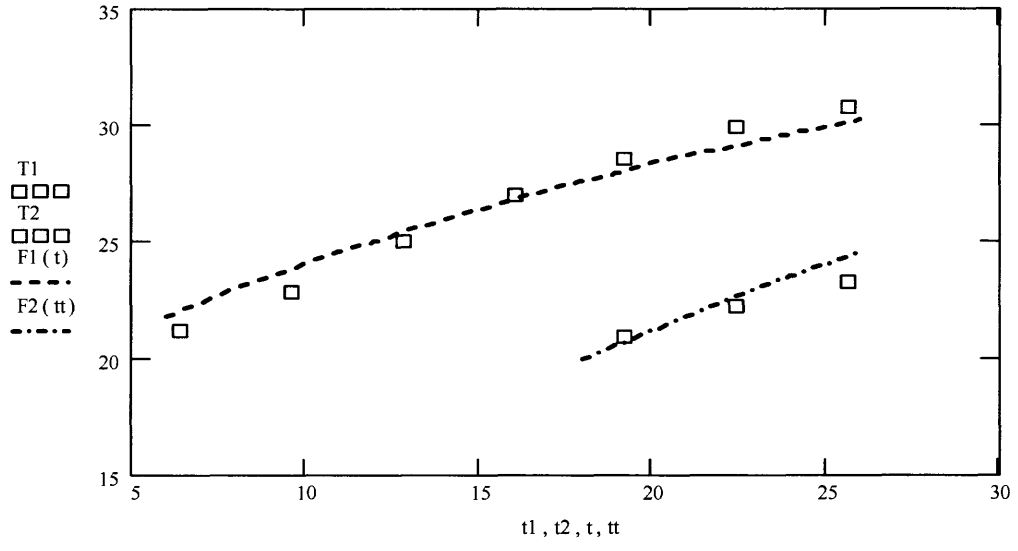

Figure C.4 MATHCAD Output. Fitting of thickness peak for thick inductive meshes for simulated data. Formula from wave vectors addition. Fitting constants.: c1=0.85, and c2=1.2. T1,T2- Simulated resonances of thickness peak(microns), F1,F2- Fitted values of thickness peak(microns), t2 actual thickness(microns). Note: Seven simulated peaks are fitted with two fitting constants.

Karlsruhe Capacitive grid Thickness peak

$$T2 := \begin{pmatrix} 25.8 \\ 27.5 \\ 27.9 \\ 28.7 \\ 29.4 \end{pmatrix} \qquad t2 := \begin{pmatrix} 12.8 \\ 16 \\ 19.2 \\ 22.4 \\ 25.6 \end{pmatrix}$$

$g := 20$ $\quad \lambda R := 40$

$c1 := 1.25$ $\quad c2 := .75$

$$F1(t2) := \sqrt{\frac{1}{\frac{1}{(\lambda R)^2} + \frac{1}{(c1 \cdot g + c2 \cdot t2)^2}}}$$

$$F1(t2) = \begin{pmatrix} 26.168 \\ 27.162 \\ 28.07 \\ 28.9 \\ 29.658 \end{pmatrix}$$

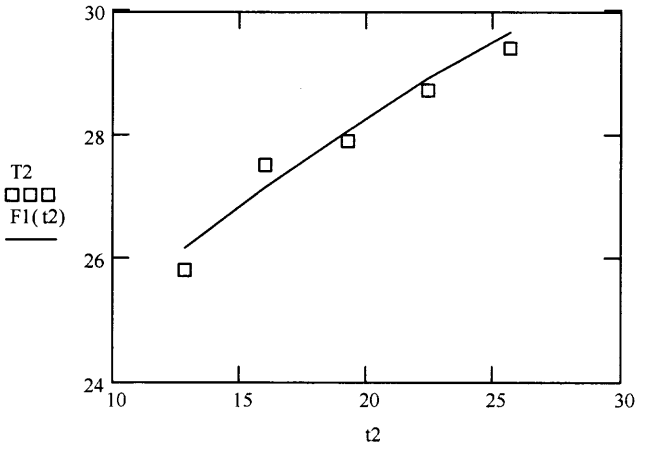

Formula C.5 MATHCAD Output. Fitting of thickness peak for thick capacitive meshes for simulated data. Formula from wave vectors addition. Fitting constants c1=1.25, and c2=1.25; T2- simulated resonances of thickness peak(microns), F1- Fitted values of thickness peak(microns), t2 actual thickness(microns).

APPENDIX D

GLOSSARY

Babinet's Principle (Electromagnetic Vector Formulation). Complementary Screens will show complementary transmittance pattern, where as the Maximum of an inductive mesh has the same wavelength as the minimum of the capacitive mesh, provided that geometrical parameters are the same

Compound modes

a. Thin free Standing Metal Meshes. The Compound mode consists of two sets of standing surface waves, each set on one side of the mesh.

b. Stacks of Thin Free Standing Metal Meshes, at Distance d. The two modes of the metal mesh and the Fabry-Perot mode form the Compound Mode.

c. Single Free Standing Metal Mesh, Substrate/Embedded Case. The Compound mode consists of two sets of resonance wavelength shifted surface waves and their interaction with the dielectric (Fabry-Perot) modes.

d. Stacks of Thin Metal Meshes, on Top of Dielectric Substrate, at Distance d. The Compound mode consists of the resonance modes of each metal mesh, the mode generated by the dielectric, and the interaction between them.

e. Thick Free Standing Metal Meshes. The compound mode consists of two sets of surface waves one on the front and the other on the backside of the mesh and interaction with the waveguide modes

Fabry-Perot Modes. Modes of two reflecting surfaces at distance d.

Oscillator Model. The model assumes the formation of resonance and waveguide modes and their coupling.

Resonance Mode. The two pairs of surface waves on the front and backside of a metal mesh oscillate with the same resonance wavelength and form the resonance mode.

Surface Wave. A longitudinal wave oscillating on the plane perpendicular to incoming propagating incident wave

Surface Wave Interaction. The governing mechanizing of a resonance mode is controlled via the interaction of surface waves. The incident light induces a pair of surface waves on both sides of the mesh, and these surface waves transfer the incident light into the reflected and transmitted light. The induced longitudinal electromagnetic surface waves are standing waves with resulting wave vector equal to zero and resonance wavelength depending on the periodicity of the mesh and geometry of the openings. Different substrate as well as different metallic thickness affects the surface waves behavior.

Transmission Line Theory and Meshes. Meshes are described by complex quantities and electrical parameters as electrical oscillators

Waveguide Modes. Modes generated with increased thickness of free standing metal meshes, also called "Thickness Peaks".

REFERENCES

1. R. Ulrich, K.F. Renk, and L. Genzel. (1963). Tunable submillimeter interferometers of the Fabry-Perot type. IEEE Trans. Micro-wave Theory Tech, MTT-11, 363-371.

2. G.M Ressler and K.D. Möller. (1967). Far infrared bandpass filters and measurements on a reciprocal grid. Applied Optics, 6, 893-896.

3. R. Ulrich. (1967). Interference filters for the far infrared. Infrared Physics, 7, 1987-1966.

4. S.T. Chase and R.D. Joseph. (1983). Resonant array bandpass filters for the far infrared. Applied Optics, 22, 1775-1779.

5. A. Goldin, University of Chicago. (1998). [FSS Code Available: http://flight.uchicago.edu/fsb/]

6. C. Compton, R.D. McPhedran, G.H Derrick, and L.C. Botten. (1983). Diffraction properties of a bandpass grid. Infrared Physics, 23, 239-245.

7. D.W. Porterfield, J.L. Hesler, R. Densing, E.R. Mueller, T.W. Crowe, and R. M. Weikle II. (1994). Resonant metal-mesh bandpass filters for the far infrared. Applied Optics, 33, 6046-6092.

8. K.D. Möller, K.R. Farmer, D.V.P. Ivanov, O. Sternberg, K.P. Stewart, and P. Lalanne. (1999). Thin and thick cross shaped metal grids. Infrared Physics, 40, 475-485.

9. K.D. Möller, J. Warren, J.B. Heaney, and C. Kotecki. (1996). Cross shaped bandpass filters for the near-and mid-infrared wave-length region. Applied Optics, 35, 6210-6215.

10. Micro-Stripes Program Ver 6.0[Computer Software]. (2002), Southborough, Massachusetts: Flomerics.

11. R. Ruprecht, W. Bacher, P. Bley, M. Harmening, and W.K. Schomburg. (1991). Kfk-Nachr. Jahrg. 23, 2-91, 18-123.

12. Max Born and Emil Wolf. (1999) Principles of Optics. UK: Cambridge.

13. J.D Jackson. (1975). Classical Electrodynamics. New York: Wiley.

14. Robert E Collin. (1992). Foundation For Microwave Engineering. New York: Mcgraw Hill.

15. K.D. Möller and W.G. Rothschild. (1971). Far Infrared Spectroscopy. New York: Wiley.

16. R. Ulrich. (1974). Modes of Propagation on an open periodic waveguide for the far infrared. Proceedings of the Symposium of Optical and Acoustical Micro-Electronics, Vol. XXIII. 359-376.

17. O. Sternberg, K.D. Möller, H. Grebel K.P Stewart, and R. M. Henry. (2002) Submited Journal of Infrared Physics.

18. Karl D. Möller, Oren Sternberg, Haim Grebel, and Kenneth P. Stewart. (2002). Near-field effects in multilyer inductive metal meshes. Applied Optics, 41, 1942-1948.

19. L. B. Whitbourn and R.C. Compton. (1985). Equivalent-circuit formulas for metal grids reflectors at dielectric boundary. Applied Optics, 24, 217-220.

20. T. Timusk and P. L. Richards. (1981). Near_Millimeter wave band-pass filters. Applied Optics, 20, 1355-1360.

21. B. C. Hicks, M. Rebbert, P. Isaacson, D. Ma, C. Marrian, J. Fischer, H. A. Smith, P. Ade, R. Sudiwala, M. Greenhouse, H. Moseley, and Ken Stewart. (1998). NASA Space Science Workshop, Harvard-Smithsonian Center for Astrophysics.

22. Karl D. Möller, Oren Sternberg, Haim Grebel, and Kenneth P. Stewart. (2002). Inductive cross-shaped metal meshes and dielectrics. Applied Optics, 41, 3919-3919- 3919.

23. K.D. Möller, Oren Sternberg, H. Grebel , Philippe Lalanne. (2002). Thick inductive cross shaped metal meshes. Applied Physics, 91, 9461-9465.

24. T. W. Ebbesen, H..J. Lezec, H.F. Ghaemi, T. Thio, and P.A. Wolff. (1998). Extraordinary optical transmission thorough sub-wavelength hole arrays. Nature, 391, 667-669.

25. D. E. Grupp, H. J. Lezec, T. W. Ebbesen, K. M. Pellerin, and T. Thio. (2000). Crucial role of metal surface in enhanced transmission through subwavelength apertures. Applied. Physics Letters. 77, 1569-1571.

26. L. Martin-Moreno, F.J Garcia-Vidal, H.J. Lezec. K. M. Pellerin, T. Thio, J. B. Pendry, and T. W. Ebbesen. (2001). Theory of Extraordinary Optical Trasnmission through Subwavelength Hole Arrays. Physical Review Letters, 86, 1114-1117 (2001).

27. Ph Lalanne, J P Hugonin, S Astilean, M Palmaru and K D Möller. (2000). One-mode model and Airy-like formulae for one-dimensional metallic gratings. Pure Applied Optics(UK), 2, 48-51.

28. J. S. McCalmont, M. M. Sigalas, G. Tuttle, K.-H. Ho and C. M. Soukolis. (1996). A layer-by-layer metallic photonic band-gap structure. Appl. Phys. Lett, 68, 2759-2765.

29. J. G. Fleming, S. Y. Lin, I. El-Kady, R. Biswas and K. M. Ho. (2002). All-Metallic three-dimensional photonic crystals with a large infrared bandgap. Nature, 417, 52-55.

30. Ali Serpenguzel. (2002). Transmission Characteristics of Metallodielectric Photonic Crystals and Resonators. IEEE Microwave and Wireless Components Letters, 12, 134-136.

31. S. Wolf and R.N. Tauber. (2000). Silicon Processing For the VLSI Era. California: Lattice Press.

32. D. M Kearns and R. W Beatty. (1967). Basic Theory of Waveguide Functions and Introductory Microwave Network Analysis. Pergamon, Oxford.

33. D. H. Dawes, R. C. McPhedran, and L. B. Whitbourn. (1989). Thin capacitive meshes on a dielectric boundary: theory and experiment. Applied Optics, 28, 3498-3510.

34. E. Popov, M. Neviere, S. Enoch, and R. Reinisch. (2002). Theory of light transmission through subwavelength periodic hole arrays. Physical Review B, 62 16100 – 16108.

35. D. M. Byrne. (1985). Diffraction Phenomena in Optical Engineering Diffractive Infrared filters Fabricated by Electron-beam Lithography, SPIE, 560, 70-81.

36. S. Astilean, Ph. Lalanne and M. Palamaru. (2000). Light transmission through metallic channels much smaller than the wavelength. Optical Communication, 175, 265-273.

37. High Frequency Structure Simulator (HFSS). Hewlett-Packard

38. Heinz Raether. (1998). Surface Plasmons on Smooth and Rough Surfaces and on Gratings Berlin: Springer 1988.